From DEPARTMENT OF CLINICAL NEUROSCIENCE
Karolinska Institutet, Stockholm, Sweden

PET STUDIES ON THE MECHANISMS OF ACTION OF ANTIDEPRESSANT AND ANTIPSYCHOTIC DRUGS

Kai-Chun Yang

Stockholm 2017

Cover illusion:

Parasagittal PET-section of a nonhuman primate brain showing regional reductions of [^{11}C]AZ10419369 binding to the 5-HT$_{1B}$ receptor after administration of vortioxetine, a novel antidepressant.

Published by Karolinska Institutet.
Printed by E-Print AB 2017

ISBN 978-91-7676-786-3

PET Studies on the Mechanisms of Action of Antidepressant and Antipsychotic Drugs

THESIS FOR DOCTORAL DEGREE (Ph.D.)

By

Kai-Chun Yang

Principal Supervisor:
Dr Sjoerd J. Finnema
Karolinska Institutet
Department of Clinical Neuroscience

Co-supervisor(s):
Professor Lars Farde
Karolinska Institutet
Department of Clinical Neuroscience

Professor Christer Halldin
Karolinska Institutet
Department of Clinical Neuroscience

Dr Akihiro Takano
Karolinska Institutet
Department of Clinical Neuroscience

Opponent:
Professor Yasuyoshi Watanabe
RIKEN
Center for Life Science Technologies

Examination Board:
Professor Sven Ove Ögren
Karolinska Institutet
Department of Neuroscience

Professor Hans Ågren
University of Gothenburg
Institute of Neuroscience and Physiology

Professor Mark Lubberink
Uppsala University
Department of Surgical Sciences

In memory of my father,

楊正宗 *(Yang, Cheng-Tsung),*

1945-2011

“I couldn't reduce it to the freshman level.
That means we don't really understand it.”

Richard Feynman, 1918-1988

ABSTRACT

Positron emission tomography (PET) is a non-invasive molecular imaging technique suitable for examination of neurochemical biomarkers in the living brain. Among these applications, PET studies are used to facilitate the development of novel psychotropic drugs. The general aim of this thesis work was to develop and implement novel PET imaging paradigms suitable for research and drug development in psychiatry. The work was carried out in nonhuman primates (NHP) with the intention to prepare for future human applications.

The first part of the thesis work was to develop improved PET imaging paradigms sensitive to changes in serotonin (5-HT) concentration. In Study I, the binding of [^{11}C]Cimbi-36, a novel 5-HT$_{2A}$ receptor agonist radioligand, was found to be sensitive to fenfluramine-induced 5-HT release. The 5-HT sensitivity of [^{11}C]Cimbi-36 was comparable to that of [^{11}C]AZ10419369, a 5-HT$_{1B}$ receptor radioligand with established 5-HT sensitivity. In Study II, [^{11}C]AZ10419369 binding was found to be sensitive to pretreatment with 5-HT concentration enhancers (amphetamine, MDMA or 5-HTP) at clinically relevant doses that may be safely applied in human studies. After validation, these PET methodologies were used in Study III to assess the mechanisms of action of vortioxetine, a novel antidepressant. At doses with comparable and clinically relevant occupancy of the 5-HT transporter, vortioxetine induced larger reductions in [^{11}C]AZ10419369 binding than citalopram, and had no significant effect on [^{11}C]Cimbi-36 binding. The results suggest that vortioxetine binds to the 5-HT$_{1B}$ receptor when administered at clinically relevant doses.

The second part of the thesis work extended the application of PET imaging from neuroreceptors to intracellularly located enzymes, such as phosphodiesterase 10A (PDE10A). In Study IV, we characterized the binding of [^{11}C]Lu AE92686 to PDE10A in the NHP brain and validated the quantification methods. In Study V, we examined the effect of changes in the concentration of 3',5'-cyclic adenosine monophosphate (cAMP) on [^{11}C]Lu AE92686 binding. Decreasing cAMP concentration by administration of SCH 23390 alone or in combination with *R*-apomorphine significantly decreased striatal [^{11}C]Lu AE92686 binding. The combination of SCH 23390 and *R*-apomorphine also significantly increased binding in substantia nigra. The decrease in striatal [^{11}C]Lu AE92686 binding may reflect a decrease in PDE10A affinity induced by cAMP depletion. The effect of changes in cAMP concentration on PDE10A binding should thus be considered when [^{11}C]Lu AE92686 is used in human studies.

In conclusion, the current thesis work has advanced the PET imaging paradigms for examining changes in 5-HT concentration. The validation of [^{11}C]Lu AE92686 as a PDE10A PET radioligand and understanding the modulatory role of cAMP on [^{11}C]Lu AE92686 binding will facilitate the application of this PDE10A radioligand in future studies. The developed PET methodologies were applied to evaluate the mechanisms of action of psychotropic drugs and can be translated into future human studies.

LIST OF SCIENTIFIC PAPERS

I. **Kai-Chun Yang**, Vladimir Stepanov, Stefan Martinsson, Anders Ettrup, Akihiro Takano, Gitte M. Knudsen, Christer Halldin, Lars Farde, Sjoerd J. Finnema. (2017) Fenfluramine reduces [^{11}C]Cimbi-36 binding to the 5-HT_{2A} receptor in the nonhuman primate brain. *International Journal of Neuropsychopharmacology* 20, 683–691. doi:10.1093/ijnp/pyx051

II. **Kai-Chun Yang**, Akihiro Takano, Christer Halldin, Lars Farde, Sjoerd J. Finnema. Serotonin concentration enhancers at clinically relevant doses reduce [^{11}C]AZ10419369 binding to the 5-HT_{1B} receptors in the nonhuman primate brain. (Manuscript).

III. **Kai-Chun Yang**, Vladimir Stepanov, Nahid Amini, Stefan Martinsson, Akihiro Takano, Christoffer Bundgaard, Benny Bang-Andersen, Connie Sanchez, Christer Halldin, Lars Farde, Sjoerd J. Finnema. Comparison of serotonin system PET markers after administration of clinically relevant doses of vortioxetine and citalopram in the nonhuman primate brain. (Manuscript).

IV. **Kai-Chun Yang**, Vladimir Stepanov, Nahid Amini, Stefan Martinsson, Akihiro Takano, Jacob Nielsen, Christoffer Bundgaard, Benny Bang-Andersen, Sarah Grimwood, Christer Halldin, Lars Farde, Sjoerd J. Finnema. (2017) Characterization of [^{11}C]Lu AE92686 as a PET radioligand for phosphodiesterase 10A in the nonhuman primate brain. *European Journal of Nuclear Medicine and Molecular Imaging* 44, 308–320. doi:10.1007/s00259-016-3544-9

V. **Kai-Chun Yang**, Sarah Grimwood, Jacob Nielsen, Vladimir Stepanov, Nahid Amini, Stefan Martinsson, Christoffer Bundgaard, Benny Bang-Andersen, Mohammed Shahid, Akihiro Takano, Christer Halldin, Lars Farde, Sjoerd J. Finnema. Changes in cAMP concentration modify [^{11}C]Lu AE92686 binding to phosphodiesterase 10A in the nonhuman primate brain. (Manuscript).

CONTENTS

LIST OF ABBREVIATIONS

1TCM	1-tissue compartment model
2TCM	2-tissue compartment model
5-HT	Serotonin
5-HTP	5-hydroxytryptophan
5-HTT	Serotonin transporter
AADC	Aromatic *L*-amino-acid decarboxylase
ANTs	Advanced Normalization Tools
B/I	Bolus and constant infusion
BBB	Blood-brain barrier
B_{max}	Receptor density
BP_{ND}	Binding potential refer to non-displaceable compartment
cAMP	3',5'-cyclic adenosine monophosphate
cGMP	3',5'-cyclic guanosine monophosphate
CNS	Central nervous system
D_1R	Dopamine D_1 receptor
D_2R	Dopamine D_2 receptor
D_3R	Dopamine D_3 receptor
DRN	Dorsal rahpe nucleus
f_P	Free fraction of compound in plasma
GABA	γ-aminobutyric acid
GPCR	G-protein coupled receptor
K_D	Dissociation constant at equilibrium
K_i	Inhibition constant at equilibrium
Loganref	Logan reference tissue model
MDMA	3,4-methylenedioxymethamphetamine
MRI	Magnetic resonance imaging
NHP	Nonhuman primate
PBS	Phosphate buffered saline
PDE10A	Phosphodiesterase 10A
PET	Positron emission tomography

SN	Substantia nigra
SRTM	Simplified reference tissue model
SSRI	Selective serotonin re-uptake inhibitor
t^*	Starting time of linearization
TAC	Time–activity curve
V_{ND}	Distribution volume for non-displaceable compartment
VOI	Volume of interest
V_T	Total distribution volume
ΔBP_{ND}	Relative changes in BP_{ND}
ΔF_{NT}	Changes in neurotransmitter concentration

1 INTRODUCTION

1.1 RATIONALE FOR THE THESIS

Neuropsychiatric disorders are chronic illnesses with high levels of morbidity and mortality (Carpenter and Koenig, 2008; Hayes *et al*, 2015; Whiteford *et al*, 2013). According to a recent survey conducted by the World Health Organization, these disorders are the leading causes of disease burden worldwide (Whiteford *et al*, 2013). Although several psychotropic drugs have been developed for the treatment of these disorders, the therapeutic outcomes are still suboptimal (Miyamoto *et al*, 2012; Papakostas and Ionescu, 2015; Perlis *et al*, 2006; Rush *et al*, 2006). For mood disorders, only about 60–70% of patients achieve remission after several courses of treatment and most of them will undergo relapse of mood episodes within 1–2 years (Perlis *et al*, 2006; Rush *et al*, 2006). The treatment outcome of schizophrenia is also poor, resulting in profound functional impairment in most patients (Carpenter and Koenig, 2008; Miyamoto *et al*, 2012). Accordingly, there is a large unmet need for better pharmacological treatment of neuropsychiatric disorders.

However, the success rate of drug discovery for the central nervous system (CNS) is low when compared to other therapeutic domains (DiMasi *et al*, 2009). Several factors contribute to the difficulty in developing novel psychotropic drugs. The etiology and pathophysiology of most neuropsychiatric disorders are complex and unknown (Matthews *et al*, 2012; Miyamoto *et al*, 2012; Papakostas and Ionescu, 2015; Roth *et al*, 2004; Wong *et al*, 2010). Although many new target proteins have been identified, the role of these proteins in the pathophysiology and treatment of neuropsychiatric disorders remains unclear (Miyamoto *et al*, 2012; Papakostas and Ionescu, 2015; Roth *et al*, 2004; Wong *et al*, 2010). The failure of a candidate CNS drug might originate from several causes, including inadequate CNS exposure, inability to achieve optimal level of binding to the target, or lack of expected biological effects/therapeutic efficacy from the drug (Hargreaves and Rabiner, 2014; Lee and Farde, 2006; Morgan *et al*, 2012).

Positron emission tomography (PET) is a non-invasive molecular imaging technique that enables quantification of neurochemical biomarkers in the living brain. PET can facilitate the development of novel CNS drugs using different approaches as shown in Table 1 (page 2) (Farde, 1996; Halldin *et al*, 2001a; Hargreaves and Rabiner, 2014; Lee and Farde, 2006; Matthews *et al*, 2012; Varnäs *et al*, 2013; Wong *et al*, 2009). First, the role of target proteins in the pathophysiology of neuropsychiatric disorders (neuropathy) can be evaluated by cross-sectional (comparing patients and healthy controls) or longitudinal (within patients) PET studies (Gunn *et al*, 2015; Lee and Farde, 2006; Varnäs *et al*, 2013). The established neuropathy biomarker can potentially also be used to monitor treatment effects from a candidate drug (Halldin *et al*, 2001a; Lee and Farde, 2006; Varnäs *et al*, 2013; Wong *et al*, 2009). Second, the biodistribution and CNS exposure of the candidate drug can be assessed by microdosing studies which include PET measurements with the radiolabeled candidate drug (Farde, 1996; Halldin *et al*, 2001a; Lee and Farde, 2006; Matthews *et al*,

2012; Varnäs *et al*, 2013; Wong *et al*, 2009). Third, PET occupancy experiments can be used to investigate target engagement of the candidate drug in the living brain and can also guide drug dose selection for future studies (Farde, 1996; Halldin *et al*, 2001a; Hargreaves and Rabiner, 2014; Lee and Farde, 2006; Matthews *et al*, 2012; Varnäs *et al*, 2013; Wong *et al*, 2009). Final, the expected biological effects of the candidate drug (proof of mechanism) and the interaction between the effect and pathophysiology (proof of principle) could be examined by the PET measurements for the targets related to these effects (Hargreaves and Rabiner, 2014; Lee and Farde, 2006; Matthews *et al*, 2012; Wong *et al*, 2009). Linking the results of target engagement and proof of principle to the clinical outcomes could provide information for proof of concept (Hargreaves and Rabiner, 2014; Wong *et al*, 2009).

Table 1. The roles of PET imaging studies in the development of CNS drugs

Stages of drug development	Description of the stage	PET study type
Target engagement	Distribution/reaching target Target occupancy	Microdosing PET occupancy studies
Proof of mechanism	Target mechanisms = pharmacodynamic effects	PET studies on targets related to pharmacodynamic effects or pathophysiology
Proof of principle	Target mechanisms influence pathophysiology	
Proof of concept	Target mechanisms improve clinical outcomes	Relating the results of PET occupancy/ pharmacodynamic/ pathophysiology studies to clinical outcomes

For the recent two decades, it has been of particular interest to develop PET imaging methodology to detect changes in the concentration of endogenous neurotransmitters (Finnema *et al*, 2015c; Laruelle, 2000; Paterson *et al*, 2010). For example, several radioligands have been validated for the detection of changes in the concentration of endogenous dopamine in the living human brain (Finnema *et al*, 2015c; Laruelle, 2000). These imaging paradigms have been applied in the examination of neuropathy and in different stages of drug development (van Berckel *et al*, 2006; Laruelle, 2000; Paterson *et al*, 2010; Tokunaga *et al*, 2009). Importantly, these studies have provided useful information that could not be obtained by imaging dopamine receptors themselves (Finnema *et al*, 2015c; Laruelle, 2000). Therefore, PET imaging paradigms for assessing changes in the concentration of endogenous neurotransmitters are important tools to facilitate the development of CNS drugs.

Much effort has been made to extend the use of PET imaging to detect changes in the concentration of neurochemicals other than dopamine, including serotonin (5-HT) (Finnema *et al*, 2015c; Paterson *et al*, 2010; Tyacke and Nutt, 2015), noradrenaline (Finnema *et al*, 2015b; Lehto *et al*, 2015), γ-aminobutyric acid (GABA) (Frankle *et al*, 2009, 2012, 2015; Stokes *et al*, 2014), glutamate (Delorenzo *et al*, 2015; Miyake *et al*, 2011), acetylcholine (Carson *et al*, 1998; Cohen *et al*, 2006; Ding *et al*, 2000; Gallezot *et al*, 2014a; Hillmer *et al*, 2013, 2016; Nishiyama *et al*, 2001; Tsukada *et al*, 2004; Valette *et al*, 2005) and opioid (Colasanti *et al*, 2012; Guterstam *et al*, 2013; Mick *et al*, 2014, 2016). However, so far, the applicability of these novel paradigms has not been as well developed as for dopamine

(Finnema *et al*, 2015c; Paterson *et al*, 2010). Among these potential target molecules, 5-HT is one of the most promising and plays an important role in the pathophysiology and treatment of neuropsychiatric disorders (Finnema *et al*, 2015c; Krishnan and Nestler, 2008; Paterson *et al*, 2010; Tyacke and Nutt, 2015). Furthermore, since the targets of PET radioligands have been extended from membrane G-protein coupled receptors (GPCR) or transporters to intracellular molecular targets (Gunn *et al*, 2015; Holland *et al*, 2013), it is of interest to evaluate if the binding of these novel PET radioligands is sensitive to changes in the concentration of intracellular signaling molecules (Finnema *et al*, 2015c).

Considering the similarity in physiology, neuroanatomy, cognition and social behavior to humans, studies in nonhuman primates (NHP) have been shown highly valuable for translating preclinical knowledge to human beings in several research fields, such as neuroscience (Capitanio and Emborg, 2008; Phillips *et al*, 2014), pharmacology (Gould *et al*, 2014; Phillips *et al*, 2014) and PET imaging (Finnema *et al*, 2015c; Gould *et al*, 2014). Therefore, the current thesis work used NHP as a working model for the validation of the developed methodology before application in human subjects.

In summary, the current thesis work focused on the development of PET methodology to measure changes in the concentration of neurochemical molecules in the NHP brain. Drug challenge paradigms were developed with consideration of future application in human studies. The first part of the work aimed to advance and apply the methods for assessing changes in the concentration of 5-HT, and the second part aimed to evaluate the sensitivity of radioligand binding to changes in the concentration of 3',5'-cyclic adenosine monophosphate (cAMP) using phosphodiesterase 10A (PDE10A) as the target for PET measurements.

1.2 PRINCIPLES OF PET

PET imaging can non-invasively trace the anatomical distribution and regional concentration of a radiolabeled molecule (radioligand) in the living brain and thereby allows for extracting biologically relevant information of the study target. There are two critical components of the radioligand: a molecule that selectively binds to the biological target and a short-lived positron (β+) emission radionuclide. The molecule makes it possible to examine the biological target and the acquisition of PET signals requires the radionuclide (Halldin *et al*, 2001b; Phelps, 2000).

After application of the radioligand (typically via intravenous route) into the body of a subject, the radioligand distributes throughout the whole body via the blood circulation system and then binds to the target protein. Importantly, although the radioligand is a biologically active molecule, the dose used for PET imaging (tracer dose) is much lower than the dose which typically displays pharmacological effects. Therefore, the applied mass dose of the radioligand only occupies a small portion of examined target and minimally influences the target function. During this dynamic process, the positron from the decay of radionuclide will travel randomly over a short distance (less than one millimeter for low-energy positron emitters, such as carbon-11) until it annihilates with an electron in the surrounding tissue at

which the emission of a pair of γ-particles (photons) is induced. The photons are able to escape from the body due to their high energy (511 keV) and therefore can be detected outside the body. Furthermore, the location of the positron-electron annihilation inside the body can be estimated based on the known direction of the movement of the pair of photons (approximately 180 degree) (Cherry, 2001; Gulyás and Sjöholm, 2007).

In a typical PET system, multiple γ-ray detectors are equipped. When there are two photons hitting two detectors located at opposite direction (180 degree) within a short predefined time window, a coincidence event is registered. A line connecting these two photons will pass through the position of annihilation. During the period of a PET measurement, a large number of coincidence events will be recorded by multiple combinations of different detectors. The raw data are then reconstructed into the final three-dimensional PET images using a sophisticated algorithm which also corrects for γ-ray attenuation in the tissue, scatter and random coincidences (Cherry, 2001; Gulyás and Sjöholm, 2007; Varrone *et al*, 2009).

1.3 QUANTIFICATION OF PET SIGNALS

1.3.1 Outcome measures of PET measurements

Under the framework of neuroreceptor PET imaging, determination of the density of the examined target is the primary goal of a PET measurement. Furthermore, the current thesis work only utilizes radioligands that bind reversibly to the target. Based on the law of mass action, the *in vitro* binding of radioligand to receptor under equilibrium condition can be described as the following equation (Ichise *et al*, 2001; Innis *et al*, 2007):

$$B = \frac{B_{max} \times F}{K_D + F}, \quad (1)$$

where B is the concentration of receptor bound radioligand, B_{max} is the total receptor density, F is the concentration of free radioligand and K_D is the radioligand equilibrium dissociation constant. For *in vitro* saturation studies, different F values are applied and corresponding B values are measured. Then, B_{max} and K_D can be estimated by fitting the model using different sets of F and B values.

Similarly, for *in vivo* PET studies, at least two PET measurements with high and low specific radioactivity (the ratio of radiolabeled to unlabeled molecules) are required to calculate B_{max} and K_D and such might not be easily feasible in routine clinical PET studies (Farde *et al*, 1989; Ichise *et al*, 2001; Mintun *et al*, 1984). Alternatively, binding potential (*BP*) has been proposed to be a suitable outcome parameter which describes the capacity of radioligand-binding site interaction in a given region (Mintun *et al*, 1984). *BP* is defined as the ratio of B_{max} to K_D according to the following equation (affinity of the radioligand to the target receptor is the inverse of K_D):

$$BP = \frac{B_{max}}{K_D} = B_{max} \times \frac{1}{K_D} = B_{max} \times \text{affinity}. \quad (2)$$

In a typical PET measurement, a tracer dose of radioligand is injected (K_D >> F), and equation (1) may be reduced and rearranged to

$$\frac{B}{F} = \frac{B_{max}}{K_D} = BP. \quad (3)$$

Therefore, *BP* also equals the equilibrium ratio of *B* over *F*. In addition, although nearly all receptors are available for radioligand binding in the well-controlled *in vitro* system, several factors might limit the availability of receptors for radioligand binding in the *in vivo* PET experiments such as cellular compartmentalization, receptor trafficking, and affinity states. For the potential differences between *in vitro* and *in vivo* conditions, the total available receptor concentration (B_{avail}), instead of B_{max}, was used to formulate *BP* in the *in vivo* PET experiments (Innis *et al*, 2007).

Volume of distribution is another outcome measure frequently used in PET imaging studies. The definition of the volume of distribution is the ratio of concentration of radioligand in one compartment to that in plasma (C_P) when at equilibrium conditions. As the radioactivity in tissue originates from the radioligand binding to the target receptor (C_S, as *B* in equation (3)), the nonspecifically bound radioligand (C_{NS}) and the free concentration in tissue water (C_F, as *F* in equation (3)), the total concentration of radioligand in tissue (C_T) can be described as

$$C_T = C_S + C_{NS} + C_F. \quad (4)$$

The nonspecific compartment (C_{NS}) and the free compartment (C_F) can be combined into a nondisplaceable concentration (C_{ND}). In this same manner, the total volume of distribution (V_T) can be expressed as

$$V_T = V_S + V_{ND}, \quad (5)$$

where V_S and V_{ND} refer to the distribution volume for corresponding compartments (Innis *et al*, 2007).

There are three versions of *BP* derived according to the different types of reference concentrations of the radioligand used in the model. First, as the original definition of *BP*, the concentration of free radioligand (C_F) was applied as reference concentration in the formulation of BP_F:

$$BP_F = \frac{Cs}{C_F} = \frac{B}{F} = \frac{B_{avail}}{K_D}. \quad (6)$$

Second, BP_P is defined when plasma concentration of radioligand (C_P, which could be described as C_F/f_P, where f_P is the free fraction of radioligand in plasma) is applied as reference concentration.

$$BP_P = \frac{Cs}{C_P} = \frac{Cs}{C_F/f_P} = \frac{B}{F/f_P} = f_P \times \frac{B_{avail}}{K_D}. \quad (7)$$

Finally, if the concentration of nondisplaceable radioligand in tissue (C_{ND}) indicates the reference concentration, BP_{ND} is specified.

$$BP_{ND} = \frac{Cs}{C_{ND}} = \frac{Cs}{C_F/f_{ND}} = \frac{B}{F/f_{ND}} = f_{ND} \times \frac{B_{avail}}{K_D}, \quad (8)$$

where f_{ND} is the fraction of free radioligand in the nondisplaceable compartment (Innis *et al*, 2007). In general, the test-retest variability of BP_{ND} is lower than that of BP_F or BP_P. Therefore, BP_{ND} is considered to be the choice of outcome measure when examining alterations in the concentration of endogenous neurotransmitters (Finnema *et al*, 2015c; Laruelle, 2000; Paterson *et al*, 2010).

Based on the definition of BP_{ND}, the relationship between BP_{ND} and volume of distribution can be formulated as follows,

$$BP_{ND} = \frac{C_S}{C_{ND}} = \frac{V_S}{V_{ND}} = \frac{V_T - V_{ND}}{V_{ND}}. \quad (9)$$

1.3.2 Kinetic modeling

In order to obtain outcome parameters of PET measurements as described in the previous section, the acquired dynamic PET data are quantified by kinetic modeling. The general principle of kinetic modeling is to determine if a mathematical model can adequately describe the measured changes in the decay-corrected radioactivity over time. If the model is able to describe the dynamic PET data, the outcome measures can be calculated from the values of the relevant parameters included in the model (Ichise *et al*, 2001; Slifstein and Laruelle, 2001).

1.3.2.1 Compartmental modeling

Compartmental modeling is the foundation of PET data quantification. Other quantification methods are mainly simplifications and/or rearrangements of equations used to describe compartments based on different assumptions. The strength of compartmental modeling is the possibility to obtain detailed information of several physiological processes in the system. A compartment is not a physical space but a biochemical volume where the concentration of molecules is homogenous and they behave uniformly (Slifstein and Laruelle, 2001).

For quantification of dynamic PET data, the 1-tissue compartment model (1TCM) and the 2-tissue compartment model (2TCM) are the two most commonly applied models (Figure 1). Although the model with more compartments might have larger capacity to describe the data, it will provide more challenges to derive reliable values of outcome parameters due to the increased number of parameters in the model (Ichise *et al*, 2001; Slifstein and Laruelle, 2001).

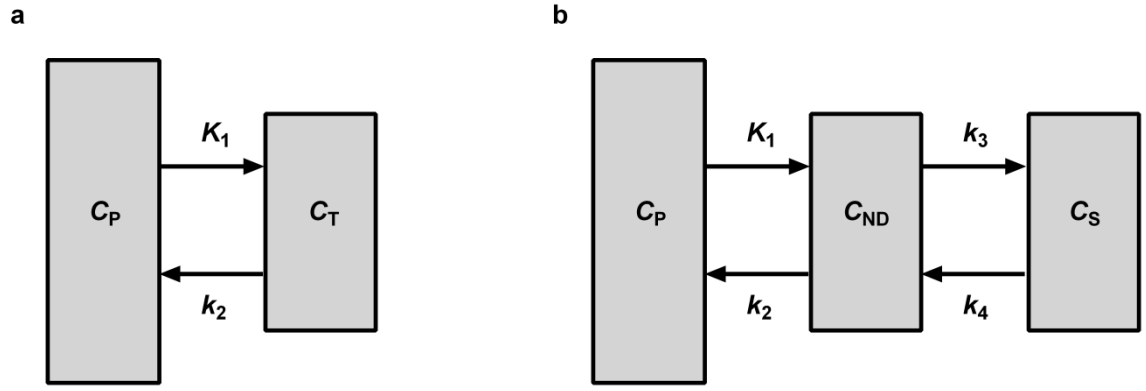

Figure 1. The two most common compartment models. (a) 1TCM. (b) 2TCM. C_{ND}: concentration of nondisplaceable radioligand; C_P: plasma concentration of radioligand; C_S: concentration of specific bound radioligand; C_T: total tissue concentration of radioligand; K_1 (ml·cm^{-3}·min^{-3}): the rate constant of influx across BBB; k_2 (min^{-3}): the rate constant of efflux across BBB; k_3 (min^{-3}): the rate constant of transport from C_{ND} to C_S; k_4 (min^{-3}): the rate constant of transport from C_S to C_{ND}.

In each compartment, the changes in radioligand concentration can be described by the parameters related to the compartment. At equilibrium, there is no net change in radioligand concentration among each compartment and the outcome measures can be formulated by model parameters. For example, the following equations describe V_T in 1TCM and 2TCM,

$$\text{1TCM: } V_T = \frac{K_1}{k_2}, \tag{10}$$

$$\text{2TCM: } V_T = \frac{K_1}{k_2} \times (1 + \frac{k_3}{k_4}), \tag{11}$$

where K_1 (ml·cm^{-3}·min^{-3}) is the rate constant of influx across blood brain barrier (BBB), k_2 (min^{-3}) is the rate constant of efflux across BBB, k_3 (min^{-3}) is the rate constant of transport from C_{ND} to C_S and k_4 (min^{-3}) is the rate constant of transport from C_S to C_{ND}. Although it is possible to estimate several microparameters (e.g. K_1 to k_4) or macroparameters (e.g. V_{ND} or BP_{ND}) in the model, not all parameters may be reliably derived. The choice of suitable model structure and the availability of reliable parameters needs to be investigated specifically for each radioligand (Ichise *et al*, 2001; Slifstein and Laruelle, 2001).

1.3.2.2 Graphical modeling

The basis of graphical modeling is that, using a transformation of variables, there will be a linear relationship between transformed dependent and predictor variables after a certain time period following the radioligand injection. Linear regression analysis is applied to the linear part of the transformed data and the slope of the regression line will approximate the outcome measures (Ichise *et al*, 2001; Logan *et al*, 1990; Slifstein and Laruelle, 2001). Logan plot analysis (Logan *et al*, 1990) is a graphical method for reversible radioligand binding and the equation of the plot is as follows,

$$\frac{\int_0^t C_T(\tau)d\tau}{C_T(t)} = (V_T + Vol_P) \times \frac{\int_0^t C_P(\tau)d\tau}{C_T(t)} + \text{intercept}, \quad (12)$$

where Vol_P is the plasma volume in the tissue which might be ignored and V_T will equal the slope. The advantages of the Logan plot analysis are less computational demand than the iterative fitting process in compartmental modeling, and no assumptions of model configuration are needed as equation (12) can describe both the 1TCM and 2TCM (Logan *et al*, 1990; Slifstein and Laruelle, 2001). However, the contribution of Vol_P and the values of microparameters cannot be determined by the Logan plot analysis.

1.3.2.3 Reference tissue modeling

Both compartmental and graphical modeling require arterial input function ($C_P(t)$) which can be obtained from arterial blood sampling and related analyses to determine radioactivity and metabolite fractions. The need of arterial input function is one major limitation for the clinical applicability of quantitative PET imaging. Therefore, it is of great interest to develop methods to quantify PET outcome parameters that do not require measurement of an arterial input function. In case there exists a brain region devoid of target receptors, this region might serve as a reference region for quantification methods and negate the need of arterial input function. The model structures of two commonly used reference tissue models are displayed in Figure 2.

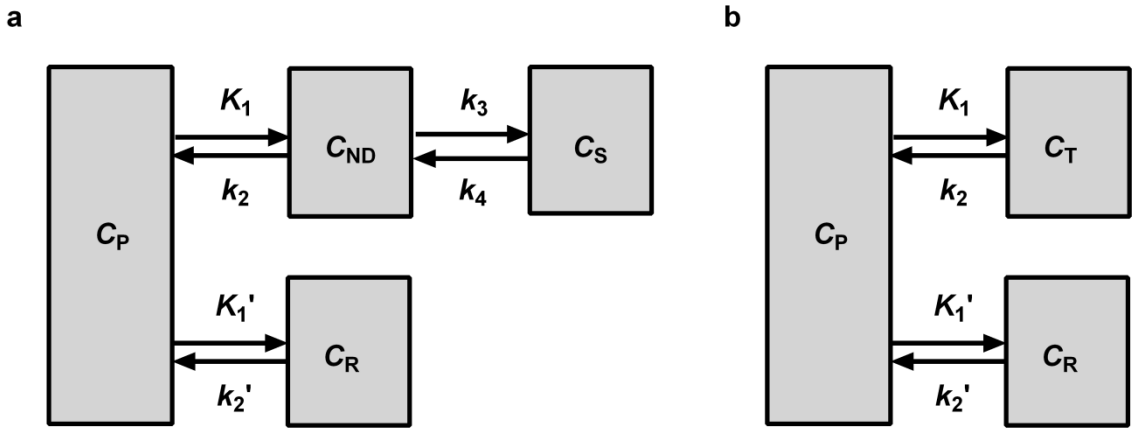

Figure 2. Model structures of two commonly used reference tissue models. (a) 2TCM for target region and 1TCM for reference region. (b) 1TCM for both target and reference regions. C_{ND}: concentration of nondisplaceable radioligand; C_P: plasma concentration of radioligand; C_R: tissue concentration of radioligand in the reference region; C_S: concentration of specific bound radioligand; C_T: total tissue concentration of radioligand; K_1 and K_1' ($ml \cdot cm^{-3} \cdot min^{-3}$): the rate constant of influx across BBB; k_2 and k_2' (min^{-3}): the rate constant of efflux across BBB; k_3 (min^{-3}): the rate constant of transport from C_{ND} to C_S; k_4 (min^{-3}): the rate constant of transport from C_S to C_{ND}.

In the model in which the target region and the reference region could be described adequately by the 2TCM and 1TCM, respectively (Figure 2a), assuming the concentration in reference region (C_R) is equal to C_{ND} and defining $R_1 = \frac{K_1}{K_1'}$, BP_{ND} can be derived from the model by determining 4 fitting parameters (R_1, k_2, k_3 and BP_{ND}), which is referred to as the

full reference tissue model (FRTM) (Hume *et al*, 1992; Lammertsma *et al*, 1996). The FRTM can be further simplified into the simplified reference tissue model (SRTM) if both target and reference regions can be described properly by the 1TCM (Figure 2b) and the 3 remaining fitting parameters (R_1, k_2 and BP_{ND}) in the model (Lammertsma and Hume, 1996). The operational equation of the SRTM is as follows,

$$C_T(t) = R_1 C_R(t) + \left\{ k_2 - \frac{R_1 k_2}{1 + BP_{ND}} \right\} C_R(t) \otimes e^{-\frac{k_2 t}{1 + BP_{ND}}}. \quad (13)$$

Moreover, the Logan plot analysis can also be adapted to use a reference region instead of an arterial input function as input. If equation (12) was applied to the reference region (C_R), an analytical expression for C_P (as a function of C_R) can be obtained. Then, the expression for C_P can be inserted back into equation (12) resulting in the following equation,

$$\frac{\int_0^t C_T(\tau)d\tau}{C_T(t)} = \text{DVR} \times \frac{\int_0^t C_R(\tau)d\tau + C_R(t) / k_2'}{C_T(t)} + \text{intercept}, \quad (14)$$

where DVR (distribution volume ratio) = $\frac{V_T}{V_{ND}} = BP_{ND} + 1$ and the described method is referred to as Logan reference tissue model (Loganref) (Logan *et al*, 1996).

1.3.2.4 Validation of reference tissue models

As described in 1.3.2.3, the reference tissue models are based on several assumptions (Hume *et al*, 1992; Lammertsma *et al*, 1996; Lammertsma and Hume, 1996). Therefore, for each radioligand, it is important to validate the application of reference tissue modeling by examination of the fulfillment of related assumptions and the potential bias of BP_{ND} values calculated by the reference tissue models (Sandiego *et al*, 2015; Zanderigo *et al*, 2013).

1.3.3 The equilibrium method

One of the main reasons for the need of kinetic modeling in the quantification of dynamic PET data is that the outcome measures of PET measurements (e.g. V_T or BP_{ND}) are defined under true equilibrium states that cannot be achieved following the bolus injection of radioligand (Slifstein and Laruelle, 2001). Alternatively, a protocol including a bolus and a constant infusion for injection of radioligand can be applied to achieve and sustain true equilibrium for a period of time (Carson, 2000; Carson *et al*, 1993; Slifstein and Laruelle, 2001). Using this method, V_T can be calculated directly from the tissue-to-plasma concentration ratio and BP_{ND} can be derived from the tissue concentration in the target and reference regions. However, the optimal bolus to infusion rate ratio of each radioligand should be determined on forehand to ensure that the binding reaches equilibrium within the time interval of the PET measurements (Carson, 2000; Martinez *et al*, 2003; Slifstein and Laruelle, 2001).

1.4 EVALUATING CHANGES IN THE CONCENTRATION OF ENDOGENOUS MOLECULES

1.4.1 The competition model

The application of PET imaging for the assessment of changes in the concentration of endogenous neurotransmitters was initially based on the competition model (Finnema *et al*, 2015c; Friedman *et al*, 1984; Ginovart, 2005; Laruelle, 2000; Paterson *et al*, 2010). The model hypothesized that the changes in neurotransmitter concentration induced by a challenge will alter the occupancy of endogenous neurotransmitters to the target receptor. As there is competition between neurotransmitter and radioligand for binding to the receptor, there will be a change in radioligand binding. As illustrated in Figure 3, according to the competition model, an increase in neurotransmitter concentration will decrease the binding of radioligand to the receptors and vice versa.

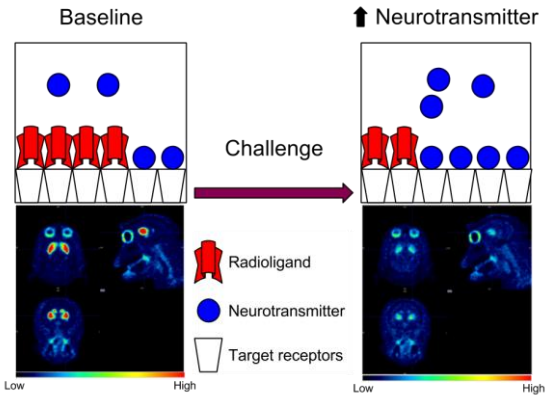

Figure 3. Schematic representation of the competition model and corresponding changes in radioligand binding.

1.4.2 Changes in BP_{ND} under the competition model

Following the principle of competitive inhibition, adding endogenous neurotransmitter into the system of radioligand binding will not affect B_{avail} but will increase the apparent K_D by a factor of $(1+ F_{NT}/K_{i\_NT})$, where F_{NT} is the basal neurotransmitter concentration and K_{i_NT} is the inhibition constant of the neurotransmitter for binding of the radioligand to the receptor (Farde *et al*, 1995; Narendran *et al*, 2004; Ross and Jackson, 1989). Therefore, the equation (8) of BP_{ND} (page 6) could be expanded to (Farde *et al*, 1995; Laruelle, 2000; Narendran *et al*, 2004; Paterson *et al*, 2010; Ross and Jackson, 1989)

$$BP_{ND\_baseline} = f_{ND} \times \frac{B_{avail}}{K_D \times (1+\frac{F_{NT}}{K_{i\_NT}})}. \quad (15)$$

After a drug challenge, based on the competition model, f_{ND}, B_{avail}, K_D, K_{i_NT} and F_{NT} remain the same. The influence of the changes in neurotransmitter concentration (ΔF_{NT}) on BP_{ND} can be described as the following equation (Farde *et al*, 1995; Narendran *et al*, 2004; Paterson *et al*, 2010; Ross and Jackson, 1989)

$$BP_{\mathrm{ND\_challenge}} = f_{\mathrm{ND}} \times \frac{B_{\mathrm{avail}}}{K_{\mathrm{D}} \times (1+\frac{F_{\mathrm{NT}}+\Delta F_{\mathrm{NT}}}{K_{\mathrm{i\_NT}}})}. \quad (16)$$

For evaluation of ΔF_{NT} induced by a drug challenge, the relative change in BP_{ND} (ΔBP_{ND}) is a common outcome measure. The definition of ΔBP_{ND} and its relationship to ΔF_{NT} can be described as (Paterson *et al*, 2010)

$$\Delta BP_{\mathrm{ND}} = \frac{BP_{\mathrm{ND\_challenge}} - BP_{\mathrm{ND\_baseline}}}{BP_{\mathrm{ND\_baseline}}} = \frac{-\Delta F_{\mathrm{NT}}}{K_{\mathrm{i\_NT}}+F_{\mathrm{NT}}+\Delta F_{\mathrm{NT}}}. \quad (17)$$

1.4.3 Availability of receptors

Since *BP* is a composite outcome measure of B_{avail} and K_{D}, in addition to the changes in apparent K_{D} as predicted by the competition model, potential changes in B_{avail} should also be considered when interpreting results of PET challenge experiments. There are several factors that might influence the B_{avail} for endogenous neurotransmitter or radioligand such as functional states of receptors and the cellular location of receptors (Abi-Dargham *et al*, 2000; Ginovart *et al*, 1997; Laruelle *et al*, 1997; Paterson *et al*, 2010).

1.4.3.1 Functional states of receptors

Based on the extended ternary complex model, the B_{avail} of GPCR might be partially determined by the functional states of the receptors (Paterson *et al*, 2010; Skinbjerg *et al*, 2010). The model hypothesizes that there are two functional state of the receptors, G protein-coupled and uncoupled (Finnema *et al*, 2010a; De Lean *et al*, 1980). Whereas agonists have high affinity to the functional G-protein coupled receptor and low affinity to the G-protein uncoupled receptor, antagonists have similar affinity to both states of the receptor. Therefore, neurotransmitters (being endogenous agonists) may more markedly compete with radioligand for binding to the high-affinity state receptor than to the low-affinity state receptor (Paterson *et al*, 2010; Skinbjerg *et al*, 2010). Accordingly, the relative low affinity of the endogenous agonist to the low-affinity state receptor decreases the sensitivity of the binding of antagonist radioligand to ΔF_{NT} (Narendran *et al*, 2004; Paterson *et al*, 2010).

1.4.3.2 Estimation of the ratio of high-affinity state receptors

Under the assumptions that [1] endogenous neurotransmitter mainly binds to the synaptic high-affinity state receptor (R_{HS}), [2] the non-synaptic high-affinity state receptor (R_{HNS}) is defined as the high-affinity state receptor that is not accessible by endogenous neurotransmitter due to compartmentalization or other factors, [3] agonist radioligand can bind to R_{HS} and R_{HNS} and [4] antagonist radioligand can bind to R_{HS}, R_{HNS} and the low-affinity state receptor (R_{L}) and [5] $B_{\mathrm{avail}} = R_{\mathrm{HS}} + R_{\mathrm{HNS}} + R_{\mathrm{L}}$, we can expand equation (15) to include the functional states of receptor, baseline occupancy of receptor by endogenous neurotransmitter and the non-synaptic distribution of receptor following the method proposed by Narendran (Narendran *et al*, 2004).

For an antagonist radioligand, the baseline BP_{ND} can be expressed as

$$BP_{ND\_anta\_baseline} = f_{ND} \times \left(\frac{R_{HS}}{K_{D\_anta} \times \left(1 + \frac{F_{NT}}{K_{i\_NT}}\right)} + \frac{R_{HNS} + R_L}{K_{D\_anta}} \right). \quad (18)$$

After a drug challenge, the BP_{ND} can be expressed as

$$BP_{ND\_anta\_challenge} = f_{ND} \times \left(\frac{R_{HS}}{K_{D\_anta} \times \left(1 + \frac{F_{NT} + \Delta F_{NT}}{K_{i\_NT}}\right)} + \frac{R_{HNS} + R_L}{K_{D\_anta}} \right). \quad (19)$$

For an agonist radioligand, the baseline BP_{ND} can be expressed as

$$BP_{ND\_ago\_baseline} = f_{ND} \times \left(\frac{R_{HS}}{K_{D\_ago} \times \left(1 + \frac{F_{NT}}{K_{i\_NT}}\right)} + \frac{R_{HNS}}{K_{D\_ago}} \right). \quad (20)$$

After a drug challenge, the BP_{ND} can be expressed as

$$BP_{ND\_ago\_challenge} = f_{ND} \times \left(\frac{R_{HS}}{K_{D\_ago} \times \left(1 + \frac{F_{NT} + \Delta F_{NT}}{K_{i\_NT}}\right)} + \frac{R_{HNS}}{K_{D\_ago}} \right). \quad (21)$$

Based on equations (18) to (21), the ratio of ΔBP_{ND_anta} to ΔBP_{ND_ago} can be expressed and reorganized as

$$\frac{\Delta BP_{ND\_anta}}{\Delta BP_{ND\_ago}} = \frac{R_{HS} + \left(1 + \frac{F_{NT}}{K_{i\_NT}}\right) \times R_{HNS}}{R_{HS} + \left(1 + \frac{F_{NT}}{K_{i\_NT}}\right) \times (R_{HNS} + R_L)}. \quad (22)$$

If $F_{NT} << K_{i\_NT}$, equation (22) can be simplified to

$$\frac{\Delta BP_{ND\_anta}}{\Delta BP_{ND\_ago}} = \frac{R_{HS} + R_{HNS}}{R_{HS} + R_{HNS} + R_L} = \frac{R_{HS} + R_{HNS}}{B_{avail}} = \text{the fraction of high affinity state receptors.} \quad (23)$$

1.4.4 Factors influencing the sensitivity of radioligand binding

It is worth noting that based on equation (17) (page 11), the ΔBP_{ND} can be much smaller than the ΔF_{NT}. For example, using the optimal values from preclinical studies (K_{i_NT} = 50 nM and F_{NT} = 3.9 nM), a 14-fold increase in 5-HT (ΔF_{NT} = 54.6 nM) will only induce around 50% decrease in BP_{ND} values of 5-HT_{1A} receptor radioligands (Paterson *et al*, 2010). Considering the relatively low sensitivity of ΔBP_{ND} when compared to ΔF_{NT}, it is important to choose an adequate radioligand for reliable detection of ΔF_{NT}.

1.4.4.1 Target related factors

According to the competition model and equation (17) (page 11), for the same neurotransmitter, the target receptor with lower K_{i_NT} value (higher NT affinity) will provide higher sensitivity to ΔF_{NT}. In addition, the target receptor with higher fraction in high-affinity state, lower fraction in non-synaptic location and lower fraction in intracellular compartment will also provide higher sensitivity to ΔF_{NT} because there will be smaller differences in receptor availability between neurotransmitter and radioligand.

1.4.4.2 Radioligand related factors

Under equilibrium conditions, ΔBP_{ND} will be independent of radioligand properties as based on the competition model and equation (17) (page 11). However, differences in dopamine sensitivity among different dopamine D_2 receptor (D_2R) radioligands did not support this hypothesis and a radioligand property explaining the different sensitivities could not be identified (Laruelle, 2000; Paterson *et al*, 2010). The different dopamine sensitivities might originate from the non-equilibrium states of PET measurements following drug challenges and in which dopamine concentrations change prominently during the PET measurement (Finnema *et al*, 2015c; Laruelle, 2000; Paterson *et al*, 2010). For example, one simulation study has reported that the dopamine sensitivity of radioligand binding will be higher if the rate of clearance from the brain (k_2) is faster (Endres and Carson, 1998).

Although some controversy existed, agonist radioligands were expected to be more sensitive to ΔF_{NT} than antagonist radioligands for the same target, as described in 1.4.3.1 (Finnema *et al*, 2015c; Paterson *et al*, 2010; Skinbjerg *et al*, 2010). The differences in dopamine sensitivity between agonist and antagonist radioligands for dopamine D_2/D_3 receptors have been observed in anesthetized NHPs (Gallezot *et al*, 2014b; Narendran *et al*, 2004; Seneca *et al*, 2006). On the other hand, one study in conscious NHPs has reported that there was similar sensitivity between agonist and antagonist radioligands and the authors attributed the observed difference in dopamine sensitivity in other studies to an anesthesia effect (Ohba *et al*, 2009). However, the difference in dopamine sensitivity has also been observed in conscious humans (Narendran *et al*, 2010; Shotbolt *et al*, 2012) and support a minimal effect of anesthesia on the difference in dopamine sensitivity between agonist and antagonist radioligands.

1.4.5 Evaluation of dopamine release by PET

The PET imaging paradigm enabling detection of ΔF_{NT} has been applied in a number of preclinical and clinical studies. Importantly, these studies have prominently improved our understanding of the role of the dopamine system in brain functions (Finnema *et al*, 2015c; Laruelle, 2000). For example, compared to healthy controls, blunted dopamine release induced by amphetamine has been observed in addiction patients while their baseline radioligand binding was similar to that in healthy controls (Volkow *et al*, 2011). Similarly, the effect size of differentiating schizophrenic patients from healthy controls was larger when using the dopamine release paradigm than imaging dopamine receptors themselves (Howes *et al*, 2012). Moreover, the level of dopamine release might relate to behavior or clinical outcomes and provide new insights on the pathophysiology of neuropsychiatric disorders (Nutt *et al*, 2015). Therefore, it is of great interest to extend the PET imaging paradigm to evaluate ΔF_{NT} for targets other than dopamine, and 5-HT is one of the promising targets.

1.5 THE SEROTONIN SYSTEM

1.5.1 Overview of serotonin system

The 5-HT system has important roles in the regulation of basic physiological functions, as well as in higher brain functions such as emotion and cognition (Chou *et al*, 2012; Cools *et al*, 2011; Lesch and Waider, 2012; Selvaraj *et al*, 2014). Since 5-HT cannot pass the BBB, the synthesis of 5-HT occurs via a two-step reaction in serotonergic neurons. First, *L*-tryptophan is hydroxylated into 5-hydroxytryptophan (5-HTP) by tryptophan hydroxylase. 5-HTP is then decarboxylated into 5-HT via the enzyme aromatic *L*-amino-acid decarboxylase (AADC). Moreover, the enzymes monoamine oxidase and aldehyde dehydrogenase degrade 5-HT into an inactive metabolite, 5-hydroxyindoleacetic acid (van Donkelaar *et al*, 2011; Turner *et al*, 2006).

The cell bodies of the serotonergic neurons are mainly concentrated in the raphe nuclei (RN) and project to almost the entire brain, including cerebral cortex, limbic regions, basal ganglia and subcortical structures (Hornung, 2003; Lechin *et al*, 2006; Steinbusch, 1981). In the projection regions, 5-HT is released from the presynaptic serotonergic neurons and binds to a number of subtypes of presynaptic and/or postsynaptic 5-HT receptors that can regulate different brain functions. Therefore, for maintaining normal brain functions, it is critical to maintain adequate regional 5-HT concentrations by modulation of the release and re-uptake of 5-HT (Best *et al*, 2010; Piñeyro and Blier, 1999; Wong-Lin *et al*, 2012). Several factors might contribute to the regulation of 5-HT concentrations such as neuronal firing in the 5-HT neurons (Gartside *et al*, 2000), 5-HT autoreceptors (Piñeyro and Blier, 1999) and serotonin transporter (5-HTT) (Kristensen *et al*, 2011). It is worth noting that there might be different mechanisms and patterns in the regulation of 5-HT concentrations between RN and projection regions (Adell *et al*, 2002; Lanzenberger *et al*, 2012)

1.5.2 The subtypes of serotonin receptors and serotonin transporter

Hitherto, fourteen 5-HT receptor subtypes have been identified in human and they have been grouped into seven families (5-HT_1 to 5-HT_7) based on their structural, functional and pharmacological features (Barnes and Sharp, 1999). Thirteen 5-HT receptors are G-protein coupled and the 5-HT_3 receptor is the only ion channel linked 5-HT receptor (Hannon and Hoyer, 2008). In addition, the 5-HTT is also distributed both in RN and projection regions (Mantere *et al*, 2002; Varnäs *et al*, 2004).

1.5.2.1 The serotonin 1B receptor

The density of the 5-HT_{1B} receptor has been reported to be highest in the globus pallidus, substantia nigra (SN) and occipital cortex; intermediate in the striatum and other neocortical regions; low in the amygdala and hippocampus as well as negligible in the cerebellar cortex (Varnäs *et al*, 2004). The 5-HT_{1B} receptor acts as a presynaptic autoreceptor on serotonergic axon terminals or as a postsynaptic heteroreceptor on axon terminals of non-

serotonergic neurons. Therefore, the 5-HT_{1B} receptor has been suggested to play an important role in the regulation of the release of 5-HT and several other neurotransmitters such as GABA, glutamate and acetylcholine (Ruf and Bhagwagar, 2009; Sari, 2004). Moreover, the 5-HT_{1B} receptor has been implicated in the pathophysiology of several neuropsychiatric disorders, such as depression, anxiety and substance abuse (Ruf and Bhagwagar, 2009; Sari, 2004; Svenningsson, 2006).

1.5.2.2 The serotonin 2A receptor

The 5-HT_{2A} receptor has been reported to mainly distribute in the neocortical regions, with low densities in the hippocampus, basal ganglia and thalamus and negligible density in the cerebellar cortex (Hall *et al*, 2000; Varnäs *et al*, 2004). The 5-HT_{2A} receptor is one of the main modulators of excitatory neurotransmission via interactions with the monoaminergic, GABAergic and glutamatergic systems (Guiard and DiGiovanni, 2015; Millan *et al*, 2008). Dysfunction of 5-HT_{2A} receptors has been reported in several neuropsychiatric disorders, including depression and schizophrenia (Savitz and Drevets, 2013; Selvaraj *et al*, 2014).

Table 2. Summary of the 5-HT targets with PET radioligands examined in primates

Targets	K_i (nM)*	Distribution	High affinity state	Extrasynaptic	Regulation
5-HT_{1A}	0.3–166; 0.2–0.8	RN (autoreceptors); HIPP, cortex (heteroreceptors) (Lanfumey and Hamon, 2000; Riad *et al*, 2000; Varnäs *et al*, 2004)	4–25% (Clawges *et al*, 1997; Watson *et al*, 2000)	High (Lanfumey and Hamon, 2000; Riad *et al*, 2000)	Internalization (autoreceptors) (Bouaziz *et al*, 2014; Riad *et al*, 2001)
5-HT_{1B}	0.6–38; 1–40	Basal ganglia, cortex (autoreceptors and heteroreceptors) (Sari, 2004; Varnäs *et al*, 2004)	31–85% (Clawges *et al*, 1997; Grånäs *et al*, 2001; Newman-Tancredi *et al*, 2003)	High (Belenky and Pickard, 2001; Riad *et al*, 2000; Sari *et al*, 1997, 1999)	Internalization (Carrel *et al*, 2011; Chen *et al*, 2009; Liebmann *et al*, 2012)
5-HT_{2A}	8–3171; 4–1000	Cortex, HIPP, basal ganglia (Nichols and Nichols, 2008; Varnäs *et al*, 2004)	4–79% (Fitzgerald *et al*, 1999; López-Giménez *et al*, 2001, 2013)	High (Jansson *et al*, 2001; Miner *et al*, 2003; Nichols and Nichols, 2008)	Internalization (Bhattacharyya *et al*, 2002; Raote *et al*, 2013; Schmid *et al*, 2008)
5-HT_4	126–316; 100–1259	Basal ganglia, cortex, HIPP (Bockaert *et al*, 2008; Nichols and Nichols, 2008; Varnäs *et al*, 2003, 2004)	17% (Mikami *et al*, 2008)	High (Bockaert *et al*, 2008; Vilaró *et al*, 2005)	Internalization (Mnie-Filali *et al*, 2010; Pindon *et al*, 2005)
5-HT_6	56–132; 32–159	Striatum, AMYG, HIPP, cortex (Gérard *et al*, 1997; Roberts *et al*, 2002; Woolley *et al*, 2004)	?	High (Brailov *et al*, 2000; Gérard *et al*, 1997)	possible internalization (Brailov *et al*, 2000; Dayer *et al*, 2015; Kim *et al*, 2014)
5-HTT	17–552 (rat); No data	RN, striatum, AMYG (Kish *et al*, 2005; Varnäs *et al*, 2004)	Not applicable	High (Miner *et al*, 2000; Zhou *et al*, 1998)	Internalization (Chanrion *et al*, 2007; Jørgensen *et al*, 2014; Lau *et al*, 2008)

*The values of K_i (inhibition constant at equilibrium) were extracted from the data for cloned or native human receptors in the National Institute of Mental Health's Psychoactive Drug Screening Program, Contract # HHSN-271–2013-00017-C (NIMH PDSP) (upper row) and from the International Union of Basic and Clinical Pharmacology (IUPHAR) GPCR database (lower row).

AMYG: Amygdala; HIPP: Hippocampus; RN: Raphe nucleus.

1.5.3 Current states of the 5-HT radioligands

Of the fourteen 5-HT receptor subtypes, PET radioligands have been developed and evaluated in the primate for five subtypes (5-HT_{1A}, 5-HT_{1B}, 5-HT_{2A}, 5-HT_4, and 5-HT_6 receptors) as well as for the 5-HTT (Paterson *et al*, 2013). The properties of these six targets are summarized in Table 2 (page 15). Except for the 5-HT_6 receptor, radioligands for the other five targets have been examined for 5-HT sensitivity in the primate brain (Finnema *et al*, 2015c; Paterson *et al*, 2010; Tyacke and Nutt, 2015).

1.5.4 Increasing 5-HT concentration via different mechanisms

The available 5-HT concentration enhancers have different mechanisms of action (Paterson et al., 2010; Rothman and Baumann, 2002; Turner et al., 2006). Selective serotonin re-uptake inhibitors (SSRIs) bind to the 5-HTT and block the re-uptake of 5-HT from the synapse. Substrate-type releasers also bind to the 5-HTT and are then transported into the presynaptic nerve terminal. Amphetamine is a prototypic substrate of monoamine transporters and there are a variety of substituted amphetamines, such as fenfluramine and 3,4-methylenedioxymethamphetamine (MDMA) that release 5-HT. These 5-HT releasers might increase the endogenous 5-HT concentration by competitive inhibition of 5-HT uptake, reversing transport of 5-HT, transporter trafficking, or inhibition of monoamine oxidase (Fleckenstein et al., 2007; Heal et al., 2013; Rothman and Baumann, 2002). On the other hand, the 5-HT precursor 5-HTP increases the endogenous 5-HT concentration by facilitating the 5-HT synthesis and thereby has a more limited effect on the concentration of other monoamines (Baumann *et al*, 2011; Turner *et al*, 2006).

However, most of these pharmacological challenges are difficult to translate into clinical 5-HT release studies (Finnema *et al*, 2015c; Paterson *et al*, 2010). For example, although fenfluramine has provided the largest reductions in radioligand binding in the primate brain (Finnema *et al*, 2010b, 2012), it has been removed from the market because of cardiovascular toxicity (Hutcheson *et al*, 2011; Montani *et al*, 2013). Clinically relevant doses of SSRI have not provided a method suitable for measurement of acute 5-HT release (Nord *et al*, 2013; Pinborg *et al*, 2012; Selvaraj *et al*, 2012). Therefore, a pharmacological challenge suitable to examine the changes in the endogenous 5-HT concentration in the human brain is still warranted.

1.5.5 Evaluating changes in 5-HT concentration by PET in primates

The results of the evaluation of the 5-HT sensitivity of PET radioligands for 5-HT_{1A} receptors, 5-HT_{1B} receptors, 5-HT_{2A} receptors, 5-HT_4 receptors or 5-HTT in healthy primates are summarized in Tables 3–6 (Finnema *et al*, 2015c; Paterson *et al*, 2010).

For the 5-HT_{1A} receptor antagonist radioligands (Table 3), it has been reported that SSRIs at high (paroxetine) and clinically relevant doses (fluoxetine) could significantly decrease [^{18}F]FPWAY and [^{18}F]MPPF BP_{ND} in dorsal raphe nucleus (DRN) in NHP (Giovacchini *et al*, 2005) and human (Sibon *et al*, 2008), respectively. Interestingly, the cortical [^{18}F]FPWAY BP_{ND} in the NHP brain also significantly increased after administration

of paroxetine (Giovacchini *et al*, 2005). For [^{11}C]CUMI-101, the only 5-HT$_{1A}$ receptor agonist radioligand, one study has reported that both fenfluramine and high doses of SSRI (citalopram) significantly decreased BP_{ND} values both in the DRN and projection regions in the NHP brain (Milak *et al*, 2011). However, another two human studies have reported either no changes (Pinborg *et al*, 2012) or increased BP_{ND} values in the projection regions (Selvaraj *et al*, 2012) induced by clinically relevant doses of citalopram.

Table 3. Summary of studies evaluating 5-HT sensitivity of 5-HT$_{1A}$ receptor radioligands in healthy primates

Radioligands	Challenge	Species	Outcome	Effects
[^{11}C]CUMI-101 (Milak *et al*, 2011)	Citalopram (2 and 4 mg/kg i.v., 30 min prior–?)	Monkey (n = 3 and 3)	OC plot	↓15 % and ↓30 % (both DRN and projection regions)*
[^{11}C]CUMI-101 (Milak *et al*, 2011)	Fenfluramine (2.5 mg/kg i.v., 30 min prior–?)	Monkey (n = 3)	OC plot	↓24 % (both DRN and projection regions)*
[^{11}C]CUMI-101 (Pinborg *et al*, 2012)	Citalopram (0.15 mg/kg i.v., 30 min prior–30 min post)	Human (n = 6)	BP_{ND}	NS
[^{11}C]CUMI-101 (Selvaraj *et al*, 2012)	Citalopram (10 mg i.v., 45–15 min prior)	Human (n = 13)	OC plot	↑14 % projection regions#
			BP_{ND}	↑7 % projection regions #
[^{11}C]WAY100635 (Rabiner *et al*, 2002)	Tryptophan depletion/ infusion	Human (n = 4/4)	BP_{ND}	NS
[^{18}F]FPWAY (Giovacchini *et al*, 2005)	Paroxetine (5 mg/kg i.v., 90 min post)	Monkey (n = 4)	BP_P / BP_{ND}	NS / ↑ 7–13% cortex# and ↓ 8–27% DRN*
[^{18}F]MPPF (Udo De Haes *et al*, 2002)	Tryptophan depletion/ infusion	Human (n = 6)	BP_{ND}	NS
[^{18}F]MPPF (Udo de Haes *et al*, 2006)	Fenfluramine (10 mg/kg i.v., 90–130 min post)	Monkey (n = 5, awake)	BP_{ND}	NS
[^{18}F]MPPF (Sibon *et al*, 2008)	Fluoxetine (20 mg p.o., 5 h prior)	Human (n = 8)	BP_{ND}	↓ 44% DRN*

*Consistent with the competition model; #Opposite to the direction predicted by the competition model.
DRN: Dorsal raphe nucleus; OC plot: Occupancy plot, the direction of effect was adjusted to be consistent with BP_{ND}.

For the 5-HT$_{1B}$ receptor radioligands (Table 4) (page 18), several studies using different radioligands, challenge drugs and quantification methods have consistently reported that fenfluramine, amphetamine and high doses of SSRIs (citalopram and escitalopram) could significantly decrease BP_{ND} values (Cosgrove *et al*, 2011; Finnema *et al*, 2010b, 2012; Nord *et al*, 2013; Ridler *et al*, 2011; Yamanaka *et al*, 2014). Similar to the PET studies using 5-HT$_{1A}$ receptor radioligands, a clinically relevant dose of escitalopram has been reported to significantly increase BP_{ND} values in the projection regions in the human brain (Nord *et al*, 2013).

One possible explanation for the unexpected effects of SSRIs at clinically relevant doses on radioligand binding is the modulation of 5-HT release by the autoreceptors in DRN. The acute increases in 5-HT concentration induced by SSRIs might stimulate the autoreceptors in DRN that then inhibit the 5-HT release in the projection regions. Consequently, the net effects of SSRIs might be acute decreases in 5-HT concentrations in the projection regions (Giovacchini *et al*, 2005; Milak *et al*, 2011; Nord *et al*, 2013). Moreover, this inhibitory effect might be overcome by higher levels of 5-HT release induced

by high doses of fenfluramine or SSRIs (David *et al*, 2003; Finnema *et al*, 2015a, 2015c; Invernizzi *et al*, 1992; Nord *et al*, 2013). Therefore, these unexpected increases in BP_{ND} values might still be interpreted under the framework of the competition model. Furthermore, these observations also support the assumption that the inhibition of 5-HT release from autoreceptors in the DRN is one of the factors contributing to the delayed onset of clinical efficacy of SSRIs (Blier and de Montigny, 1994; Sanchez *et al*, 2015).

Table 4. Summary of studies evaluating 5-HT sensitivity of 5-HT_{1B} receptor radioligands in healthy primates

Radioligands	Challenge	Species	Outcome	Effects
[^{11}C]AZ10419369 (Finnema *et al*, 2010b)	Fenfluramine (1.0 and 5.0 mg/kg i.v., 15–20 min post)	Monkey (n = 3)	Specific biding ratio	↓ 27 and 50%$^{*\$}$
[^{11}C]AZ10419369 (Finnema *et al*, 2012)	Fenfluramine (1.0 and 5.0 mg/kg i.v., 80–85 min post)	Monkey (n = 3)	BP_{ND}	↓ 12 and 33%$^{*\$}$
[^{11}C]AZ10419369 (Finnema *et al*, 2012)	Fenfluramine (5.0 mg/kg i.v., 30–25 min prior)	Monkey (n = 3)	BP_{ND}	↓ 34%$^{*\$}$
[^{11}C]AZ10419369 (Nord *et al*, 2013)	Escitalopram (2.0 mg/kg i.v., 45–15 min prior)	Monkey (n = 7)	BP_{ND}	↓ 11–25% (DRN)*
[^{11}C]AZ10419369 (Nord *et al*, 2013)	Escitalopram (20 mg p.o., 3 h prior)	Human (n = 9)	BP_{ND}	↑ 5% cortex$^{\#}$
[^{11}C]AZ10419369 (Yamanaka *et al*, 2014)	Fenfluramine (5.0 mg/kg i.v., 15 min prior–?)	Monkey (n = 4, awake)	BP_{ND}	↓22–41%*
[^{11}C]AZ10419369 (Yamanaka *et al*, 2014)	Fenfluramine (5.0 mg/kg i.v., 15 min prior–?) + continuous infusion of subanesthetic dose of ketamine	Monkey (n = 4, awake)	BP_{ND}	↓20–38%*
[^{11}C]P943 (Ridler *et al*, 2011)	Amphetamine (1 mg/kg i.v., prior? for 5 min)	Monkey (n = 1)	OC plot	↓25%$^{*\$}$
[^{11}C]P943 (Ridler *et al*, 2011)	Citalopram (4 mg/kg i.v., prior? for 10 min)	Monkey (n = 2)	OC plot	↓9–24%$^{*\$}$
[^{11}C]P943 (Ridler *et al*, 2011)	Fenfluramine (0.8 and 2.5 mg/kg i.v., prior ? for 10 min)	Monkey (n = 2)	OC plot	↓5–20% and ↓39–41%$^{*\$}$
[^{11}C]P943 (Cosgrove *et al*, 2011)	Fenfluramine (1 mg/kg i.v., 5 min prior–?)	Monkey (n = 2)	OC plot	↓25–29%$^{*\$}$
[^{11}C]P943 (Cosgrove *et al*, 2011)	Fenfluramine (5 mg/kg i.v., 75–70 min post)	Monkey (n = 1)	OC plot	↓42%$^{*\$}$

*Consistent with the competition model; $^{\#}$Opposite to the direction predicted by the competition model;
$^{\$}$No statistical analyses were reported.
DRN: Dorsal raphe nucleus; OC plot: Occupancy plot, the direction of effect was adjusted to be consistent with BP_{ND}.

For the 5-HT_{2A} receptor antagonist radioligands (Table 5), one study has reported that fenfluramine significantly decreased [^{18}F]altanserin binding in the human brain (Quednow *et al*, 2012). Tryptophan depletion which results in deceases in the 5-HT concentration has been reported to decrease [^{18}F]setoperone and [^{11}C]MDL100907 BP_{ND} in two human studies (Talbot *et al*, 2012; Yatham *et al*, 2001). The mechanism for these paradoxical effects was unclear and acute downregulation of the 5-HT_{2A} receptor might be the cause (Gray and Roth, 2001; Talbot *et al*, 2012; Yatham *et al*, 2001). Furthermore, the binding of [^{11}C]Cimbi-36, a novel 5-HT_{2A} receptor agonist radioligand has been characterized in the primate brain (Ettrup *et al*, 2014, 2016; Finnema *et al*, 2014). One recent study demonstrated that [^{11}C]Cimbi-36 binding was sensitive to 4- to 11-fold increases in 5-HT concentration in the pig brain (Jørgensen et al., 2016). Therefore, [^{11}C]Cimbi-36 might be a promising radioligand for the detection of increases in 5-HT concentration in the living primate brain.

Table 5. Summary of studies evaluating 5-HT sensitivity of 5-HT_{2A} receptor radioligands in healthy primates

Radioligands	Challenge	Species	Outcome	Effects
[^{11}C]MDL100907 (Talbot *et al*, 2012)	Tryptophan depletion	Human (n = 10)	BP_{ND}	↓ 8–20%[#]
[^{18}F]altanserin (Pinborg *et al*, 2004)	Citalopram (0.25 mg/kg i.v., 1 h post for 20 min) + pindolol pretreatment	Human (n = 7)	BP_P	NS
[^{18}F]altanserin (Matusch *et al*, 2007)	Ketamine (0.05 mg/kg i.v., 2 h post + 0.2 mg/kg/h infusion)	Human (n = 3)	BP_P	NS
[^{18}F]altanserin (Quednow *et al*, 2012)	Dexfenfluramine (40 and 60 mg p.o., 2 h prior)	Human (n = 6 and 7)	V_T	↓14–16%[*]
			BP_P	↓~ 17%[*]
[^{18}F]deutero-altanserin (Staley *et al*, 2001)	Fenfluramine (1.0 and 1.5 mg/kg i.v., 6 h post)	Monkey (n = 2)	Uptake	NS[$]
[^{18}F]setoperone (Meyer *et al*, 1999)	Paroxetine (20 mg p.o., 4.5 h prior)	Human (n = 5)	BP_{ND}	NS
[^{18}F]setoperone (Yatham *et al*, 2001)	Tryptophan depletion	Human (n = 10)	BP_{ND}	↓ 8%[#]

[*]Consistent with the competition model; [#]Opposite to the direction predicted by the competition model; [$]No statistical analyses were reported.

For studies evaluating the 5-HT sensitivity of 5-HTT radioligands (Table 6), one study has reported decreased BP_{ND} values after administration of 5-HTP which increased 5-HT concentration in awake monkeys (Yamamoto *et al*, 2007). Decreased V_T values in thalamus but no change in BP_{ND} values after administration of tranylcypromine which increased 5-HT concentration has been reported in another study in anesthetized monkeys (Lundquist *et al*, 2007). Decreased radioligand binding after tryptophan depletion has been observed in one NHP study (Milak *et al*, 2005), although no significant changes after tryptophan depletion have been observed in two human studies (Praschak-Rieder *et al*, 2005; Talbot *et al*, 2005). Trafficking (internalization) of 5-HTT after 5-HT depletion has been proposed to explain these paradoxical effects (Milak *et al*, 2005). Moreover, the only study using a 5-HT_4 radioligand reported no effect of a clinically relevant dose of citalopram on BP_{ND} values (Marner *et al*, 2010) (Table 6).

Table 6. Summary of studies evaluating 5-HT sensitivity of 5-HTT and 5-HT_4 receptor radioligands ([^{11}C]-DASB and [^{11}C]-SB207145, respectively) in healthy primates

Radioligands	Challenge	Species	Outcome	Effects
[^{11}C]DASB (Milak *et al*, 2005)	Tryptophan depletion	Monkey (n = 2, 18 scans)	BP_P	↓27–33%[#]
[^{11}C]DASB (Praschak-Rieder *et al*, 2005)	Tryptophan depletion	Human (n = 14)	BP_{ND}	NS
[^{11}C]DASB (Talbot *et al*, 2005)	Tryptophan depletion	Human (n = 8)	V_T / BP_P / BP_{ND}	NS
[^{11}C]DASB (Lundquist *et al*, 2007)	Tranylcypromine (0.2 and 2 mg/kg i.v., 1 h prior for 3–5 min)	Monkey (n = 3)	V_T	NS and ↓30% thalamus[*]
			BP_{ND}	NS and NS
[^{11}C]DASB (Yamamoto *et al*, 2007)	5-HTP (20 mg/kg i.v., 30 min prior–?)	Monkey (n = 5, awake)	BP_{ND}	↓35–45% striatum[*]
[^{11}C]SB207145 (Marner *et al*, 2010)	Citalopram (0.25 mg/kg i.v., 30 min prior–30 min post) + pindolol pretreatment	Human (n = 6 and 7)	BP_{ND}	NS

[*]Consistent with the competition model; [#]Opposite to the direction predicted by the competition model.

1.5.6 Vortioxetine

Vortioxetine is a novel multimodal antidepressant which has been approved for the treatment of major depressive disorder (MDD) in the US and EU since 2013 (Garnock-Jones, 2014; Sanchez *et al*, 2015). In addition to 5-HTT inhibition, vortioxetine is a 5-HT_3, 5-HT_7 and 5-HT_{1D} receptor antagonist, 5-HT_{1B} receptor partial agonist and 5-HT_{1A} receptor agonist (Bang-Andersen *et al*, 2011; Mørk *et al*, 2012; Sanchez *et al*, 2015). Rodent studies have reported that vortioxetine induced larger increases in 5-HT concentration than SSRIs and achieved antidepressant effects by direct modulation of several subtypes of 5-HT receptors (du Jardin *et al*, 2014; Pehrson *et al*, 2013; Sanchez *et al*, 2015). Thus, in rodents the mechanisms of action of vortioxetine differ from SSRIs. It remains to be seen whether similar differences in mechanisms of action translate into human. Species differences in the binding profile of vortioxetine to some 5-HT receptor subtypes may exist, e.g., higher affinity for 5-HT_{1B} and 5-HT_{1D} receptors and lower affinity for 5-HT_{1A} and 5-HT_7 receptors for the rat than for the recombinant human receptors (Sanchez *et al*, 2015). It is therefore important as a next step to evaluate the mechanisms of action of vortioxetine in the primate brain. Moreover, although occupancy of vortioxetine on the 5-HT_{1B} receptor has been observed in rats (30–45% at doses with 70–85% 5-HTT occupancy) (Mørk *et al*, 2012; Pehrson *et al*, 2013), whether vortioxetine significantly binds to the 5-HT_{1B} receptor at clinically relevant doses in the primate brain remained unclear. Considering the important role of 5-HT_{1B} receptor in depression (Ruf and Bhagwagar, 2009; Sari, 2004; Svenningsson, 2006), it is warranted to examine the engagement of vortioxetine on the 5-HT_{1B} receptor in the primate brain.

1.6 CYCLIC AMP AND PDE10A

1.6.1 Overview of cAMP and PDE

The cAMP is an intracellular second messenger that plays an important role in multiple neuronal and physiological functions, e.g. learning, memory, mood and neurodegeneration (Beavo and Brunton, 2002; Millar *et al*, 2005; Pierre *et al*, 2009). A number of methods have been developed for measuring cAMP concentration in living cells, such as genetically-encoded fluorescence or bioluminescence resonance energy transfer (Paramonov *et al*, 2015). However, it is currently not possible to monitor cAMP concentration in the living human brain and a non-invasive imaging approach could be useful for this purpose.

Although there is no available PET radioligand for imaging cAMP *in vivo* directly, there have been several radioligands targeting the downstream effectors of cAMP, especially for phosphodiesterases (PDEs) (Finnema *et al*, 2015c; Gunn *et al*, 2015; Holland *et al*, 2013). PDEs modulate the function of cAMP and/or 3',5'-cyclic guanosine monophosphate (cGMP) by catabolizing these signaling messengers (Conti and Beavo, 2007; Maurice *et al*, 2014). The close and direct interactions between cAMP and PDEs suggest that PDEs are potential PET imaging targets for detection of changes in cAMP concentration. There are 11 families of PDEs, and radioligands have been developed and validated in the primate brain for PDE4

and PDE10A (Conti and Beavo, 2007; Holland *et al*, 2013; Maurice *et al*, 2014; Schröder *et al*, 2016).

Several studies have demonstrated that the binding of [^{11}C]-(*R*)-rolipram, a PDE4 radioligand, was sensitive to alterations in cAMP concentration in the primate brain (Harada *et al*, 2002; Tsukada *et al*, 2001). Notably, the direction of changes in [^{11}C]-(*R*)-rolipram binding were inconsistent with the competition model. The cAMP induced alterations in PDE4 activity and the affinity of cAMP and [^{11}C]-(*R*)-rolipram to PDE4 have been suggested to be the cause of these unexpected effects (Itoh *et al*, 2010). Currently, [^{11}C]-(*R*)-rolipram binding is being used as an index of PDE4 activity (Fujita *et al*, 2017).

1.6.2 The PDE10A system

PDE10A can break down both cAMP and cGMP but its affinity for cAMP is much higher than that for cGMP (Fujishige *et al*, 1999; Jäger *et al*, 2012; Soderling *et al*, 1999). PDE10A is one of the major PDEs in the striatum (Russwurm *et al*, 2015). There might be a competition between radioligand and cAMP for binding to the catalytic domain of PDE10A. Furthermore, striatal PDE10A is almost exclusively located in GABAergic medium spiny neurons and projects to the substantia nigra (SN) and globus pallidus via the striatonigral and the striatopallidal pathway, respectively (Coskran *et al*, 2006; Seeger *et al*, 2003). These characteristics suggest that PDE10A is a promising target for detecting *in vivo* alterations in cAMP concentration in striatum and related projection regions.

It is worth noting that binding of cAMP to the GAF-B domain of PDE10A might influence the affinity of cAMP and radioligand to the catalytic domain (Jäger *et al*, 2012; Ooms *et al*, 2016; Russwurm *et al*, 2015). One recent PET study in rodents has reported that striatal binding of the PDE10A radioligand [^{18}F]JNJ42259152 was increased after acute elevations in cAMP concentration by PDE4 or PDE2 inhibition, opposite of what would be expected based on the competition model (Ooms *et al*, 2016). These changes might originate from increased affinity of [^{18}F]JNJ42259152 to PDE10A induced by elevations in cAMP concentration. As PDE10A has been proposed to be a novel target for several neuropsychiatric disorders and a growing number of PET studies have evaluated PDE10A binding in patients (Bodén *et al*, 2017; Marques *et al*, 2016), it is important to evaluate if similar effect of alterations in cAMP concentration on PDE10A radioligand binding exists in the primate brain.

1.6.3 Interaction between dopamine and PDE10A system

The postsynaptic dopamine receptors in striatal medium spiny neurons segregated into the striatonigral pathway and the striatopallidal pathway where dopamine D_1 receptor (D_1R) and D_2R are the dominant receptors, respectively (Calabresi *et al*, 2014; Nishi *et al*, 2011). The D_1R like receptors (dopamine D_1 and D_5 receptors) are coupled to $G_{s/olf}$ proteins that stimulate adenylyl cyclase and increase cAMP production. The D_2R like receptors (dopamine D_2, D_3 and D_4 receptors) are coupled to $G_{i/o}$ proteins that inhibit adenylyl cyclase (Kelly *et al*, 2007; Nishi *et al*, 2011). Therefore, D_1R agonism and/or D_2R antagonism will increase

cAMP concentrations and D_1R antagonism and/or D_2R agonism will decrease cAMP concentrations.

1.6.4 Current status of PDE10A radioligands

Numerous potential PET radioligands for imaging PDE10A have been developed and several have been examined in the NHP or human brain (Barret *et al*, 2014; Celen *et al*, 2013; Hwang *et al*, 2014, 2015; Kehler *et al*, 2014; Van Laere *et al*, 2013; Lin *et al*, 2015; Liu *et al*, 2015; Niccolini *et al*, 2015; Plisson *et al*, 2011, 2014; Takano *et al*, 2015). Most of these radioligands provide adequate target-to-background signal for the striatum and globus pallidus, but so far, radioligand binding in the SN has been examined only for [^{18}F]JNJ-42259152 and [^{11}C]IMA107. Both studies reported BP_{ND} values of approximately 0.5 for SN in healthy human subjects with corresponding striatal BP_{ND} values of 3.5 and 2.2, respectively (Van Laere *et al*, 2013; Niccolini *et al*, 2015). This low BP_{ND} value might limit the application of these radioligands for quantitative examinations of PDE10A binding in SN (Laruelle *et al*, 2003). Considering that the SN is a key nucleus in relation to the basal ganglia (Perez-Costas *et al*, 2010), and that regional differences in PDE10A functioning may be a part of the pathophysiology of neuropsychiatric disorders (Charych *et al*, 2010; Giorgi *et al*, 2011; Nishi *et al*, 2011), it is important to develop a PET methodology enabling quantification of PDE10A binding in the SN of the primate brain.

[^{11}C]Lu AE92686 is a recently developed radioligand with high affinity for PDE10A and an evaluation of the radioligand in humans has previously been reported (Kehler *et al*, 2014). The characteristics of this radioligand were promising, with striatal BP_{ND} value around 7.5 which is higher than those reported for other PDE10A radioligands (typical range: 2–5) (Barret *et al*, 2014; Celen *et al*, 2013; Hwang *et al*, 2014, 2015; Kehler *et al*, 2014; Van Laere *et al*, 2013; Lin *et al*, 2015; Liu *et al*, 2015; Niccolini *et al*, 2015; Plisson *et al*, 2011, 2014; Takano *et al*, 2015). Preliminary examination of [^{11}C]Lu AE92686 in cynomolgus monkeys has suggested that [^{11}C]Lu AE92686 binding is high in the striatum (BP_{ND} around 6.5) (Kehler *et al*, 2014). However, the initial study in monkeys did not include a full kinetic evaluation of [^{11}C]Lu AE92686 or examination of binding in the SN. Accordingly, further characterization of the binding properties of [^{11}C]Lu AE92686 and the sensitivity of [^{11}C]Lu AE92686 binding to changes in cAMP concentration in the primate brain were warranted.

2 AIMS

The general aim of the thesis work was to develop and implement novel PET imaging paradigms suitable for research and drug development in psychiatry. The work was carried out in nonhuman primates with the intention to prepare for future human applications.

The specific aims of the thesis work were as below:

1. The first specific aim was to evaluate the sensitivity of the recently developed radioligands [^{11}C]Cimbi-36 and [^{11}C]AZ10419369 for changes in the endogenous 5-HT concentration and subsequently to apply the methodology to examine the mechanisms of action of the novel antidepressant vortioxetine.

2. The second specific aim was to evaluate the novel radioligand [^{11}C]Lu AE92686 and its binding to the intraneuronal enzyme PDE10A. The sensitivity to changes in cAMP concentration was examined by challenges with dopaminergic agonists and antagonists.

3 MATERIALS AND METHODS

The following sections describe the general methods applied in the current thesis work. For the specific methods for each study, the reader is referred to each respective paper or manuscript.

3.1 ETHICAL APPROVALS

All NHP studies were approved by the Animal Research Ethical Committee of the Northern Stockholm region and the reference numbers for each study were Dnr N386/09 and N452/11 for Study I, Dnr N145/08, N399/08, N362/10, N452/11 and N185/14 for Study II, Dnr N185/14 for Study III and Dnr N452/11, N632/12, N633/12 and N185/14 for both Study IV and V, respectively. The caring and experimental procedures were performed according to the 'Guidelines for planning, conducting and documenting experimental research' (Dnr 4820/06-600) of Karolinska Institutet and the 'Guide for the Care and Use of Laboratory Animals: Eighth Edition' (Council, 2011). In study V, mice studies were performed in accordance with the Guide for the Care and Use of Laboratory Animals as adopted and promulgated by the National Institutes of Health (Pub. 85-23, revised 1996) under the approval of the Pfizer Cambridge site Institutional Animal Care and Use Committee.

3.2 STUDY SUBJECTS

Female rhesus monkeys (*Macaca mulatta*) and cynomolgus monkeys (*Macaca fascicularis*) were included in the thesis work.

3.3 STUDY DRUGS

3.3.1 Drugs used for increasing the 5-HT concentration

The dose, formulation and administration protocol for each drug are summarized in Table 7.

Table 7. Summary of the drugs for increasing the 5-HT concentration

Drugs	Formulation	Start time*	Duration	Study
Racemic fenfluramine 5.0 mg/kg	Saline	30 min	10 min	I
D-amphetamine 1.0 mg/kg (sulfate salt)	PBS	25 min	15 min	II
MDMA 1.0 mg/kg (hydrochloride salt)	PBS	25 min	15 min	II
5-HTP 5.0 mg/kg	PBS	25 min	15 min	II
Citalopram 0.3 or 2.0 mg/kg	PBS	45 min	30 min	III
Vortioxetine 0.1, 0.3, 1.0 or 3.0 mg/kg	10% HPBCD in PBS	45 min	30 min	III

*The interval between start of pretreatment infusion and intravenous injection of radioligand.

HPBCD: hydroxypropyl beta cyclodextrin; PBS: phosphate buffered saline.

3.3.2 Drugs used for blocking PDE10A binding

In Study IV, MP-10 (Verhoest *et al*, 2009), a PDE10A inhibitor was formulated in a mixture of PEG 400 (25%, v/v) and 0.9% saline (75%, v/v). Unlabeled Lu AE92686 was formulated in a mixture of 10% hydroxypropyl beta cyclodextrin dissolved in phosphate

buffered saline (PBS). All drug solutions were infused intravenously (~1 mL/kg) over 15 min, starting 45 min before the injection of [^{11}C]Lu AE92686.

3.3.3 Drugs used for increasing the cAMP concentration

In Study V, the cAMP concentration was increased by using D_2R antagonist haloperidol (0.05 mg/kg) in combination with functional D_1R agonism achieved by using *D*-amphetamine (1.0 mg/kg). Haloperidol and *D*-amphetamine were formulated in water and PBS, respectively. The administration protocol is described in the next section.

3.3.4 Drugs used for decreasing the cAMP concentration

In Study V, the cAMP concentration was decreased by using a combination of D_1R antagonist SCH 23390 (2.0 mg/kg) and functional D_2R agonist *R*-apomorphine (1.0 mg/kg), or by SCH 23390 alone (2.0 mg/kg). SCH 23390 and *R*-apomorphine were formulated in PBS and water with ascorbate, respectively. In all the regimens, the antagonist drug (haloperidol or SCH 23390) solution was infused intravenously over 15 min, starting 45 min prior to the injection of [^{11}C]Lu AE92686. The second drug (*D*-amphetamine or *R*-apomorphine) was infused intravenously over 15 min, starting 30 min prior to the injection of [^{11}C]Lu AE92686.

3.4 PET MEASUREMENTS IN NHP

3.4.1 Radioligands

[^{11}C]Cimbi-36 (Ettrup *et al*, 2011) in Study I and III, [^{11}C]MDL 100907 (Lundkvist *et al*, 1996) in Study I, [^{11}C]AZ10419369 (Andersson *et al*, 2011; Pierson *et al*, 2008) in Study I, II and III, [^{11}C]MADAM (Halldin *et al*, 2005) in Study III as well as [^{11}C]Lu AE92686 (Kehler *et al*, 2014) in Study IV and V were prepared according to the procedures reported previously.

3.4.2 PET experimental procedures

Anesthesia was initiated by intramuscular injection of ketamine hydrochloride (~10 mg/kg) and maintained by a mixture of sevoflurane (2–8%), oxygen and medical air. PET measurements were conducted in the High Resolution Research Tomograph. Following a six min transmission measurement (using a single ^{137}Cs source), the list-mode data was acquired for 123 min after intravenous bolus injection of radioligand in all PET measurements except for Study II. In Study II, [^{11}C]AZ10419369 was administered using a B/I protocol with the bolus-to-infusion rate ratio ranging from 80 to 180 min and 123-min PET data was acquired. This B/I protocol has been validated in previous NHP studies (Finnema *et al*, 2012; Nord *et al*, 2013). On each experimental day, a baseline PET measurement was performed in the morning followed by a second PET measurement in the afternoon with or without pretreatment. The two PET measurements were performed approximately 3 hours apart.

Venous blood samples were collected at several time points for determination of the plasma drug concentrations (Study I, III and V). In Study IV, arterial blood samples were collected for determination of the protein binding of radioligand, blood and plasma radioactivity, radiometabolite fractions as well as plasma drug concentrations.

3.5 MAGNETIC RESONANCE IMAGING

T1-weighted magnetic resonance imaging (MRI) images were acquired for each NHP on a GE 1.5 Tesla Signa MRI scanner (Milwaukee, WI) using a 3D spoiled gradient recalled protocol with repetition time 21 ms, flip angle 35°, FOV 12.8, matrix 256 × 256 × 128, 128 × 1.0 mm^2 slices.

3.6 IMAGE DATA ANALYSIS AND QUANTIFICATION

Unless otherwise specified, analyses of imaging data were performed using PMOD (PMOD Technologies, Zurich, Switzerland): version 3.704 for Study I and II, 3.604 for Study III and 3.403 for study IV and V.

3.6.1 Image preprocessing

The PET images were preprocessed according to previously reported methods (Varrone *et al*, 2009) with the frames of the reconstructed image binned as 9 × 10 s, 2 × 15 s, 3 × 20 s, 4 × 30 s, 4 × 60 s, 4 × 180 s and 17 × 360 s. The MRI images were manually reoriented to the anterior-posterior commissure plane in all studies. Moreover, for Study I to III, non-brain tissues were removed manually and the processed brain MRI images were then corrected for inhomogeneous intensity by the N4 algorithm (Tustison *et al*, 2010) using the software Advanced Normalization Tools (ANTs) (http://stnava.github.io/ANTs/).

3.6.2 PET-MRI co-registration

For each baseline PET measurement, a summed PET image was generated for PET-MRI co-registration. Time frames for the summed PET image were chosen based on high tissue counts and optimal tissue contrast to enable co-registration. The applied time frames were 12–63 min for [^{11}C]Cimbi-36, 21–75 min for [^{11}C]MDL 100907, 5–18 min and 0–57 min for bolus and B/I administration of [^{11}C]AZ10419369, respectively, 15–69 min for [^{11}C]MADAM as well as 0–9 min for [^{11}C]Lu AE92686. For Study I to III, each summed image was co-registered to its individual MRI brain image by the Rigid matching algorithm using the default settings for primates in the PMOD Fuse It Tool. For Study IV and V, the summed image was co-registered manually to its individual MRI image. For all studies, the resulting transformation matrices were applied to the two PET measurements obtained for each monkey on the same day.

3.6.3 Volumes of interest

The volumes of interest (VOIs) were selected based on the regional distribution of each target protein. For Study I and III (rhesus monkeys), VOIs were defined based on the

NeuroMaps atlas in the INIA19 rhesus template (Rohlfing *et al*, 2012). Each monkey's brain MRI image was normalized to the INIA19 rhesus template by the Deformable matching algorithm with the default settings for primate in the PMOD Fuse It Tool and the resulting normalization matrix was used to inversely transform the template VOIs into the individual MRI space. Moreover, in Study III, the DRN was manually delineated on each monkey's coregistrated summed [^{11}C]MADAM PET image in a sagittal plane, including 5-6 slices from the level of the superior colliculus to the level of the inferior colliculus (Kranz *et al*, 2012).

For Study II (cynomolgus monkeys), VOIs were defined on an in-house cynomolgus brain template that was generated from MRI images of 36 cynomolgus monkeys using the symmetric group-wise normalization procedures (Avants *et al*, 2010) in ANTs. The automated delineation of VOIs was guided by the NeuroMaps atlas in the INIA19 template (Rohlfing *et al*, 2012) and the Paxinos' histology atlas (Paxinos *et al*, 2008) in the CIVM template (Calabrese *et al*, 2015). Each individual brain MRI image was normalized to the in-house cynomolgus brain template by the antsRegistration algorithm using the symmetric image normalization method (Avants *et al*, 2008) in ANTs. The resulting normalization matrix was used to inversely transform the template VOIs into the individual MRI space. For Study IV and V (cynomolgus monkeys), VOIs were manually defined on individual MRI images.

3.6.4 Quantification of PET data

For each VOI, a decay-corrected time–activity curve (TAC) was generated from the coregistrated dynamic PET data. In Study I, III and V, BP_{ND} values were calculated using the SRTM (Lammertsma and Hume, 1996) with cerebellum as the reference region. This method has been validated in previous primate studies for [^{11}C]Cimbi-36 (Finnema *et al*, 2014), [^{11}C]MDL 100907 (Meyer *et al*, 2010; Talbot *et al*, 2012), [^{11}C]AZ10419369 (Varnäs *et al*, 2011) and [^{11}C]MADAM (Lundberg *et al*, 2005). For [^{11}C]Lu AE92686, the validation of the use of reference tissue models and the selection of reference region was performed in Study IV (see below description). In Study II, BP_{ND} values were calculated using the equilibrium method (integral interval: 63 to 123 min) with cerebellum as the reference region (Finnema *et al*, 2012; Nord *et al*, 2013).

In Study IV, kinetic analysis was performed by applying the 1TCM and the 2TCM. Logan plot analysis (Logan *et al*, 1990) was also used and the starting time of linearization (t^*) was decided separately for each VOI in each experiment by examination of the V_T value and identifiability of V_T for different t^* values ranging from 6 min to a time point with 5 time frames remaining until the end of the PET measurement. The effects of PET measurement duration on V_T values were also examined by varying the time interval from 0–33 min to 0–117 min with one time frame increments. BP_{ND} was derived by 3 different approaches, the indirect method using equation (9) and two reference tissue models: SRTM and Loganref (Logan *et al*, 1996) with cerebellum as the reference region. The efflux rate constant k_2' in Loganref was derived by using SRTM and couple fitting of all target regions except SN

(excluded due to its relatively high noise levels). The t^* for Loganref was 27 minutes, based on the results of the Logan plot analysis.

3.6.5 PET related outcome measures

The ΔBP_{ND} induced by administration of pretreatment drug which represents receptor occupancy by pretreatment drug and/or endogenous neurochemical was calculated based on equation (17) (page 11) and expressed as percentage. In Study I, the fraction of 5-HT_{2A} receptors in the high-affinity state was estimated by the ratio of ΔBP_{ND} using [^{11}C]MDL 100907 to ΔBP_{ND} using [^{11}C]Cimbi-36 in the same NHPs, following the method proposed by Narendran and colleagues (Narendran *et al*, 2004) as described in equation (23) (page 12).

According to the law of mass action, the relationship between radioligand binding and the concentration of drug at equilibrium can be described by a one-site binding hyperbola, as expressed by the following equation:

$$\text{Decrease in } BP_{ND}\ (\%) = I_{max} \times \frac{\text{drug dose (or } C_{PD})}{\text{drug dose (or } C_{PD}) + ID_{50}\text{ (or } K_{i\_PD})}, \quad (24)$$

where I_{max} is the maximal inhibition (%), C_{PD} is the plasma drug concentration and ID_{50} or K_{i_PD} corresponds to the drug dose or the plasma drug concentration at which 5-HTT occupancy is 50%, respectively (Farde *et al*, 1988; Finnema *et al*, 2015a).

In Study III, based on equation (24), the drug-induced decreases in [^{11}C]MADAM BP_{ND} (%) (equal to the ΔBP_{ND} (%) with opposite sign) in putamen and caudate nucleus were plotted against the corresponding drug dose or plasma drug concentration (Finnema *et al*, 2015a). The mean plasma drug concentration value of 8 blood samples taken during the PET measurement period was used to represent the C_{PD}. An unconstrained I_{max} value was applied to the model (Finnema *et al*, 2015a) and the ID_{50} or K_{i_PD} value was calculated using GraphPad Prism (version 6.05; GraphPad, San Diego, CA, USA).

In Study I and III, equation (24) was modified to estimate the receptor occupancy by direct binding of pretreatment drugs following a previously proposed method (Tyacke and Nutt, 2015). The receptor occupancy can be calculated according to equation (25):

$$\text{Receptor occupancy } (\%) = 100 \times \frac{C_{BD}}{C_{BD} + K_{i\_BD}}, \quad (25)$$

where C_{BD} is the extracellular drug concentration in the brain and K_{i_BD} is the drug's inhibition constant to the receptor. For each receptor, K_{i_BD} was based on the K_i value of pretreatment drugs for the receptor and was obtained from the National Institute of Mental Health's Psychoactive Drug Screening Program (NIMH PDSP) (Besnard *et al*, 2012) or literature (Bang-Andersen *et al*, 2011; Rothman *et al*, 2000).

C_{BD} was estimated according to the equation:

$$C_{BD} = C_{PD} \times f_P \times K_P, \quad (26)$$

where C_{PD} is the plasma drug concentration, f_P is the free fraction of the drug in plasma and K_P is the brain to plasma partition factor of unbound drug. The values of f_P and K_P were obtained from the literature (Bundgaard *et al*, 2016; Caccia *et al*, 1979; Garnock-Jones, 2014; Kaddoumi *et al*, 2003). The parameters used for estimation of direct occupancy by pretreatment drugs are summarized in Table 8.

Table 8. Summary of parameters used for estimation of receptor occupancy by pretreatment drugs

Parameters	Fenfluramine	Norfenfluramine	Vortioxetine
5-HT_{1B} K_{i_BD} (nM)*	1837	2444	33
5-HT_{2A} K_{i_BD} (nM)#	5216	2316	N/A
5-HT_{2B} K_{i_BD} (nM)*	4134	52	N/A
5-HT_{2C} K_{i_BD} (nM)#	3183	557	N/A
f_P (%)	3.0	3.0	2.0
K_P	2.6	1.9	3.1

*Cloned human receptors; #Cloned rat receptors.

f_P: the free fraction of the drug in plasma; K_{i_BD}: the drug's equilibrium dissociation constant to the receptor; K_P: the brain to plasma partition factor of unbound drug; N/A: not applicable.

In Study V, for test-retest characterization, the absolute variability was calculated according to the equation:

$$\text{Absolute variability (\%)} = \frac{|BP_{ND}\text{Retest} - BP_{ND}\text{Test}|}{(BP_{ND}\text{Retest} + BP_{ND}\text{Test})/2} \times 100. \quad (27)$$

3.7 BLOOD SAMPLE ANALYSIS

3.7.1 Determination of plasma drug concentrations

In Study I, norfenfluramine, the main metabolite of fenfluramine, is also a potent 5-HT releaser (Rothman and Baumann, 2002). Therefore, the plasma concentrations of both fenfluramine and norfenfluramine were determined using liquid chromatography–mass spectrometry. In Study III to V, the plasma drug concentrations of pretreatment drugs were determined using ultra performance liquid chromatography followed by tandem mass spectrometry detection according to the procedures reported previously (Finnema *et al*, 2015a).

3.7.2 Determination of plasma protein binding and radiometabolite fractions

In Study IV, the f_p of [^{11}C]Lu AE92686 in plasma was estimated by ultrafiltration and the percentages of radioactivity for unchanged radioligand and radiometabolites in plasma were determined by the reversed-phase high-performance liquid chromatography according to the procedures reported previously (Finnema *et al*, 2014; Takano *et al*, 2015).

3.8 *EX VIVO* BINDING AND IMMUNOBLOTTING EXPERIMENTS

In Study V, for binding experiments, CD-1 mice (~30 g; Charles River Laboratories) were subcutaneously administered with either vehicle (H_2O), *R*-apomorphine (3 mg/kg; Sigma-Aldrich, St Louis, MO) and/or SCH 23390 (2 mg/kg; Sigma-Aldrich, St Louis, MO) in a dose volume of 10 mL/kg. [^{3}H]Lu AE92686 (75 μCi/kg; Lundbeck A/S) (Kehler *et al*, 2014) was intravenously administered in a dose volume of 5 mL/kg, 15 min prior to euthanasia by rapid decapitation, either 20 min after *R*-apomorphine administration, or at 5, 10, 20, 30 or 60 min after SCH 23390 administration. In the immunoblotting studies, mice were subcutaneously dosed with 2 mg/kg of SCH 23390 (in saline) or vehicle 60 min before decapitation.

3.9 STATISTICAL ANALYSIS

In Study I, II, III and V, a paired *t*-test was used to assess changes in parameters between the two NHP PET measurements performed on the same day. The statistical analyses were performed in GraphPad Prism (version 6.05; GraphPad Software Inc., La Jolla, CA, USA). The threshold of significance was set as $P < 0.05$ (one-tailed) for fenfluramine induced decreases in BP_{ND} and $P < 0.05$ (two-tailed) for changes in other parameters. In Study V, *ex vivo* [^{3}H]Lu AE92686 binding studies and *ex vivo* immunoblotting experiments in mice were evaluated using ANOVA analysis and unpaired *t*-tests, respectively.

4 RESULTS AND COMMENTS

4.1 STUDY I: 5-HT SENSITIVITY OF [^{11}C]CIMBI-36 BINDING

Eighteen PET measurements, 6 for each radioligand, were performed in 3 rhesus monkeys before or after administration of 5.0 mg/kg fenfluramine. Fenfluramine significantly decreased [^{11}C]Cimbi-36 BP_{ND} (26–62%) and [^{11}C]AZ10419369 BP_{ND} (35–58%) in most regions. Fenfluramine-induced decreases in [^{11}C]MDL 100907 BP_{ND} were 8–30%, and statistically significant in three regions including temporal cortex, anterior cingulate cortex and thalamus (Table 9 and Figure 4, page 34). Decreases in [^{11}C]Cimbi-36 BP_{ND} were larger than for [^{11}C]AZ10419369 in neocortical and limbic regions (~35%), but smaller in striatum and thalamus (~40%). Decreases in [^{11}C]Cimbi-36 BP_{ND} were 0.9–2.8 times larger than for [^{11}C]MDL 100907.

Table 9. Effect of fenfluramine on regional BP_{ND} values (n = 3)

Region	[^{11}C]MDL 100907			[^{11}C]Cimbi-36			[^{11}C]AZ10419369		
	BAS	FEN	ΔBP_{ND} (%)	BAS	FEN	ΔBP_{ND} (%)	BAS	FEN	ΔBP_{ND} (%)
Put	1.05	0.94	-10.3	0.69	0.61	-11.4	0.78	0.44	-46.5*
CN	1.15	0.93	-17.4	0.86	0.53	-38.0*	0.65	0.37	-46.1*
VS	1.16	0.91	-21.4	0.80	0.56	-30.4*	1.36	0.66	-51.9**
FC	3.53	2.39	-29.9	1.73	0.83	-51.3*	0.78	0.51	-35.2*
PC	2.95	1.98	-30.0	1.44	0.68	-51.8*	0.67	0.40	-42.6*
TC	2.95	2.05	-28.9*	1.79	0.80	-54.6*	0.72	0.42	-42.3*
OC	2.47	1.73	-26.1	1.17	0.45	-62.2**	1.17	0.51	-58.2*
ACC	3.46	2.41	-29.3*	2.14	1.03	-51.1*	0.91	0.59	-37.0*
Amyg	1.02	0.76	-25.2	0.86	0.54	-36.6*	1.05	0.55	-47.6*
HC	1.27	0.85	-29.8	1.03	0.49	-51.5**	0.63	0.37	-41.3*
Thal	0.78	0.72	-8.2*	0.70	0.52	-25.8**	0.94	0.49	-48.1*
MB	0.84^	0.67	-16.3	0.66	0.37	-43.3**	0.92	0.50	-46.3*
WB	2.03	1.46	-25.8	1.19	0.60	-49.4**	0.69	0.38	-46.3*

Data presented as mean (n = 3). Modified from (Yang *et al*, 2017b).

Abbreviations: ACC, anterior cingulated cortex; Amyg, amygdala; BAS, baseline; CN, caudate nucleus; FEN, fenfluramine; FC, frontal cortex; HC, hippocampus; MB, midbrain; OC, occipital cortex; PC, parietal cortex; Put, putamen; TC, temporal cortex; Thal, thalamus; VS, ventral striatum; WB, whole brain.

*P < 0.05, **P < 0.01 (one-tailed) by paired t-test.

These observations suggested that [^{11}C]Cimbi-36 binding was sensitive to 5-HT release induced by fenfluramine. Moreover, the agonist radioligand [^{11}C]Cimbi-36 was more sensitive to 5-HT release than [^{11}C]MDL100907, an antagonist radioligand for the same target. The results are thus consistent with the view that agonist radioligands are more sensitive to the changes in the concentration of neurotransmitter than antagonists. The estimated fraction of 5-HT_{2A} receptor in the high-affinity state (54% in the neocortex) in Study I was slightly higher than previously reported values from *in vitro* binding assays (13–45%) (Fitzgerald *et al*, 1999; Gray *et al*, 2003; Hazelwood and Sanders-Bush, 2004; Sleight *et al*, 1996). The present *in vivo* estimates should be taken with caution since they were based on data obtained in only three NHPs but support the view that high- and low-affinity states are valid concepts also *in vivo*. In addition, the 5-HT sensitivity of [^{11}C]Cimbi-36 binding was comparable to that for [^{11}C]AZ10419369 binding. Due to the relative high density of 5-

HT_{2A} receptors in neocortical and limbic regions (Paterson *et al*, 2010), [^{11}C]Cimbi-36 may be advantageous to [^{11}C]AZ10419369 for examination of serotonergic neurotransmission in these regions.

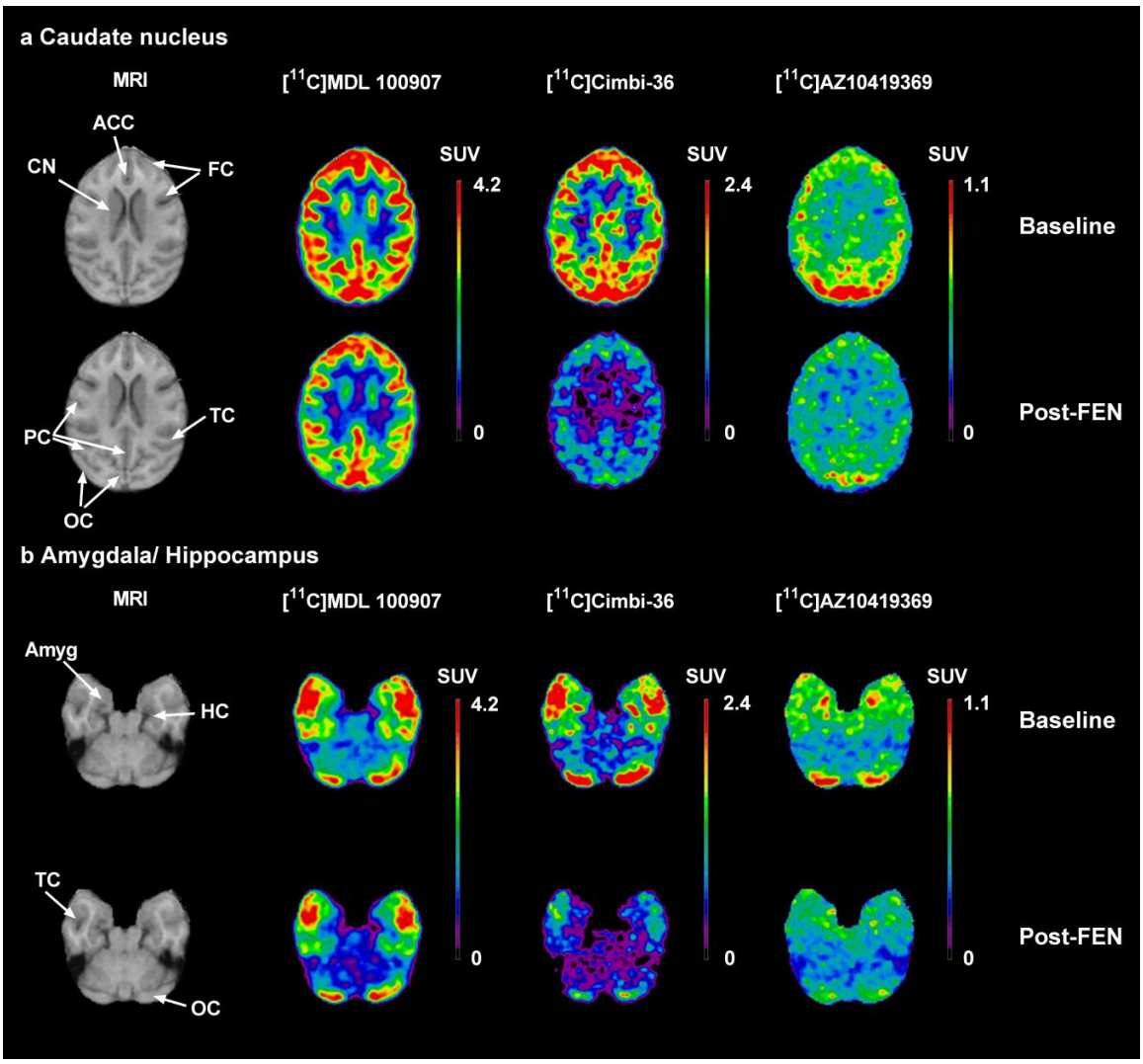

Figure 4. Magnetic resonance images and corresponding coregistrated PET summation images (average of frames from 9 to 123 min) of [^{11}C]MDL 100907, [^{11}C]Cimbi-36 and [^{11}C]AZ10419369 during baseline and post-fenfluramine (FEN) conditions in one NHP. (a) Axial view of images at the level of caudate nucleus. (b) Axial view of images at the level of amygdala/hippocampus; note the difference in the range of the standardized uptake values (SUV) color bars for the different radioligands. SUV values were calculated from the radioactivity concentration as [kBq/cm^3] / (radioactivity injected [MBq] / body weight [kg]). Abbreviations: ACC, anterior cingulate cortex; Amyg, amygdala; CN, caudate nucleus; FC, frontal cortex; HC, hippocampus; PC, parietal cortex; OC, occipital cortex; TC, temporal cortex. Modified from (Yang *et al*, 2017b).

4.2 STUDY II: TRANSLATIONAL 5-HT SENSITIVITY OF [^{11}C]AZ10419369 BINDING

This study applied 5-HT concentration enhancers which can be safely studied in humans, and examined their effects on [^{11}C]AZ10419369 binding at clinically relevant doses, including amphetamine (1 mg/kg), MDMA (1 mg/kg) or 5-HTP (5 mg/kg). Twenty-six PET measurements (14 for amphetamine, 6 for MDMA and 6 for 5-HTP) using a B/I protocol were performed in four cynomolgus monkeys before or after drug administration. The BP_{ND}

values were significantly decreased in several brain regions after administration of amphetamine (18–31%), MDMA (16–25%) or 5-HTP (13–31%) (Table 10 and Figure 5, page 36). The reductions in [^{11}C]AZ10419369 binding were greater in striatum than cortical regions after administration of 5-HTP, while no prominent regional differences were found for amphetamine and MDMA.

Table 10. Effect of pretreatment drugs on regional BP_{ND} values

	AMPH 1.0 mg/kg (n = 7)			MDMA 1.0 mg/kg (n = 3)			5-HTP 5.0 mg/kg (n = 3)		
Region	BAS	PreTx	ΔBP_{ND} (%)	BAS	PreTx	ΔBP_{ND} (%)	BAS	PreTx	ΔBP_{ND} (%)
FC	0.86	0.69	-19**	0.81	0.65	-19*	0.80	0.68	-14*
OC	1.40	0.98	-30***	1.28	1.03	-20*	1.29	1.17	-10
HC	0.87	0.69	-21**	0.89	0.71	-22	0.83	0.73	-13*
CN	0.96	0.72	-24**	0.92	0.78	-16*	0.82	0.57	-31*
Put	1.09	0.85	-22**	1.10	0.87	-23*	1.08	0.79	-26*
VS	1.50	1.20	-18*	1.44	1.08	-25*	1.55	1.13	-27*
GP	1.96	1.43	-27***	1.86	1.44	-24*	1.90	1.63	-14
Thal	1.07	0.73	-31***	0.99	0.77	-24*	0.98	0.80	-17
MB	1.32	1.00	-23**	1.17	0.96	-18*	1.15	1.04	-9
WB	0.83	0.64	-23**	0.78	0.62	-20*	0.79	0.68	-14

Data presented as mean values.

Abbreviations: AMPH, amphetamine; BAS, baseline; CN, caudate nucleus; FC, frontal cortex; GP, globus pallidus; HC, hippocampus; MB, midbrain; OC, occipital cortex; PreTx, pretreatment; Put, putamen; Thal, thalamus; VS, ventral striatum; WB, whole brain.

*P < 0.05, **P < 0.01, ***P < 0.001 (two-tailed) by paired t-test.

Amphetamine has been widely applied in human PET studies to evaluate dopamine release (Finnema *et al*, 2015c; Jayaram-Lindström *et al*, 2017; Laruelle, 2000; Oswald *et al*, 2015; Volkow *et al*, 2015). Interestingly, the amphetamine (1 mg/kg) induced reduction in [^{11}C]AZ10419369 BP_{ND} in Study II was comparable to that for [^{11}C]raclopride BP_{ND} (23–44%) in the NHP brain (Narendran *et al*, 2004; Seneca *et al*, 2006). Importantly, [^{11}C]raclopride binding has been demonstrated to be sensitive to lower doses of amphetamine (e.g. 0.3 mg/kg intravenous with ~16% reduction) in human studies (Finnema *et al*, 2015c; Laruelle, 2000; Martinez *et al*, 2003). Altogether, it is expected that in the human brain, the current PET imaging paradigm will be sensitive to 5-HT release induced by amphetamine with doses that have been applied in previous human PET studies (~0.5 mg/kg oral or ~0.3 mg/kg intravenous) (Aalto *et al*, 2009).

The dose of MDMA (1mg/kg) used in Study II is comparable to those in previous human studies (~1.7 mg/kg oral) and is unlikely to give rise to significant adverse events (Bowyer *et al*, 2003; Gamma *et al*, 2000; Tyacke and Nutt, 2015; Vizeli and Liechti, 2017). Considering the similar decreases in [^{11}C]AZ10419369 binding between MDMA and amphetamine in Study II, MDMA may thus serve as an alternative to the use of amphetamine for examination of the 5-HT release in future clinical studies.

The 5-HTP (5 mg/kg) induced a 30% decrease in striatal [^{11}C]AZ10419369 BP_{ND} in Study II. This marked effect is consistent with a previous report in which 20 mg/kg of 5-HTP reduced [^{11}C]DASB binding to the 5-HTT in the NHP brain (~43% in striatum) (Yamamoto *et al*, 2007). The current dose of 5-HTP was comparable to the clinical dose range of 200 to

300 mg/day, typically administered per os or intravenous (Turner *et al*, 2006). Furthermore, a slow-release formulation of 5-HTP has been shown to provide more stable increases in 5-HT concentration and less adverse effects than the immediate release form in rodent studies (Jacobsen *et al*, 2016). Therefore, PET measurement with [^{11}C]AZ10419369 and pretreatment with oral administration of slow-release formulation of 5-HTP is a promising paradigm to investigate 5-HT release in the human brain.

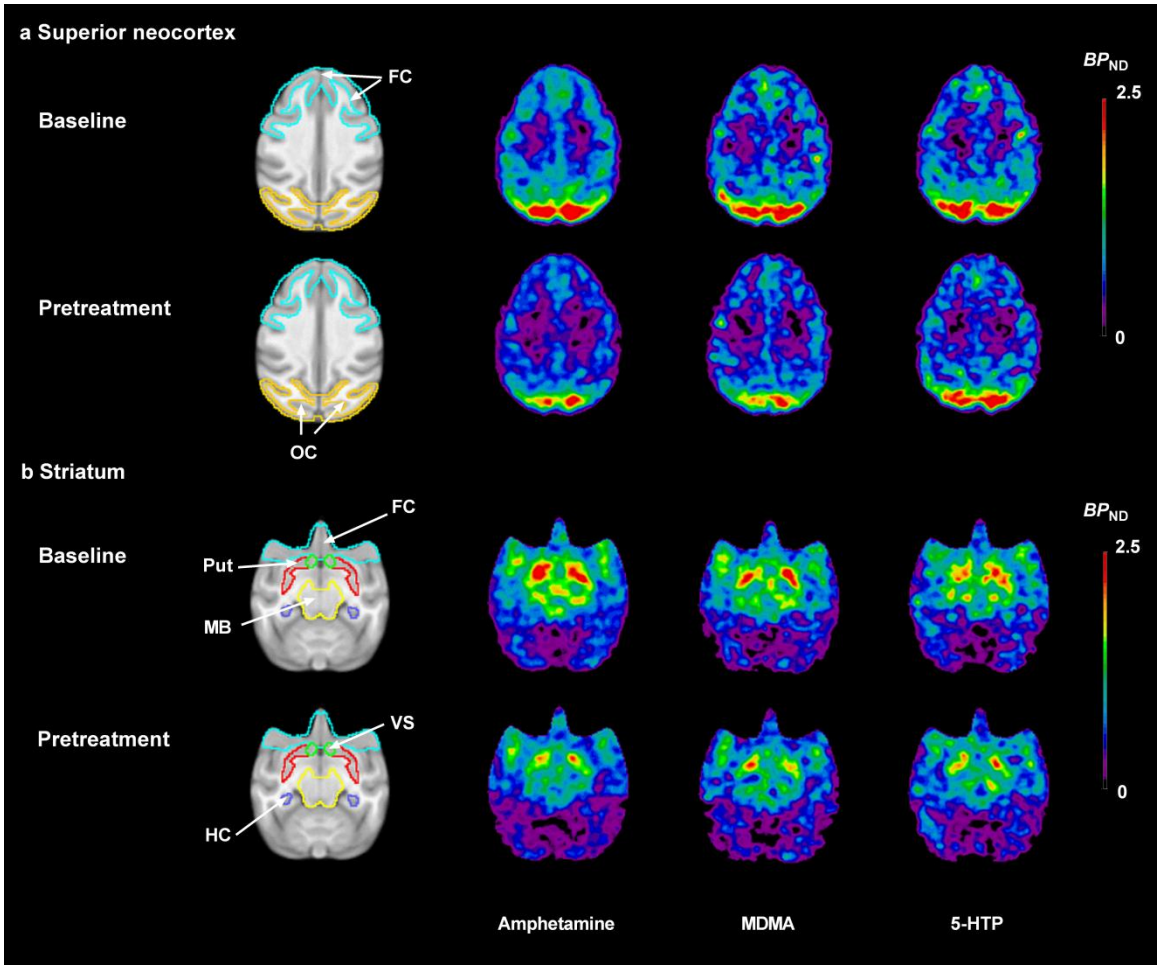

Figure 5. Mean parametric BP_{ND} images of [^{11}C]AZ10419369 derived by the equilibrium method at baseline and following pretreatment with 3 different experimental drugs: Amphetamine 1 mg/kg (n = 7), 3,4-methylenedioxymethamphetamine (MDMA) 1 mg/kg (n = 3) and 5-hydroxy-L-tryptophan (5-HTP) 5 mg/kg (n = 3). The images were normalized to an in-house cynomolgus brain template. (a) Axial view of images at the level of superior neocortex. (b) Axial view of images at the level of striatum. Abbreviations: FC, frontal cortex; HC, hippocampus; MB, midbrain; OC, occipital cortex; Put, putamen; VS, ventral striatum.

The observed larger 5-HTP induced reduction in [^{11}C]AZ10419369 binding in striatum than cortical regions is also consistent with previous results using [^{11}C]DASB in the NHP brain (Yamamoto *et al*, 2007). This regional effect is in line with the microdialysis studies in NHP demonstrating a larger increase (~27-fold) in the 5-HT concentration in striatum than in prefrontal cortex (Yamamoto *et al*, 2007). Interestingly, 5-HTP has been labeled with carbon-11 and examined as a PET-marker for the 5-HT synthesis (Visser *et al*, 2011). The [^{11}C]5-HTP influx rate has been shown to be higher in striatum than in prefrontal cortex in the NHP brain (Yamamoto *et al*, 2007). Together, the observed regional effect is likely attributed to

the regional differences in the activity of AADC which converts 5-HTP to 5-HT (Yamamoto *et al*, 2007). In summary, the regional difference in the effect of 5-HTP on [^{11}C]AZ10419369 binding supports the use of this PET imaging paradigm to detect changes in 5-HT concentration, primarily in subcortical regions.

4.3 STUDY III: EFFECTS OF VORTIOXETINE ON SEROTONIN SYSTEM

The affinity of vortioxetine to 5-HTT was evaluated by 8 PET measurements with [^{11}C]MADAM before and after administration of vortioxetine (0.1–3.0 mg/kg) in 4 monkeys. The estimated dose and plasma concentration of vortioxetine for 50% 5-HTT occupancy were 0.25±0.09 mg/kg and 39±12 nM, respectively. The doses of the pretreatment drugs were selected to achieve 80% (vortioxetine 1.0 mg/kg or citalopram 0.3 mg/kg) or 55% (vortioxetine 0.3 mg/kg) 5-HTT occupancy. The effects of pretreatment drugs on radioligand binding were evaluated by 18 PET measurements with [^{11}C]AZ10419369 in 3 NHPs and 4 PET measurements with [^{11}C]Cimbi-36 in 2 NHPs before and after administration of each regimen of pretreatment drug and vortioxetine 1.0 mg/kg, respectively. [^{11}C]AZ10419369 binding was significantly decreased in DRN after citalopram 0.3 mg/kg (5%), in 6 regions after vortioxetine 0.3 mg/kg (~25%) and in all 12 examined regions after vortioxetine 1.0 mg/kg (~48%). There was no effect of vortioxetine 1.0 mg/kg on [^{11}C]Cimbi-36 binding (Table 11 and Figure 6, page 38).

Table 11. Effect of citalopram and vortioxetine on regional BP_{ND} values

Region	[^{11}C]AZ10419369 ΔBP_{ND} (%)			[^{11}C]Cimbi-36 ΔBP_{ND} (%)	
	CIT 0.3[a]	VOR 1.0[a]	VOR 0.3[a]	VOR 1.0[b]	VOR 1.0[c]
Put	10.0	-34.2**	-15.1[#]	-5.7	7.9
CN	9.1	-40.8***	-22.3*	1.7	-18.1
VS	5.1	-41.6**	-24.5**	-0.4	-23.9
GP	-0.4	-38.1**	-20.3*	17.3	34.3
FC	14.7[#]	-27.2**	-9.0	1.0	-4.6
OC	18.1	-48.3*	-22.4*	10.9	22.8
ACC	12.1	-29.2**	-11.5	8.8	-21.2
Amyg	6.4	-34.9***	-13.6	-37.1	-10.6
HC	4.5	-20.4*	-12.0[#]	-4.3	7.1
Thal	1.4	-37.2***	-24.3*	-2.9	2.2
MB	4.8	-43.2*	-22.7***	38.2	13.5
DRN	-4.8**	-44.0*	-19.2[#]	-24.5	-22.0

Abbreviations: ACC, anterior cingulated cortex; Amyg, amygdala; Bas, baseline; CIT 0.3, citalopram 0.3 mg/kg; CN, caudate nucleus; DRN, dorsal raphe nucleus; FC, frontal cortex; GP, globus pallidum; HC, hippocampus; MB, midbrain; OC, occipital cortex; Put, putamen; Thal, thalamus; VOR 0.3, vortioxetine 0.3 mg/kg; VOR 1.0, vortioxetine 1.0 mg/kg; VS, ventral striatum.

[a]Mean value of 3 monkeys for each experimental condition; [b]NHP2; [c]NHP3.

[#]$0.05 \leq P < 0.1$, *$P < 0.05$, **$P < 0.01$, ***$P < 0.001$ (two-tailed) by paired *t*-test.

The significantly decreased BP_{ND} in the DRN and the numerically increased BP_{ND} in the projection regions induced by citalopram 0.3 mg/kg are in good agreement with previous human studies using clinically relevant doses of SSRIs (Nord *et al*, 2013; Selvaraj *et al*, 2012). It is worth noting that these BP_{ND} changes are in contrast to the significant reductions in several brain regions induced by high doses of SSRIs in previous NHP PET studies (Milak

et al, 2011; Nord *et al*, 2013; Ridler *et al*, 2011). Previous microdialysis studies in rats have also reported that, although high doses of SSRIs increased the 5-HT concentration both in the DRN and projection regions (DRN > projection regions), lower and more clinically relevant doses of SSRIs only increased the 5-HT concentration in the DRN (Gartside *et al*, 1995; Hervás and Artigas, 1998; Invernizzi *et al*, 1992). The current results thus support that the different direction of BP_{ND} changes induced by SSRIs between previous human and NHP studies are related to the applied doses of SSRIs (Finnema *et al*, 2015a; Nord *et al*, 2013; Selvaraj *et al*, 2012).

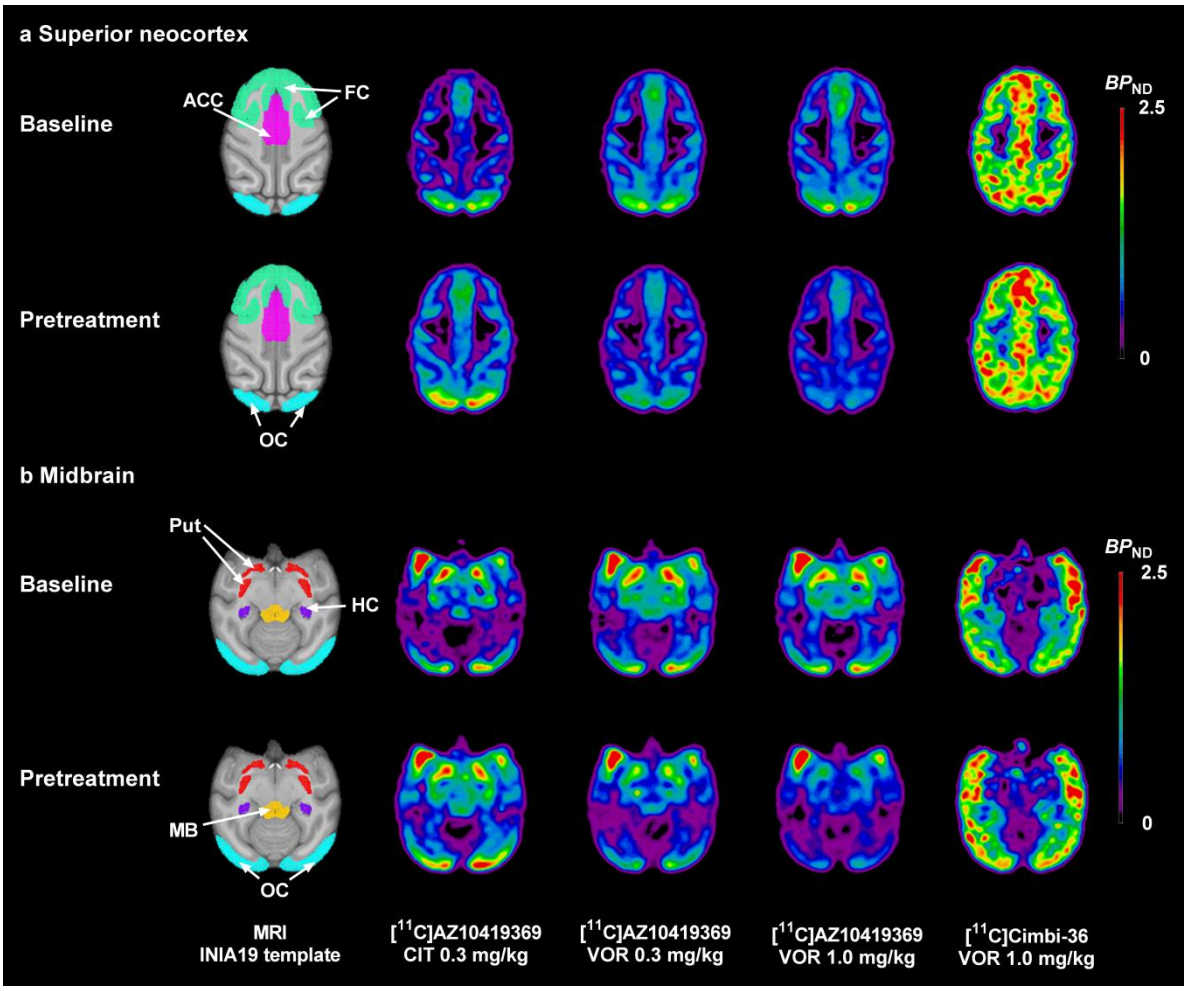

Figure 6. BP_{ND} images of [^{11}C]AZ10419369 or [^{11}C]Cimbi-36 derived by SRTM2 at baseline and after pretreatment with citalopram (CIT) or vortioxetine (VOR) (n = 3 for each pretreatment condition measured by [^{11}C]AZ10419369 and n = 2 for vortioxetine 1.0 mg/kg and [^{11}C]Cimbi-36). The images were normalized to the INIA19 rhesus template. (a) Axial view of images at the level of superior neocortex. (b) Axial view of images at the level of midbrain. Abbreviations: ACC, anterior cingulated cortex; frontal cortex; HC, hippocampus; MB, midbrain; OC, occipital cortex; Put, putamen.

The different effects between vortioxetine and citalopram on [^{11}C]AZ10419369 binding might originate from their differences in 5-HT_{1B} receptor occupancy and/or changes in 5-HT concentration. According to microdialysis data in rodents, the increases in 5-HT concentration induced by vortioxetine were about twice those induced by escitalopram (Pehrson *et al*, 2013). Considering the limited sensitivity of PET methodology for measuring changes in neurotransmitter concentration (Paterson *et al*, 2010), the relative large difference

in [^{11}C]AZ10419369 BP_{ND} reduction between vortioxetine 1.0 mg/kg and citalopram 0.3 mg/kg (~65% in OC) is likely not only explained by the magnitude of difference in 5-HT release. This observation was also consistent with the nanomolar range affinity of vortioxetine to recombinant human 5-HT$_{1B}$ receptors (Bang-Andersen *et al*, 2011; Sanchez *et al*, 2015). In summary, there might be direct occupancy of 5-HT$_{1B}$ receptor by the applied doses of vortioxetine.

To differentiate the potential causes of vortioxetine induced decreases in [^{11}C]AZ10419369 binding, we assessed the effects of vortioxetine 1.0 mg/kg on [^{11}C]Cimbi-36 binding which has previously been demonstrated to have comparable 5-HT sensitivity as [^{11}C]AZ10419369 binding in Study I. After excluding the estimated occupancy of the 5-HT$_{1B}$ receptor by vortioxetine based on *in vitro* determined binding affinities (7 and 21% for 0.3 and 1.0 mg/kg, respectively), the anticipated decrease in [^{11}C]AZ10419369 binding induced by 5-HT release would be 13–18% and 0–27% for vortioxetine 0.3 mg/kg and 1.0 mg/kg, respectively. Interestingly, this level of BP_{ND} reductions were comparable to those induced by high doses of SSRIs (12–30%) in previous NHP studies (Milak *et al*, 2011; Nord *et al*, 2013; Ridler *et al*, 2011). Accordingly, it was anticipated that [^{11}C]Cimbi-36 binding would also be sensitive to this magnitude of 5-HT release. The lack of effect of vortioxetine 1.0 mg/kg on [^{11}C]Cimbi-36 binding suggested that the actual level of 5-HT$_{1B}$ receptor occupancy by vortioxetine was higher than the estimated values based on *in vitro* measurements.

The results in Study III suggest that vortioxetine binds to the 5-HT$_{1B}$ receptor at clinically relevant doses. The 5-HT$_{1B}$ receptor occupancy by vortioxetine 0.3 mg/kg or 1.0 mg/kg might range from 7% to 25% or from 21% to 48%, respectively. Although the 5-HT$_{1B}$ receptor plays an important role in the pathophysiology of depression (Ruf and Bhagwagar, 2009; Sari, 2004; Svenningsson, 2006), the required 5-HT$_{1B}$ receptor occupancy by vortioxetine in relation to its antidepressant effect remains unclear. Target occupancy by partial agonists resulting in functional effects has been reported to range from <10% to >90% among different molecular targets (Grimwood and Hartig, 2009). Interestingly, using the study design of 5-HT depletion, preclinical studies have demonstrated that some therapeutic effects of vortioxetine were mediated by direct modulation of 5-HT receptors, independent of the increases in 5-HT concentration (du Jardin *et al*, 2014, 2016). So far, the mechanistic studies for the antidepressant effects of vortioxetine mainly focused on 5-HT$_{1A}$ and 5-HT$_3$ receptors (Sanchez *et al*, 2015). Our results suggest that the 5-HT$_{1B}$ receptor is also engaged by clinically relevant doses of vortioxetine in the primate brain.

4.4 STUDY IV: CHARACTERIZATION OF [^{11}C]LU AE92686 BINDING

A total of 11 PET measurements, 7 baseline and 4 following pretreatment with unlabeled Lu AE92686 or the structurally unrelated PDE10A inhibitor MP-10, were performed in 5 NHPs. [^{11}C]Lu AE92686 was rapidly metabolized and the parent compound fraction was 18 ± 4% of the plasma radioactivity at 60 min after injection. Regional TACs were best described with the 2TCM. However, the V_T values for all regions were quantified

by Logan plot analysis, as reliable cerebellar V_T values could not be derived by the 2TCM (Figure 7).

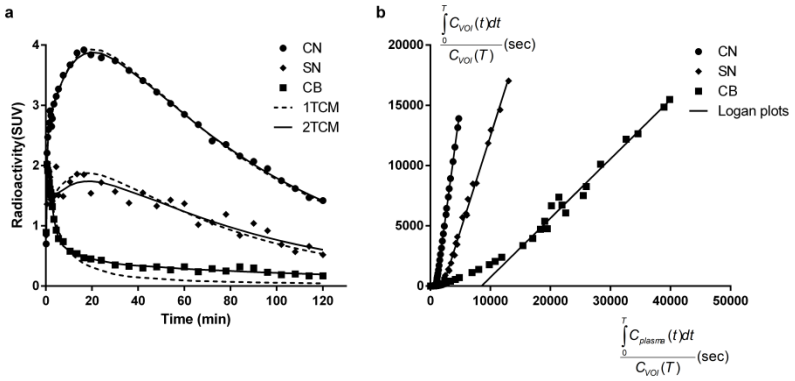

Figure 7. Representative kinetic modeling evaluation of [^{11}C]Lu AE92686 in one NHP. (a) 1TCM fits and 2TCM fits in the caudate nucleus (as in putamen and globus pallidus), substantia nigra (as in ventral striatum), and cerebellum. (b) Corresponding Logan plot analysis described the data adequately for all regions. Modified from (Yang *et al*, 2017a).

For cerebellum, a proposed reference region, V_T values increased by ~30% with increasing PET measurement duration from 63 min to 123 min, while V_T values in target regions remained stable (Figure 8). The continuous increase in the cerebellar V_T values might originate from the presence of BBB-penetrating radiometabolites (Zoghbi *et al*, 2006). To minimize the possible influence of radiometabolites, we choose 63 min as the preferred PET measurement duration. Similar approaches have been proposed for the application of other PDE10A radioligand, e.g. [^{18}F]JNJ-42259152 in rats, to overcome the confounding effects from BBB-penetrating radiometabolites (Celen *et al*, 2013).

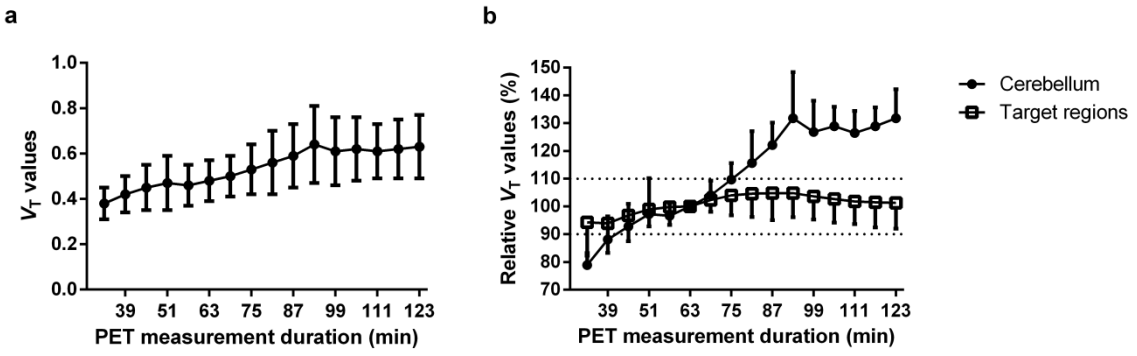

Figure 8. The effect of PET measurement duration on V_T values derived by the Logan plot analysis; Relative V_T values (%) = [(V_T values by corresponding duration of PET measurement - V_T values by reference duration of PET measurement) / V_T values by reference duration of PET measurement] x 100. (a) Cerebellar V_T values (mean ± SD). (b) Relative V_T values to 63 min data for target regions (mean – SD) and cerebellum (mean + SD). Modified from (Yang *et al*, 2017a).

Both pretreatment drugs significantly decreased [^{11}C]Lu AE92686 binding in the target regions while no significant effect on the cerebellum was observed. For the cerebellum, there was no statistical significant difference (4.8 ± 15.4 %, P = 0.55) in V_T/f_p between baseline

(8.6 ± 2.5) and pretreatment (9.0 ± 2.5) conditions. The suitability of the cerebellum as a reference region was further supported by the Lassen plots. The linear regression model could fit data from all regions well (the goodness of fit, $R^2 > 0.90$), suggesting that all examined regions, including SN, shared the same occupancy and V_{ND} values.

The BP_{ND} values calculated by SRTM in the baseline measurements were 13–17 in putamen and 3–5 in SN. These values were lower than those derived indirectly by Logan plot analysis (-19.7 ± 18.2%, median: -23.3%) and there was a significant correlation between BP_{ND} values calculated by Logan plot analysis and SRTM in the baseline measurements (Pearson $r = 0.95$, $P < 0.0001$). When pooling baseline and pretreatment data, the equation for the linear regression analysis was y = 0.601x + 1.295 ($R^2 = 0.95$; Figure 9). These results suggest that the SRTM may be used to quantify [^{11}C]Lu AE92686 binding.

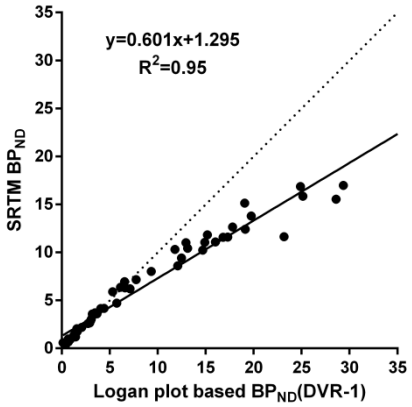

Figure 9. Linear regression analysis for BP_{ND} values calculated by SRTM and Loganref for 63 min PET data of [^{11}C]Lu AE92686. Dotted lines represent the line of identity. Modified from (Yang *et al*, 2017a).

4.5 STUDY V: CYCLIC AMP CONCENTRATIONS MODIFY [^{11}C]LU AE92686 BINDING

A total of 32 PET measurements (10 for test-retest and 22 for pretreatment studies) were performed in 5 NHPs. Elevations in cAMP concentration by haloperidol (0.05 mg/kg) plus *D*-amphetamine (1.0 mg/kg; $n = 3$) did not significantly alter [^{11}C]Lu AE92686 binding. In cAMP depletion paradigms, administration of SCH 23390 alone (2.0 mg/kg; $n = 3$) or in combination with *R*-apomorphine (1.0 mg/kg; $n = 5$) significantly decreased striatal [^{11}C]Lu AE92686 binding (-17±5%). The combination of SCH 23390 and *R*-apomorphine also significantly increased [^{11}C]Lu AE92686 binding in the SN (22±14%) (Figure 11, page 42). These effects were larger than the observed test-retest variability (6–16%).

Consistent with the NHP results, striatal *ex vivo* [^{3}H]Lu AE92686 specific binding in mice after 20, 30 and 60 min post SCH 23390 treatment was significantly lower than in the vehicle group, $t(24) = 3.32$, $P < 0.0143$ and $t(24) = 3.56$, $P < 0.008$, and $t(24) = 5.0$, $P < 0.0002$, respectively. Moreover, in both striatum and SN, there was no significant difference in PDE10A protein expression between vehicle-treated and SCH 23390-treated groups.

The striatal BP_{ND} changes observed in Study V were inconsistent with the competition model. This observation is in line with the previous PET study using PDE4 or PDE2A inhibitors to acutely increase cAMP concentrations in rats (Ooms *et al*, 2016). These combined results might be explained by alterations in radioligand binding affinity, as recently demonstrated for [^{18}F]JNJ42259152 in a tissue homogenate binding study in rats (Ooms *et al*, 2016). This alteration in affinity might be attributed to a conformational change in the catalytic domain of PDE10A induced by binding of cAMP to the GAF-B domain. Moreover, our studies also revealed that in mice *ex vivo* striatal [^{3}H]Lu AE92686 binding decreased after pretreatment with SCH 23390 while striatal PDE10A protein expression did not change. These observations suggest that the decreased striatal [^{11}C]Lu AE92686 binding was not caused by reduced PDE10A expression. Accordingly, the decreased striatal [^{11}C]Lu AE92686 binding likely reflects a decrease in affinity of [^{11}C]Lu AE92686 to PDE10A.

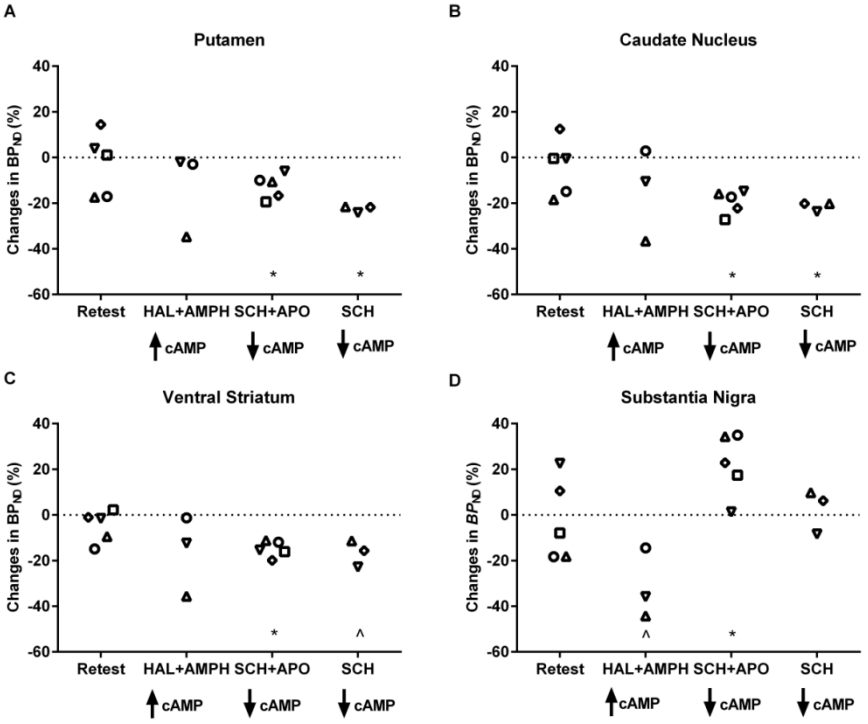

Figure 11. Relative change in regional [^{11}C]Lu AE92686 BP_{ND} values during 4 different study conditions. (A) Putamen. (B) Caudate nucleus. (C) Ventral striatum. (D) Substantia nigra. Abbreviations: HAL+AMPH, haloperidol 0.05 mg/kg + *D*-amphetamine 1.0 mg/kg; SCH, SCH 23390 2.0 mg/kg; SCH+APO, SCH 23390 2.0 mg/kg + *R*-apomorphine 1.0 mg/kg. The * indicates $P < 0.05$ and the ^ indicates $P = 0.05$-0.10 (two-tailed, paired *t*-test).

The use of [^{11}C]Lu AE92686 in Study V provided an unique opportunity to evaluate PDE10A binding both in striatum and SN (Yang *et al*, 2017a). Surprisingly, there were regional differences in the direction of BP_{ND} changes between striatum and SN. The reasons for these regional differences are not clearly understood and may relate to a different direction of the change in affinity and/or cAMP concentration. Since SN localized PDE10A is synthesized in the striatum and then transported to the SN (Charych *et al*, 2010; Seeger *et*

al, 2003), it is unlikely that there are regional differences in drug induced changes in the PDE10A affinity.

Moreover, we could not completely exclude the possibility that pretreatment with SCH 23390 plus *R*-apomorphine decreased striatal cAMP concentrations and simultaneously increased cAMP concentrations in SN. One previous *ex vivo* mice study has reported that acute pretreatment with *D*-amphetamine increased cAMP concentrations in striatum but decreased cAMP concentrations in cortex. These differences might be caused by preferential activation of different dopamine receptor subtypes (Kelly *et al*, 2007). The relative expression of dopamine D_3 receptors (D_3Rs) vs. D_1Rs or D_2Rs has been reported to be higher in SN than striatum (Sun *et al*, 2012). *R*-apomorphine has previously been reported to have high affinity for D_3Rs (Millan *et al*, 2002). Interestingly, a high fraction of D_3Rs in the SN is reported to form D_1Rs–D_3Rs heteromers and activation of D_3Rs within the heteromers could potentiate cAMP production, opposite to the effect by activation of individually expressed D_3Rs (Fiorentini *et al*, 2015). Therefore, it is possible that the combination of SCH 23390 and *R*-apomorphine increased and decreased cAMP concentrations in striatum and SN, respectively.

5 METHODOLOGICAL CONSIDERATIONS

5.1 SMALL SAMPLE SIZE

A limitation of the thesis work is the small sample size of PET measurements in each study (typical 3–5 for each experimental condition). Although this number of sample size is common and acceptable for NHP PET studies under the consideration of costs and ethics, this sample size is too small to provide adequate power in several experimental conditions and is consistent with a general statistical problem in neuroscience studies (Button *et al*, 2013). Consequently, the interpretation of the current results mainly focused on the statistically significant findings. It is worth noting that this number of sample size also made non-parametric statistical methods (e.g. Wilcoxon rank-sum test) unsuitable for data analysis due to their extremely low power (Janušonis, 2009). The use of a paired *t*-test is a better choice because of its relative high power and acceptable level of Type I error (Janušonis, 2009; De Winter, 2013).

5.2 INFLUENCE OF ANESTHESIA

Another potential limitation of the performed PET studies is the use of anesthesia. The effects of the applied anesthetics (induction by ketamine and maintenance by sevoflurane) on the binding of [^{11}C]Cimbi-36 or [^{11}C]MDL 100907 were unknown, although ketamine and isoflurane have previously been shown not to affect binding of [^{18}F]altanserin to the 5-HT$_{2A}$ receptor in the rodent brain (Elfving *et al*, 2003). It has been reported that anesthetic doses of ketamine increased [^{11}C]AZ10419369 binding in the NHP brain. Importantly, in the same study, decreases in [^{11}C]AZ10419369 binding induced by fenfluramine were similar between awake and anesthetized NHPs (Yamanaka *et al*, 2014). Therefore, the effect of ketamine on 5-HT sensitivity of [^{11}C]AZ10419369 binding was expected to be minimal. Currently, no data were available for the effect of sevoflurane on [^{11}C]AZ10419369 binding and for the effect of the applied anesthetics on [^{11}C]Lu AE92686 binding or cAMP concentrations. As the same anesthesia regimen was applied across the experiments, potential anesthesia effects were similar between citalopram and vortioxetine in 5-HTT occupancy studies and between [^{11}C]AZ10419369 and [^{11}C]Cimbi-36 in studies using vortioxetine 1.0 mg/kg. Accordingly, the potential anesthesia effects were not likely to affect the main observations in Study III.

In the thesis work, the potential anesthesia effects were minimized by maintaining stable levels of sevoflurane between and during PET measurements on the same experimental day. Future studies evaluating the current PET imaging paradigms in conscious humans are warranted to exclude potential anesthesia effects. For example, ketamine/xylazine and isoflurane have been reported to elevate the dopamine sensitivity of dopamine D_2/D_3 receptor agonist radioligands in NHP and rats, respectively (McCormick *et al*, 2011; Ohba *et al*, 2009). However, the higher dopamine sensitivity of dopamine D_2/D_3 receptor agonist radioligands than antagonist radioligands has been confirmed in awake human studies (Narendran *et al*, 2010; Shotbolt *et al*, 2012). Therefore, it is warranted to compare the 5-HT sensitivity of [^{11}C]Cimbi-36 and [^{11}C]MDL 100907 in awake humans.

5.3 QUANTIFICATION OF PET DATA

The quantification of PET data obtained in this thesis work was mainly performed using SRTM, one of the most commonly applied reference tissue models (Study I, III and V). The use of SRTM with cerebellum as the reference region has been validated in previous studies for [^{11}C]Cimbi-36 (Finnema *et al*, 2014), [^{11}C]MDL 100907 (Meyer *et al*, 2010; Talbot *et al*, 2012), [^{11}C]AZ10419369 (Varnäs *et al*, 2011) and [^{11}C]MADAM (Lundberg *et al*, 2005). In Study II, the [^{11}C]AZ10419369 BP_{ND} was calculated using the equilibrium method with cerebellum as the reference region which has also been validated in previous NHP studies (Finnema *et al*, 2012). For [^{11}C]Lu AE92686, the validation of the use of reference tissue models was performed in Study IV. In general, although there might be violations of the assumptions for quantification using SRTM (e.g. both TACs of target and reference regions were better described by the 2TCM than the 1TCM), it is still possible to apply SRTM if the bias of BP_{ND} values derived by the SRTM remain within an acceptable level (Sandiego *et al*, 2015; Zanderigo *et al*, 2013).

Performance criteria for the reference tissue models have recently been proposed by Zanderigo and coworkers (Zanderigo *et al*, 2013). The current results in Study IV could fulfill two of these three criteria, there was a high correlation between the BP_{ND} values derived by SRTM and Logan plot analysis (>0.95, proposed: >0.5) and a small median percent difference in the BP_{ND} values derived by these two methods (1.5% to 23.3%, proposed: <50%). However, the regression slope (0.6) of these BP_{ND} values slightly deviated from the proposed level (0.7–1.3), suggesting that the maximum relative difference in the BP_{ND} values derived by these two methods was relative high. As shown in Figure 9 (page 41), the deviation between the regression line and the line of identity is mainly driven by regions with high PDE10A density. Similar observations have previously been reported for several other established radioligands, including [^{11}C]Cimbi-36, [^{11}C]WAY-100635 and [^{11}C]FLB 457 (Finnema *et al*, 2014; Gunn *et al*, 1998; Parsey *et al*, 2000; Sandiego *et al*, 2015). Since the BP_{ND} values of [^{11}C]Lu AE92686 in target regions are relatively high (>15), a relatively large maximum difference in the BP_{ND} values derived by SRTM and Logan plot analysis can be anticipated. As for the established radioligands, reference tissue models are thus suitable for quantification of [^{11}C]Lu AE92686 binding in the NHP studies.

5.4 OTHER CAUSES FOR DECREASED RADIOLIGAND BINDING

As discussed in Study III, in addition to increases in 5-HT concentration, other factors such as occupancy of target receptors by pretreatment drugs or other neurochemicals might contribute to the decreases in radioligand binding in Study I and II.

In Study I, it is worth noting that [^{11}C]Cimbi-36 has a relatively poor selectivity for the 5-HT$_2$ receptor subtype, the K_i is 0.5–0.8 nM for the 5-HT$_{2A}$ receptor, 0.5 nM for the 5-HT$_{2B}$ receptor and 1.7 nM for the 5-HT$_{2C}$ receptor (Ettrup *et al*, 2011). The estimated occupancy levels by fenfluramine and norfenfluramine for the 5-HT$_{2A}$, 5-HT$_{2C}$ and 5-HT$_{1B}$ receptors (5–13%) were much lower than the observed reductions in cortical binding of [^{11}C]Cimbi-36 or

[^{11}C]AZ10419369 (35–62%). Although the estimated 5-HT_{2B} receptor occupancy was relatively high (50%), the low and restricted expression of the 5-HT_{2B} receptor in brain (Nichols and Nichols, 2008) suggests that this binding would have negligible effect on [^{11}C]Cimbi-36 binding. In conclusion, a major proportion of fenfluramine induced decreases in radioligand binding can be attributed to 5-HT release and is not likely to represent the drug occupancy.

In Study II, although plasma concentrations of pretreatment drugs were not measured, the estimated direct occupancy of MDMA 75 mg or its main active metabolites, 3,4-methylenedioxyamphetamine (MDA) (both with K_i > 10,000 nM) on the human 5-HT_{1B} receptor has been reported to be <10 % or 0.6%, respectively (Tyacke and Nutt, 2015). Because the affinity of amphetamine and 5-HTP to the 5-HT_{1B} receptor could not be found in the literature, direct occupancy could not be estimated for these two drugs. Moreover, the influence of release of other neurotransmitters, such as dopamine or norepinephrine, after administration of amphetamine or MDMA on the present results should be considered. Based on data from the National Institute of Mental Health's Psychoactive Drug Screening Program (NIMH PDSP) (Besnard *et al*, 2012), the affinity of dopamine and norepinephrine to the 5-HT_{1B} receptor (both with K_i > 10,000 nM) is much lower than that of 5-HT (K_i: 2 to 24 nM). Therefore, the contributions of dopamine and norepinephrine to the reductions in [^{11}C]AZ10419369 binding can be assumed to be minimal. In conclusion, a major proportion of the drug induced decreases in [^{11}C]AZ10419369 binding can be attributed to 5-HT release.

5.5 TRANSLATIONAL CONSIDERATIONS

The translation of the observations in NHP into future human studies is one of the main considerations in this thesis work. In Study I, fenfluramine 5 mg/kg reduced [^{11}C]Cimbi-36 binding by 55% in the NHP brain. In one previous human study, dexfenfluramine (40 or 60 mg p.o.) was shown to reduce [^{18}F]altanserin antagonist binding to the 5-HT_{2A} receptor (~20%). Following safety considerations, the proposed maximal dose of dexfenfluramine suitable for human use was 1 mg/kg p.o. (Quednow *et al*, 2012). Based on the level of decreases in radioligand binding and the higher 5-HT sensitivity of [^{11}C]Cimbi-36 than antagonist radioligand, it may be anticipated that [^{11}C]Cimbi-36 binding will also be sensitive to 5-HT release induced by dexfenfluramine 1 mg/kg in the human brain.

However, since fenfluramine has been withdrawn from the market because of cardiovascular toxicity (Hutcheson *et al*, 2011; Montani *et al*, 2013), in Study II, we evaluated the sensitivity of [^{11}C]AZ10419369 binding to 5-HT concentration enhancers which can be safely studied in humans. As discussed in section 4.2, the clinically relevant doses of these drugs and the robustness of ΔBP_{ND} suggested that the applied PET imaging paradigms hold promise to be successfully used in future human studies.

In Study III, the doses of vortioxetine 1.0 mg/kg and citalopram 0.3 mg/kg were selected as they result in around 80% 5-HTT occupancy, which is the proposed occupancy level required for therapeutic effects by SSRIs (Meyer *et al*, 2004). A lower dose of

vortioxetine (0.3 mg/kg) was selected to achieve 55% 5-HTT occupancy, and to represent the lower end of clinical doses (5–10 mg/day) (Areberg *et al*, 2012a; Garnock-Jones, 2014; Stenkrona *et al*, 2013). The clinical relevance of these doses was further supported by the comparable plasma concentrations of citalopram 0.3 mg/kg (119 nM), vortioxetine 0.3 mg/kg (38 nM) and vortioxetine 1.0 mg/kg (114 nM) to the clinical data for citalopram 20–60 mg/day (130–400 nM) (Bezchlibnyk-Butler *et al*, 2000) and vortioxetine 5–20 mg/day (30–110 nM) (Garnock-Jones, 2014). Based on the clinical relevance of the applied doses, it can thus be anticipated that the current results can be successfully translated into human studies.

The determined K_i value of the plasma concentration of vortioxetine for the 5-HTT (39±12 nM) in NHP (Study III) was modestly higher than previously measured in human (16–20 nM) (Areberg *et al*, 2012a; Stenkrona *et al*, 2013). Similar level of discrepancy between monkey and human 5-HTT K_i values have been reported for escitalopram (Finnema *et al*, 2015a; Lundberg *et al*, 2007) and venlafaxine (Meyer *et al*, 2004; Takano *et al*, 2013) in previous PET studies. Differences in the pharmacokinetic profile or the route of drug administration may have contributed to these modest differences (Areberg *et al*, 2012b; Finnema *et al*, 2015a; Takano *et al*, 2013). The estimated K_i value in the NHP brain was therefore considered to be consistent with previous human results.

In Study V, from a translational perspective (Finnema *et al*, 2015c), the pretreatment drugs were selected based on their applicability in future human studies. High doses of these drugs (Farde, 1992; Farde *et al*, 1988; Finnema *et al*, 2009, 2015c) were selected to maximize their effect on cAMP concentrations. Several *in vitro* or *ex vivo* studies in rodents have reported that there were changes in cAMP concentration consistent with the hypothesized directions of effects induced by SCH 23390 (Harrison and He, 2011; Skoblenick *et al*, 2010), amphetamine (Kelly *et al*, 2007; Ren *et al*, 2009), haloperidol (Skoblenick *et al*, 2010) or D_2R agonism (Cohen *et al*, 1992). However, the effects of these pretreatment drugs on cAMP concentrations in the living NHP brain remain unclear. Future studies are thus warranted to evaluate if [^{11}C]Lu AE92686 binding is sensitive to pretreatment with more specific modulators of cAMP concentrations, such as PDE2 or PDE4 inhibitors (Ooms *et al*, 2016) or modulators of adenylyl cyclase (Pavan *et al*, 2009) although such drugs can currently not be applied in human studies.

For reliable measurement of changes in radioligand binding, the test-retest variability for the applied PET imaging paradigm should be within an acceptable range (Finnema *et al*, 2015c; Paterson *et al*, 2010). The test-retest variability of [^{11}C]Lu AE92686 binding in Study V is comparable to previous human results (6% in striatum) (Kehler *et al*, 2014). Similarly, comparable test-retest variability of [^{11}C]AZ10419369 binding between NHP and human have also been reported (Finnema *et al*, 2012; Nord *et al*, 2014). These observations further support the high possibility for the translation of current NHP results into future human studies.

6 CONCLUSIONS AND FUTURE PERSPECTIVES

The present thesis work aimed to develop PET imaging paradigms that were sensitive to changes in the concentration of 5-HT or cAMP. These paradigms were applied to evaluate the mechanisms of action of antidepressant and antipsychotic drugs and are suitable for translation into future human studies.

The results in Study I suggested that [^{11}C]Cimbi-36 appears to be one of the most sensitive radioligands so far developed for detection of changes in 5-HT concentration in the primate brain. It is warranted to assess the sensitivity of [^{11}C]Cimbi-36 binding to smaller increases in 5-HT concentration such as induced by high doses of SSRIs or the pretreatment drugs applied in Study II. Similar evaluations have been performed for [^{11}C]AZ10419369 binding and supported the use of this radioligand in different experimental conditions (Nord *et al*, 2013). In addition, as discussed in section 5.2, it is also warranted to compare the 5-HT sensitivity of [^{11}C]Cimbi-36 and [^{11}C]MDL 100907 in awake humans to exclude potential anesthesia effects and to demonstrate the existence of 5-HT$_{2A}$ receptors in different functional states in the living human brain.

In Study II, we evaluated the sensitivity of [^{11}C]AZ10419369 binding to 5-HT concentration enhancers which can be safely studied in humans. The results suggest that all three PET imaging paradigms (amphetamine, MDMA and 5-HTP) have the potential to be utilized in future human studies. Moreover, although abnormal [^{11}C]5-HTP influx rate has been reported in patients with social anxiety disorder (Frick *et al*, 2015) or depression (Agren *et al*, 1991), the clinical application of [^{11}C]5-HTP might be limited by the difficulty in quantification due to trapping of [^{11}C]5-HTP in the reference region (Hagberg *et al*, 2002; Lundquist *et al*, 2006). Therefore, the developed PET imaging paradigm using cold 5-HTP as a pretreatment drug might be an alternative way to evaluate 5-HT synthesis in the human brain.

The feasibility to use the developed PET imaging paradigms to evaluate the mechanisms of action of vortioxetine, a novel antidepressant was demonstrated in Study III. The clinical relevance of applied vortioxetine and citalopram was supported by the 5-HTT occupancy and plasma drug concentrations. Our results suggested that at comparable 5-HTT occupancy, vortioxetine induced larger reductions in [^{11}C]AZ10419369 binding than citalopram. Based on the results in Study I, the lack of the effect of vortioxetine 1.0 mg/kg on [^{11}C]Cimbi-36 binding further supported the engagement of 5-HT$_{1B}$ receptor by vortioxetine at clinically relevant doses. Future studies are warranted to evaluate the role of 5-HT$_{1B}$ receptor in the antidepressant effects of vortioxetine and as a target for future development of more selective drugs.

According to the observations in Study IV, the method proposed for quantification of [^{11}C]Lu AE92686 binding in NHP is based on 63 min PET data and SRTM using cerebellum as the reference region. Moreover, the study supports that [^{11}C]Lu AE92686 can be used for PET examinations of PDE10A binding both in the striatum and SN. For more detailed

evaluation of potential influences from radiometabolites on the quantification, further studies are needed to characterize these radiometabolites, such as identification of their structures or radiolabelling them to examine their passage across the BBB.

In Study V, the results suggest that striatal [^{11}C]Lu AE92686 binding was sensitive to decreases in cAMP concentration and the effect was not consistent with the competition model. As in previous rodent studies, the observations might reflect alterations in the affinity of [^{11}C]Lu AE92686 to PDE10A induced by cAMP depletion. Moreover, we for the first time observed that the direction of BP_{ND} changes in the SN was opposite to that in the striatum. To clarify the underlying mechanism, future studies with Scatchard approaches (Farde *et al*, 1989) and/or to assess the changes in cAMP concentration both in the striatum and SN are warranted to examine the possible contribution from changes in affinity (Ginovart *et al*, 1997) and/or cAMP concentration, respectively.

It is important to know if the sensitivity of radioligand binding to cAMP concentration is specific for [^{11}C]Lu AE92686 and [^{18}F]JNJ42259152 or is a general characteristic of PDE10A radioligands. For example, decreased striatal [^{11}C]Lu AE92686 binding in schizophrenic patients has been reported (Bodén *et al*, 2017) while another study found no significant changes in [^{11}C]IMA107 binding (Marques *et al*, 2016). In addition to different clinical characteristics of the studied patients, the differences in the observations might originate from differences in the effect of alterations in cAMP concentration on radioligand binding between [^{11}C]Lu AE92686 and [^{11}C]IMA107. Therefore, the sensitivity of radioligand binding to cAMP concentration should be taken into account when interpreting changes in the binding of PDE10A radioligands.

In conclusion, the first part of the thesis work has advanced PET imaging paradigms that can detect changes in 5-HT concentration in the NHP brain. The robustness of the BP_{ND} changes and the application of pretreatment drugs at clinically relevant doses made the translation of current results into future human studies promising. Moreover, using the developed PET methodology, the engagement of the 5-HT_{1B} receptor by vortioxetine, a novel antidepressant was demonstrated. In the second part of the thesis work, the quantification method for a novel PDE10A radioligand, [^{11}C]Lu AE92686 was validated first which could provide reliable BP_{ND} values both in the striatum and SN. The following study revealed that the striatal [^{11}C]Lu AE92686 binding was sensitive to alterations in cAMP concentration that inconsistent with the competition model. In summary, the developed PET imaging paradigms can be used to evaluate the mechanisms of action of psychotropic drugs and may be safely translated into future human studies.

7 ACKNOWLEDGEMENTS

PET research is a team work and I would like to express my sincere gratitude to all of you who have contributed. I am especially thankful to:

Dr. Sjoerd J. Finnema, my principal supervisor, for guiding me into the field of PET and neuropsychopharmacology, for your invaluable support and encouragement, and for always being available for questions and discussions. Also, thank you for giving me enough space to explore the beauty of science as well as the guidance when I needed. I am really lucky and grateful to be the first PhD student mainly supervised by you.

Professor Lars Farde, my co-supervisor and one of the pioneers in psychiatric PET research, for teaching me scientific thinking and writing, and for sharing your broad expertise in neuropsychopharmacology and PET. I have enjoyed every moment of inspiration you provided and the trial to make things clearer by embracing the complexity in a realistic and problem-solving manner. It has been a great privilege to learn from you.

Professor Christer Halldin, my co-supervisor and director of KI PET Centre, for world-renowned expertise in radiochemistry, for your generous support, and for operating the PET center in such a successful way that also creates a superb research environment. It was a pleasurable experience to work under your leadership.

Dr. Akihiro Takano, my co-supervisor, for your great daily support and kind thoughts both for work and family life, for helping me settle in more quickly, and for all interesting and fruitful lunch talks. I also appreciated the comforting work atmosphere in the NHP team.

All research nurses for NHP studies: Gudrun Nylén, for teaching us everything about how to work with NHP for PET experiments; Jonas Ahlgren, Kia Hultberg-Lundberg and Anncathrin Kallin, for excellent skills in NHP care and experimental procedures. Thanks especially to Dr. Ryosuke Arakawa, for setting up several useful routines and substantial help; Dr. Junya Matsumoto, for helpful assistance and stimulating discussions. Thanks also to the AFL staff, for outstanding housing of NHP as well as all the participated NHP cousins.

All colleagues for radiochemistry: Dr. Vladimir Stepanov, for great support for several fields of radiochemistry; Dr. Zhisheng Jia, for helping me in both my personal and work life; Prodip Datta, Dr. Mahabuba Jahan, Dr. Peter Johnström, Dr. Mikhail Kondrashov, Anton Lindberg, Dr. Jonas Malmquist, Dr. Sangram Nag, Dr. Obaidur Rahman, Dr. Evgeny Revunov, Dr. Magnus Schou, Johan Ulin and Dr. Ana María Vázquez Romero, for high-quality radioligand production; Arsalan Amir, Guennadi Jogolev and Maria Johansson, for QC; Petra Agirman, Dr. Nahid Amini, Stefan Martinsson, Dr. Mohammed Mahdi Moein and Erik Nordlinder, for radiometabolite and other analyses of blood samples; Henrik Alfredéen, Dr. Arindam Das and Jacob Kihlström, for preparation of pretreatment drugs; Dr. Kenneth Dahl and Youssef EL Khoury, for chemical engineering.

All staff members of the PET group: Karin Zahir, for always being helpful for everything; Zilla Hallman and Agnetha Helgesson, for dealing with the practicalities; Anne Axelsson, Julio Gabriel, Nadja Hellsing and Göran Rosenqvist, for the operation/care of PET system and reconstruction of PET data; Urban Hansson, for IT support.

Dr. Jacqueline Borg, associate professor Simon Cervenka, assistant professor Anton Forsberg, professor Balazs Gulyás, associate professor Johan Lundberg, assistant professor Katarina Varnäs and associate professor Andrea Varrone, the senior academics of the PET group, for sharing your in-depth expertise, fruitful scientific input and valuable feedback. To the "classmates" of research meeting: Granville Matheson, Pontus Plavén-Sigray and Emma Veldman, for your well organization and not afraid to innovate; Dr. Max Andersson, Dr. Karin Collste, Dr. Jenny Häggkvist, Dr. Pauliina Ikonen, Dr. Benny Liberg, Dr. Patrik Mattson, Dr. Patricia Miranda Azpiazu, Dr. Martin Schain, Dr. Jonas Svensson, Ämma Tangen, Lenke Tari, Dr. Mikael Tiger and Dr. Miklòs Toth, for interesting discussions and great contributions. To wonderful roommates: Dr. Patrik Fazio, for fruitful discussions on research, career and family matters as well as helpful tips for preparation of dissertation; Dr. Ming Ai, Dr. Rafael Maior and Dr. Igor Yakushev, for broad knowledge and friendship.

All other colleagues of the PET group: Opokua Britton Cavaco, Dr. Zsolt Cselényi, Dr. Aurelija Jucaite, Dr. Naoki Kanegawa, Malena Kjellén, Nina Knave, Éva Lindström Böö, Dr. Magdalena Nord, Karin Olsson and Dr. Per Stenkrona, for lunchtime talk and help; Anne Byström, Dr. Davide D'Arienzo, Hanna Elgstrand, Siv Eriksson, Mélodie Ferrat, Kaisa Horkka, Dr. Raisa Krasikova, Adam Lada, Sara Lundqvist, Emma Meyer, Susanna Nevala, Zsolt Sarnyai, Dr. Ida Sonni, Carsten Steiger, Marie Svedberg and Åsa Södergren, for creating a nice work environment.

Collaborators at Center for Integrated Molecular Brain Imaging (Copenhagen), Dr. Anders Ettrup and professor Gitte M. Knudsen; at H. Lundbeck A/S (Valby/Paramus), Dr. Benny Bang-Andersen, Dr. Christoffer Bundgaard, Dr. Jacob Nielsen and Dr. Connie Sanchez; at Pfizer (Cambridge), Dr. Sarah Grimwood; at Orion Pharma (Nottingham), Dr. Mohammed Shahid, for great collaboration and sharing your excellent scientific skills.

Associate Professor Yuan-Hwa Chou, my mentor, for guiding me the first steps in psychiatric and neuroimaging research, paving the way to KI and always being supportive.

My father, Cheng-Tsung who passed away suddenly and unexpectedly 6 years ago and my mother, Ying-Fen, for giving me a good start in life, for your unconditional love, and for always believing in me and encouraging me to do what I like; my brother, Hsin-Wei, for your continuous support, especially for taking care of the family.

My beloved wife, Ying-Hsiu, for your endless love and patience, for your devotion to our family and for all the moments we spent together. Without you, I couldn't have made this journey possible; my lovely daughter, Cing-Mei, for filling our lives with happiness and meaning.

8 REFERENCES

Aalto S, Hirvonen J, Kaasinen V, *et al* (2009). The effects of d-amphetamine on extrastriatal dopamine D2/D 3 receptors: A randomized, double-blind, placebo-controlled PET study with [11C]FLB 457 in healthy subjects. *Eur J Nucl Med Mol Imaging* **36**: 475–483.

Abi-Dargham A, Rodenhiser J, Printz D, *et al* (2000). Increased baseline occupancy of D2 receptors by dopamine in schizophrenia. *Proc Natl Acad Sci U S A* **97**: 8104–8109.

Adell A, Celada P, Abellán MT, *et al* (2002). Origin and functional role of the extracellular serotonin in the midbrain raphe nuclei. *Brain Res Rev* **39**: 154–180.

Agren H, Reibring L, Hartvig P, *et al* (1991). Low brain uptake of L-[11C]5-hydroxytryptophan in major depression: a positron emission tomography study on patients and healthy volunteers. *Acta Psychiatr Scand* **83**: 449–455.

Andersson JD, Pierson ME, Finnema SJ, *et al* (2011). Development of a PET radioligand for the central 5-HT1B receptor: Radiosynthesis and characterization in cynomolgus monkeys of eight radiolabeled compounds. *Nucl Med Biol* **38**: 261–272.

Areberg J, Luntang-Jensen M, Søgaard B, *et al* (2012a). Occupancy of the serotonin transporter after administration of Lu AA21004 and its relation to plasma concentration in healthy subjects. *Basic Clin Pharmacol Toxicol* **110**: 401–404.

Areberg J, Sogaard B, Hojer AM (2012b). The clinical pharmacokinetics of Lu AA21004 and its major metabolite in healthy young volunteers. *Basic Clin Pharmacol Toxicol* **111**: 198–205.

Avants BB, Epstein CL, Grossman M, *et al* (2008). Symmetric diffeomorphic image registration with cross-correlation: Evaluating automated labeling of elderly and neurodegenerative brain. *Med Image Anal* **12**: 26–41.

Avants BB, Yushkevich P, Pluta J, *et al* (2010). The optimal template effect in hippocampus studies of diseased populations. *Neuroimage* **49**: 2457–2466.

Bang-Andersen B, Ruhland T, Jørgensen M, *et al* (2011). Discovery of 1-[2-(2,4-dimethylphenylsulfanyl)phenyl]piperazine (Lu AA21004): a novel multimodal compound for the treatment of major depressive disorder. *J Med Chem* **54**: 3206–3221.

Barnes NM, Sharp T (1999). A review of central 5-HT receptors and their function. *Neuropharmacology* **38**: 1083–1152.

Barret O, Thomae D, Tavares A, *et al* (2014). In vivo assessment and dosimetry of 2 novel PDE10A PET radiotracers in humans: 18F-MNI-659 and 18F-MNI-654. *J Nucl Med* **55**: 1297–1304.

Baumann MH, Williams Z, Zolkowska D, *et al* (2011). Serotonin (5-HT) precursor loading with 5-hydroxy-l-tryptophan (5-HTP) reduces locomotor activation produced by (+)-amphetamine in the rat. *Drug Alcohol Depend* **114**: 147–152.

Beavo JA, Brunton LL (2002). Cyclic nucleotide research -- still expanding after half a century. *Nat Rev Mol Cell Biol* **3**: 710–718.

Belenky MA, Pickard GE (2001). Subcellular distribution of 5-HT1B and 5-HT7 receptors in the mouse suprachiasmatic nucleus. *J Comp Neurol* **432**: 371–388.

Berckel BNM van, Kegeles LS, Waterhouse R, *et al* (2006). Modulation of amphetamine-induced dopamine release by group II metabotropic glutamate receptor agonist LY354740 in non-human primates studied with positron emission tomography. *Neuropsychopharmacology* **31**: 967–977.

Besnard J, Ruda GF, Setola V, *et al* (2012). Automated design of ligands to polypharmacological profiles. *Nature* **492**: 215–220.

Best J, Nijhout HF, Reed M (2010). Serotonin synthesis, release and reuptake in terminals: A mathematical model. *Theor Biol Med Model* **7**: 34.

Bezchlibnyk-Butler K, Aleksic I, Kennedy SH (2000). Citalopram--a review of pharmacological and clinical

effects. *J Psychiatry Neurosci* **25**: 241–254.

Bhattacharyya S, Puri S, Miledi R, *et al* (2002). Internalization and recycling of 5-HT2A receptors activated by serotonin and protein kinase C-mediated mechanisms. *Proc Natl Acad Sci U S A* **99**: 14470–14475.

Blier P, Montigny C de (1994). Current advances and trends in the treatment of depression. *Trends Pharmacol Sci* **15**: 220–226.

Bockaert J, Claeysen S, Compan V, *et al* (2008). 5-HT4 receptors: History, molecular pharmacology and brain functions. *Neuropharmacology* **55**: 922–931.

Bodén R, Persson J, Wall A, *et al* (2017). Striatal phosphodiesterase 10A and medial prefrontal cortical thickness in patients with schizophrenia: a PET and MRI study. *Transl Psychiatry* **7**: e1050.

Bouaziz E, Emerit MB, Vodjdani G, *et al* (2014). Neuronal phenotype dependency of agonist-induced internalization of the 5-HT(1A) serotonin receptor. *J Neurosci* **34**: 282–294.

Bowyer JF, Young JF, Slikker W, *et al* (2003). Plasma levels of parent compound and metabolites after doses of either d-fenfluramine or d-3,4-methylenedioxymethamphetamine (MDMA) that produce long-term serotonergic alterations. *Neurotoxicology* **24**: 379–390.

Brailov I, Bancila M, Brisorgueil MJ, *et al* (2000). Localization of 5-HT6 receptors at the plasma membrane of neuronal cilia in the rat brain. *Brain Res* **872**: 271–275.

Bundgaard C, Eneberg E, Sánchez C (2016). P-glycoprotein differentially affects escitalopram, levomilnacipran, vilazodone and vortioxetine transport at the mouse blood-brain barrier in vivo. *Neuropharmacology* **103**: 104–111.

Button KS, Ioannidis JPA, Mokrysz C, *et al* (2013). Power failure: why small sample size undermines the reliability of neuroscience. *Nat Rev Neurosci* **14**: 365–376.

Caccia S, Ballabio M, Ponte P De (1979). Pharmacokinetics of fenfluramine enantiomers in man. *Eur J Drug Metab Pharmacokinet* **4**: 129–132.

Calabrese E, Badea A, Coe CL, *et al* (2015). A diffusion tensor MRI atlas of the postmortem rhesus macaque brain. *Neuroimage* **117**: 408–416.

Calabresi P, Picconi B, Tozzi A, *et al* (2014). Direct and indirect pathways of basal ganglia: a critical reappraisal. *Nat Neurosci* **17**: 1022–1030.

Capitanio JP, Emborg ME (2008). Contributions of non-human primates to neuroscience research. *Lancet* **371**: 1126–1135.

Carpenter WT, Koenig JI (2008). The evolution of drug development in schizophrenia: Past issues and future opportunities. *Neuropsychopharmacology* **33**: 2061–2079.

Carrel D, Simon A, Emerit MB, *et al* (2011). Axonal targeting of the 5-HT 1B serotonin receptor relies on structure-specific constitutive activation. *Traffic* **12**: 1501–1520.

Carson RE (2000). PET physiological measurements using constant infusion. *Nucl Med Biol* **27**: 657–660.

Carson RE, Channing MA, Blasberg RG, *et al* (1993). Comparison of bolus and infusion methods for receptor quantitation: application to [18F]cyclofoxy and positron emission tomography. *J Cereb Blood Flow Metab* **13**: 24–42.

Carson RE, Kiesewetter DO, Jagoda E, *et al* (1998). Muscarinic cholinergic receptor measurements with [18F]FP-TZTP: control and competition studies. *J Cereb Blood Flow Metab* **18**: 1130–1142.

Celen S, Koole M, Ooms M, *et al* (2013). Preclinical evaluation of [18F]JNJ42259152 as a PET tracer for PDE10A. *Neuroimage* **82**: 13–22.

Chanrion B, Mannoury la Cour C, Bertaso F, *et al* (2007). Physical interaction between the serotonin transporter and neuronal nitric oxide synthase underlies reciprocal modulation of their activity. *Proc Natl Acad Sci U S A* **104**: 8119–8124.

Charych EI, Jiang L-X, Lo F, *et al* (2010). Interplay of palmitoylation and phosphorylation in the trafficking and

localization of phosphodiesterase 10A: implications for the treatment of schizophrenia. *J Neurosci* **30**: 9027–9037.

Chen L, Salinas GD, Li X (2009). Regulation of serotonin 1B receptor by glycogen synthase kinase-3. *Mol Pharmacol* **76**: 1150–1161.

Cherry SR (2001). Fundamentals of positron emission tomography and applications in preclinical drug development. *J Clin Pharmacol* **41**: 482–491.

Chou Y-H, Wang S-J, Lirng J-F, *et al* (2012). Impaired cognition in bipolar I disorder: the roles of the serotonin transporter and brain-derived neurotrophic factor. *J Affect Disord* **143**: 131–137.

Clawges HM, Depree KM, Parker EM, *et al* (1997). Human 5-HT1 receptor subtypes exhibit distinct G protein coupling behaviors in membranes from Sf9 cells. *Biochemistry* **36**: 12930–12938.

Cohen AI, Todd RD, Harmon S, *et al* (1992). Photoreceptors of mouse retinas possess D4 receptors coupled to adenylate cyclase. *Proc Natl Acad Sci U S A* **89**: 12093–12097.

Cohen RM, Carson RE, Filbey F, *et al* (2006). Age and APOE-ε4 genotype influence the effect of physostigmine infusion on the in-vivo distribution volume of the muscarinic-2-receptor dependent tracer [18F]FP-TZTP. *Synapse* **60**: 86–92.

Colasanti A, Searle GE, Long CJ, *et al* (2012). Endogenous opioid release in the human brain reward system induced by acute amphetamine administration. *Biol Psychiatry* **72**: 371–377.

Conti M, Beavo J (2007). Biochemistry and physiology of cyclic nucleotide phosphodiesterases: essential components in cyclic nucleotide signaling. *Annu Rev Biochem* **76**: 481–511.

Cools R, Nakamura K, Daw ND (2011). Serotonin and dopamine: unifying affective, activational, and decision functions. *Neuropsychopharmacology* **36**: 98–113.

Cosgrove KP, Kloczynski T, Nabulsi N, *et al* (2011). Assessing the sensitivity of [11C]p943, a novel 5-HTIB radioligand, to endogenous serotonin release. *Synapse* **65**: 1113–1117.

Coskran TM, Morton D, Menniti FS, *et al* (2006). Immunohistochemical Localization of Phosphodiesterase 10A in Multiple Mammalian Species. *J Histochem Cytochem* **54**: 1205–1213.

Council NR (National Academies Press (US): Washington, DC, 2011). *Guide for the Care and Use of Laboratory Animals*, 8th edn.

David DJP, Bourin M, Jego G, *et al* (2003). Effects of acute treatment with paroxetine, citalopram and venlafaxine in vivo on noradrenaline and serotonin outflow: a microdialysis study in Swiss mice. *Br J Pharmacol* **140**: 1128–1136.

Dayer AG, Jacobshagen M, Chaumont-Dubel S, *et al* (2015). 5-HT6 receptor: a new player controlling the development of neural circuits. *ACS Chem Neurosci* **6**: 951–960.

Delorenzo C, Dellagioia N, Bloch M, *et al* (2015). In vivo ketamine-induced changes in [11C]ABP688 binding to metabotropic glutamate receptor subtype 5. *Biol Psychiatry* **77**: 266–275.

DiMasi JA, Feldman L, Seckler A, *et al* (2009). Trends in risks associated with new drug development: success rates for investigational drugs. *Clin Pharmacol Ther* **87**: 272–277.

Ding YS, Logan J, Bermel R, *et al* (2000). Dopamine receptor-mediated regulation of striatal cholinergic activity: Positron emission tomography studies with norchloro [18F] fluoroepibatidine. *J Neurochem* **74**: 1514–1521.

Donkelaar EL van, Blokland A, Ferrington L, *et al* (2011). Mechanism of acute tryptophan depletion: is it only serotonin? *Mol Psychiatry* **16**: 695–713.

Elfving B, Bjørnholm B, Knudsen GM (2003). Interference of anaesthetics with radioligand binding in neuroreceptor studies. *Eur J Nucl Med Mol Imaging* **30**: 912–915.

Endres CJ, Carson RE (1998). Assessment of dynamic neurotransmitter changes with bolus or infusion delivery of neuroreceptor ligands. *J Cereb Blood Flow Metab* **18**: 1196–1210.

Ettrup A, Cunha-Bang S da, McMahon B, *et al* (2014). Serotonin 2A receptor agonist binding in the human brain with [11C]Cimbi-36. *J Cereb Blood Flow Metab* **34**: 1188–1196.

Ettrup A, Hansen M, Santini MA, *et al* (2011). Radiosynthesis and in vivo evaluation of a series of substituted 11C-phenethylamines as 5-HT2A agonist PET tracers. *Eur J Nucl Med Mol Imaging* **38**: 681–693.

Ettrup A, Svarer C, McMahon B, *et al* (2016). Serotonin 2A receptor agonist binding in the human brain with [11C]Cimbi-36: Test-retest reproducibility and head-to-head comparison with the antagonist [18F]altanserin. *Neuroimage* **130**: 167–174.

Farde L (1992). Selective D1- and D2-dopamine receptor blockade both induces akathisia in humans - a PET study with [11C]SCH 23390 and [11C]raclopride. *Psychopharmacology (Berl)* **107**: 23–29.

Farde L (1996). The advantage of using positron emission tomography in drug research. *Trends Neurosci* **19**: 211–214.

Farde L, Eriksson L, Blomquist G, *et al* (1989). Kinetic analysis of central [11C]raclopride binding to D2-dopamine receptors studied by PET--a comparison to the equilibrium analysis. *J Cereb Blood Flow Metab* **9**: 696–708.

Farde L, Hall H, Pauli S, *et al* (1995). Variability in D2-dopamine receptor density and affinity: A PET study with [11C]raclopride in man. *Synapse* **20**: 200–208.

Farde L, Wiesel F-A, Halldin C, *et al* (1988). Central D2-dopamine receptor occupancy in schizophrenic patients treated with antipsychotic drugs. *Arch Gen Psychiatry* **45**: 71–76.

Finnema SJ, Bang-Andersen B, Wikström H V., *et al* (2010a). Current state of agonist radioligands for imaging of brain dopamine D2/D3 receptors in vivo with positron emission tomography. *Curr Top Med Chem* **10**: 1477–1498.

Finnema SJ, Halldin C, Bang-Andersen B, *et al* (2009). Dopamine D2/3 receptor occupancy of apomorphine in the nonhuman primate brain - A comparative PET study with [11C]raclopride and [11C]MNPA. *Synapse* **63**: 378–389.

Finnema SJ, Halldin C, Bang-Andersen B, *et al* (2015a). Serotonin transporter occupancy by escitalopram and citalopram in the non-human primate brain: A [11C]MADAM PET study. *Psychopharmacology (Berl)* **232**: 4159–4167.

Finnema SJ, Hughes ZA, Haaparanta-solin M, *et al* (2015b). Amphetamine decreases α2C-adrenoceptor binding of [11C]ORM-13070: A PET study in the primate brain. *Int J Neuropsychopharmacol* **18**: 1–10.

Finnema SJ, Scheinin M, Shahid M, *et al* (2015c). Application of cross-species PET imaging to assess neurotransmitter release in brain. *Psychopharmacology (Berl)* **232**: 4129–4157.

Finnema SJ, Stepanov V, Ettrup A, *et al* (2014). Characterization of [11C]Cimbi-36 as an agonist PET radioligand for the 5-HT2A and 5-HT2C receptors in the nonhuman primate brain. *Neuroimage* **84**: 342–353.

Finnema SJ, Varrone A, Hwang T-J, *et al* (2010b). Fenfluramine-induced serotonin release decreases [11C]AZ10419369 binding to 5-HT1B-receptors in the primate brain. *Synapse* **64**: 573–577.

Finnema SJ, Varrone A, Hwang T-J, *et al* (2012). Confirmation of fenfluramine effect on 5-HT(1B) receptor binding of [(11)C]AZ10419369 using an equilibrium approach. *J Cereb Blood Flow Metab* **32**: 685–695.

Fiorentini C, Savoia P, Bono F, *et al* (2015). The D3 dopamine receptor: From structural interactions to function. *Eur Neuropsychopharmacol* **25**: 1462–1469.

Fitzgerald LW, Conklin DS, Krause CM, *et al* (1999). High-affinity agonist binding correlates with efficacy (intrinsic activity) at the human serotonin 5-HT2A and 5-HT2C receptors: evidence favoring the ternary complex and two-state models of agonist action. *J Neurochem* **72**: 2127–2134.

Fleckenstein AE, Volz TJ, Riddle EL, *et al* (2007). New insights into the mechanism of action of amphetamines. *Annu Rev Pharmacol Toxicol* **47**: 681–698.

Frankle WG, Cho RY, Mason NS, *et al* (2012). [11C]flumazenil binding is increased in a dose-dependent

manner with tiagabine-induced elevations in GABA levels. *PLoS One* **7**: e32443.

Frankle WG, Cho RY, Narendran R, *et al* (2009). Tiagabine increases [11C]flumazenil binding in cortical brain regions in healthy control subjects. *Neuropsychopharmacology* **34**: 624–633.

Frankle WG, Cho RY, Prasad KM, *et al* (2015). In vivo measurement of GABA transmission in healthy subjects and schizophrenia patients. *Am J Psychiatry* **172**: 1148–1159.

Frick A, Åhs F, Engman J, *et al* (2015). Serotonin synthesis and reuptake in social anxiety disorder: A positron emission tomography study. *JAMA Psychiatry* **72**: 794–802.

Friedman AM, Dejesus OT, Revenaugh J, *et al* (1984). Measurements in vivo of parameters of the dopamine system. *Ann Neurol* **15**: 66–76.

Fujishige K, Kotera J, Michibata H, *et al* (1999). Cloning and characterization of a novel human phosphodiesterase that hydrolyzes both cAMP and cGMP (PDE10A). *J Biol Chem* **274**: 18438–18445.

Fujita M, Richards EM, Niciu MJ, *et al* (2017). cAMP signaling in brain is decreased in unmedicated depressed patients and increased by treatment with a selective serotonin reuptake inhibitor. *Mol Psychiatry* **22**: 754–759.

Gallezot J-D, Esterlis I, Bois F, *et al* (2014a). Evaluation of the sensitivity of the novel α4β2* nicotinic acetylcholine receptor PET radioligand ^{18}F-(-)-NCFHEB to increases in synaptic acetylcholine levels in rhesus monkeys. *Synapse* **68**: 556–564.

Gallezot J-D, Kloczynski T, Weinzimmer D, *et al* (2014b). Imaging nicotine- and amphetamine-induced dopamine release in rhesus monkeys with [11C]PHNO vs [11C]raclopride PET. *Neuropsychopharmacology* **39**: 866–874.

Gamma A, Buck A, Berthold T, *et al* (2000). 3,4-Methylenedioxymethamphetamine (MDMA) modulates cortical and limbic brain activity as measured by [H(2)(15)O]-PET in healthy humans. *Neuropsychopharmacology* **23**: 388–395.

Garnock-Jones KP (2014). Vortioxetine: A review of its use in major depressive disorder. *CNS Drugs* **28**: 855–874.

Gartside SE, Hajós-Korcsok E, Bagdy E, *et al* (2000). Neurochemical and electrophysiological studies on the functional significance of burst firing in serotonergic neurons. *Neuroscience* **98**: 295–300.

Gartside SE, Umbers V, Hajós M, *et al* (1995). Interaction between a selective 5-HT1A receptor antagonist and an SSRI in vivo: effects on 5-HT cell firing and extracellular 5-HT. *Br J Pharmacol* **115**: 1064–1070.

Gérard C, Martres MP, Lefèvre K, *et al* (1997). Immune-localization of serotonin 5-HT6 receptor-like material in the rat central nervous system. *Brain Res* **746**: 207–219.

Ginovart N (2005). Imaging the dopamine system with in vivo [11C]raclopride displacement studies: Understanding the true mechanism. *Mol Imaging Biol* **7**: 45–52.

Ginovart N, Farde L, Halldin C, *et al* (1997). Effect of reserpine-induced depletion of synaptic dopamine on [11C]raclopride binding to D2-dopamine receptors in the monkey brain. *Synapse* **25**: 321–325.

Giorgi M, Melchiorri G, Nuccetelli V, *et al* (2011). PDE10A and PDE10A-dependent cAMP catabolism are dysregulated oppositely in striatum and nucleus accumbens after lesion of midbrain dopamine neurons in rat: A key step in parkinsonism physiopathology. *Neurobiol Dis* **43**: 293–303.

Giovacchini G, Lang L, Ma Y, *et al* (2005). Differential effects of paroxetine on raphe and cortical 5-HT1A binding: A PET study in monkeys. *Neuroimage* **28**: 238–248.

Gould RW, Duke AN, Nader MA (2014). PET studies in nonhuman primate models of cocaine abuse: Translational research related to vulnerability and neuroadaptations. *Neuropharmacology* **84**: 138–151.

Grånäs C, Nordquist J, Mohell N, *et al* (2001). Site-directed mutagenesis of the 5-HT1B receptor increases the affinity of 5-HT for the agonist low-affinity conformation and reduces the intrinsic activity of 5-HT. *Eur J Pharmacol* **421**: 69–76.

Gray JA, Bhatnagar A, Gurevich V V, *et al* (2003). The interaction of a constitutively active arrestin with the arrestin-insensitive 5-HT(2A) receptor induces agonist-independent internalization. *Mol Pharmacol* **63**: 961–972.

Gray JA, Roth BL (2001). Paradoxical trafficking and regulation of 5-HT2A receptors by agonists and antagonists. *Brain Res Bull* **56**: 441–451.

Grimwood S, Hartig PR (2009). Target site occupancy: Emerging generalizations from clinical and preclinical studies. *Pharmacol Ther* **122**: 281–301.

Guiard BP, Giovanni G Di (2015). Central serotonin-2A (5-HT2A) receptor dysfunction in depression and epilepsy: The missing link? *Front Pharmacol* **6**: 46.

Gulyás B, Sjöholm N (2007). Principles of positron emission tomography. *Funct neuroimaging Clin Popul* 3–30.

Gunn RN, Sargent PA, Bench CJ, *et al* (1998). Tracer kinetic modeling of the 5-HT1A receptor ligand [carbonyl-11C]WAY-100635 for PET. *Neuroimage* **8**: 426–440.

Gunn RN, Slifstein M, Searle GE, *et al* (2015). Quantitative imaging of protein targets in the human brain with PET. *Phys Med Biol* **60**: R363–R411.

Guterstam J, Jayaram-Lindström N, Cervenka S, *et al* (2013). Effects of amphetamine on the human brain opioid system--a positron emission tomography study. *Int J Neuropsychopharmacol* **16**: 763–769.

Hagberg GE, Torstenson R, Marteinsdottir I, *et al* (2002). Kinetic compartment modeling of [11C]-5-hydroxy-L-tryptophan for positron emission tomography assessment of serotonin synthesis in human brain. *J Cereb Blood Flow Metab* **22**: 1352–1366.

Hall H, Farde L, Halldin C, *et al* (2000). Autoradiographic localization of 5-HT(2A) receptors in the human brain using [3H]M100907 and [11C]M100907. *Synapse* **38**: 421–431.

Halldin C, Gulyás B, Farde L (2001a). PET studies with carbon-11 radioligands in neuropsychopharmacological drug development. *Curr Pharm Des* **7**: 1907–1929.

Halldin C, Gulyás B, Langer O, *et al* (2001b). Brain radioligands--state of the art and new trends. *Q J Nucl Med* **45**: 139–152.

Halldin C, Lundberg J, Sóvágó J, *et al* (2005). [11C]MADAM, a new serotonin transporter radioligand characterized in the monkey brain by PET. *Synapse* **58**: 173–183.

Hannon J, Hoyer D (2008). Molecular biology of 5-HT receptors. *Behav Brain Res* **195**: 198–213.

Harada N, Nishiyama S, Ohba H, *et al* (2002). Age differences in phosphodiesterase type-IV and its functional response to dopamine D1 receptor modulation in the living brain: A PET study in conscious monkeys. *Synapse* **44**: 139–145.

Hargreaves RJ, Rabiner EA (2014). Translational PET imaging research. *Neurobiol Dis* **61**: 32–38.

Harrison LM, He Y (2011). Rhes and AGS1/Dexras1 affect signaling by dopamine D1 receptors through adenylyl cyclase. *J Neurosci Res* **89**: 874–882.

Hayes JF, Miles J, Walters K, *et al* (2015). A systematic review and meta-analysis of premature mortality in bipolar affective disorder. *Acta Psychiatr Scand* **131**: 417–425.

Hazelwood L a, Sanders-Bush E (2004). His452Tyr polymorphism in the human 5-HT2A receptor destabilizes the signaling conformation. *Mol Pharmacol* **66**: 1293–1300.

Heal DJ, Smith SL, Gosden J, *et al* (2013). Amphetamine, past and present--a pharmacological and clinical perspective. *J Psychopharmacol* **27**: 479–496.

Hervás I, Artigas F (1998). Effect of fluoxetine on extracellular 5-hydroxytryptamine in rat brain. Role of 5-HT autoreceptors. *Eur J Pharmacol* **358**: 9–18.

Hillmer AT, Esterlis I, Gallezot JD, *et al* (2016). Imaging of cerebral α4β2* nicotinic acetylcholine receptors with (−)-[18F]Flubatine PET: Implementation of bolus plus constant infusion and sensitivity to

acetylcholine in human brain. *Neuroimage* **141**: 71–80.

Hillmer AT, Wooten DW, Farhoud M, *et al* (2013). PET imaging of acetylcholinesterase inhibitor-induced effects on α4β2 nicotinic acetylcholine receptor binding. *Synapse* **67**: 882–886.

Holland JP, Cumming P, Vasdev N (2013). PET radiopharmaceuticals for probing enzymes in the brain. *Am J Nucl Med Mol Imaging* **3**: 194–216.

Hornung JP (2003). The human raphe nuclei and the serotonergic system. *J Chem Neuroanat* **26**: 331–343.

Howes OD, Kambeitz J, Kim E, *et al* (2012). The nature of dopamine dysfunction in schizophrenia and what this means for treatment. *Arch Gen Psychiatry* **69**: 776–786.

Hume SP, Myers R, Bloomfield PM, *et al* (1992). Quantitation of Carbon-11-labeled raclopride in rat striatum using positron emission tomography. *Synapse* **12**: 47–54.

Hutcheson JD, Setola V, Roth BL, *et al* (2011). Serotonin receptors and heart valve disease-It was meant 2B. *Pharmacol Ther* **132**: 146–157.

Hwang D-R, Hu E, Allen JR, *et al* (2015). Radiosynthesis and initial characterization of a PDE10A specific PET tracer [18F]AMG 580 in non-human primates. *Nucl Med Biol* **42**: 654–663.

Hwang D-R, Hu E, Rumfelt S, *et al* (2014). Initial characterization of a PDE10A selective positron emission tomography tracer [11 C] AMG 7980 in non-human primates. *Nucl Med Biol* **41**: 343–349.

Ichise M, Meyer JH, Yonekura Y (2001). An introduction to PET and SPECT neuroreceptor quantification models. *J Nucl Med* **42**: 755–763.

Innis RB, Cunningham VJ, Delforge J, *et al* (2007). Consensus nomenclature for in vivo imaging of reversibly binding radioligands. *J Cereb Blood Flow Metab* **27**: 1533–1539.

Invernizzi R, Belli S, Samanin R (1992). Citalopram's ability to increase the extracellular concentrations of serotonin in the dorsal raphe prevents the drug's effect in the frontal cortex. *Brain Res* **584**: 322–324.

Itoh T, Abe K, Hong J, *et al* (2010). Effects of cAMP-dependent protein kinase activator and inhibitor on in vivo rolipram binding to phosphodiesterase 4 in conscious rats. *Synapse* **64**: 172–176.

Jacobsen JP, Rudder ML, Roberts W, *et al* (2016). SSRI Augmentation by 5-hydroxytryptophan slow release: mouse pharmacodynamic proof of concept. *Neuropsychopharmacology* **41**: 2324–2334.

Jäger R, Russwurm C, Schwede F, *et al* (2012). Activation of PDE10 and PDE11 phosphodiesterases. *J Biol Chem* **287**: 1210–1219.

Jansson A, Tinner B, Bancila M, *et al* (2001). Relationships of 5-hydroxytryptamine immunoreactive terminal-like varicosities to 5-hydroxytryptamine-2A receptor-immunoreactive neuronal processes in the rat forebrain. *J Chem Neuroanat* **22**: 185–203.

Janušonis S (2009). Comparing two small samples with an unstable, treatment-independent baseline. *J Neurosci Methods* **179**: 173–178.

Jardin KG du, Jensen JB, Sanchez C, *et al* (2014). Vortioxetine dose-dependently reverses 5-HT depletion-induced deficits in spatial working and object recognition memory: A potential role for 5-HT1A receptor agonism and 5-HT3 receptor antagonism. *Eur Neuropsychopharmacol* **24**: 160–171.

Jardin KG du, Liebenberg N, Müller HK, *et al* (2016). Differential interaction with the serotonin system by S-ketamine, vortioxetine, and fluoxetine in a genetic rat model of depression. *Psychopharmacology (Berl)* **233**: 2813–2825.

Jayaram-Lindström N, Guterstam J, Häggkvist J, *et al* (2017). Naltrexone modulates dopamine release following chronic, but not acute amphetamine administration: a translational study. *Transl Psychiatry* **7**: e1104.

Jørgensen TN, Christensen PM, Gether U (2014). Serotonin-induced down-regulation of cell surface serotonin transporter. *Neurochem Int* **73**: 107–112.

Kaddoumi A, Nakashima MN, Maki T, *et al* (2003). Liquid chromatography studies on the pharmacokinetics of phentermine and fenfluramine in brain and blood microdialysates after intraperitoneal administration to

rats. *J Chromatogr B Anal Technol Biomed Life Sci* **791**: 291–303.

Kehler J, Kilburn JP, Estrada S, *et al* (2014). Discovery and development of 11C-Lu AE92686 as a radioligand for PET imaging of phosphodiesterase10A in the brain. *J Nucl Med* **55**: 1513–1518.

Kelly MP, Isiegas C, Cheung Y-F, *et al* (2007). Constitutive activation of Galphas within forebrain neurons causes deficits in sensorimotor gating because of PKA-dependent decreases in cAMP. *Neuropsychopharmacology* **32**: 577–588.

Kim SH, Kim DH, Lee KH, *et al* (2014). Direct interaction and functional coupling between human 5-HT6 receptor and the light chain 1 subunit of the microtubule-associated protein 1B (MAP1B-LC1). *PLoS One* **9**: e91402.

Kish SJ, Furukawa Y, Chang LJ, *et al* (2005). Regional distribution of serotonin transporter protein in postmortem human brain: Is the cerebellum a SERT-free brain region? *Nucl Med Biol* **32**: 123–128.

Kranz GS, Hahn A, Savli M, *et al* (2012). Challenges in the differentiation of midbrain raphe nuclei in neuroimaging research. *Proc Natl Acad Sci U S A* **109**: E2000–E2000.

Krishnan V, Nestler EJ (2008). The molecular neurobiology of depression. *Nature* **455**: 894–902.

Kristensen AS, Andersen J, Jørgensen TN, *et al* (2011). SLC6 Neurotransmitter Transporters: Structure, Function, and Regulation. *Pharmacol Rev* **63**: 585–640.

Laere K Van, Ahmad RU, Hudyana H, *et al* (2013). Quantification of 18F-JNJ-42259152, a novel phosphodiesterase 10A PET tracer: kinetic modeling and test-retest study in human brain. *J Nucl Med* **54**: 1285–1293.

Lammertsma AA, Bench CJ, Hume SP, *et al* (1996). Comparison of methods for analysis of clinical [11C]raclopride studies. *J Cereb Blood Flow Metab* **16**: 42–52.

Lammertsma AA, Hume SP (1996). Simplified reference tissue model for PET receptor studies. *Neuroimage* **4**: 153–158.

Lanfumey L, Hamon M (2000). Central 5-HT(1A) receptors: regional distribution and functional characteristics. *Nucl Med Biol* **27**: 429–435.

Lanzenberger R, Kranz GS, Haeusler D, *et al* (2012). Prediction of SSRI treatment response in major depression based on serotonin transporter interplay between median raphe nucleus and projection areas. *Neuroimage* **63**: 874–881.

Laruelle M (2000). Imaging synaptic neurotransmission with in vivo binding competition techniques: a critical review. *J Cereb Blood Flow Metab* **20**: 423–451.

Laruelle M, D'Souza CD, Baldwin RM, *et al* (1997). Imaging D2 receptor occupancy by endogenous dopamine in humans. *Neuropsychopharmacology* **17**: 162–174.

Laruelle M, Slifstein M, Huang Y (2003). Relationships between radiotracer properties and image quality in molecular imaging of the brain with positron emission tomography. *Mol Imaging Biol* **5**: 363–375.

Lau T, Horschitz S, Berger S, *et al* (2008). Antidepressant-induced internalization of the serotonin transporter in serotonergic neurons. *FASEB J* **22**: 1702–1714.

Lean A De, Stadel JM, Lefkowitz RJ (1980). A ternary complex model explains the agonist-specific binding properties of the adenylate cyclase-coupled beta-adrenergic receptor. *J Biol Chem* **255**: 7108–7117.

Lechin F, Dijs B van der, Hernández-Adrián G (2006). Dorsal raphe vs. median raphe serotonergic antagonism. Anatomical, physiological, behavioral, neuroendocrinological, neuropharmacological and clinical evidences: Relevance for neuropharmacological therapy. *Prog Neuro-Psychopharmacology Biol Psychiatry* **30**: 565–585.

Lee C-M, Farde L (2006). Using positron emission tomography to facilitate CNS drug development. *Trends Pharmacol Sci* **27**: 310–316.

Lehto J, Johansson J, Vuorilehto L, *et al* (2015). Sensitivity of [11C]ORM-13070 to increased extracellular

noradrenaline in the CNS – a PET study in human subjects. *Psychopharmacology (Berl)* **232**: 4169–4178.

Lesch KP, Waider J (2012). Serotonin in the modulation of neural plasticity and networks: implications for neurodevelopmental disorders. *Neuron* **76**: 175–191.

Liebmann T, Kruusmägi M, Sourial-Bassillious N, *et al* (2012). A noncanonical postsynaptic transport route for a GPCR belonging to the serotonin receptor family. *J Neurosci* **32**: 17998–18008.

Lin S, Labaree D, Chen M, *et al* (2015). Further evaluation of [11C]MP-10 as a radiotracer for phosphodiesterase 10A: PET imaging study in rhesus monkeys and brain tissue metabolite analysis. *Synapse* **69**: 86–95.

Liu H, Jin H, Yue X, *et al* (2015). Preclinical evaluation of a promising C-11 labeled PET tracer for imaging phosphodiesterase 10A in the brain of living subject. *Neuroimage* **121**: 253–262.

Logan J, Fowler JS, Volkow ND, *et al* (1990). Graphical analysis of reversible radioligand binding from time-activity measurements applied to [N-11C-methyl]-(-)-cocaine PET studies in human subjects. *J Cereb Blood Flow Metab* **10**: 740–747.

Logan J, Fowler JS, Volkow ND, *et al* (1996). Distribution volume ratios without blood sampling from graphical analysis of PET data. *J Cereb Blood Flow Metab* **16**: 834–840.

López-Giménez JF, Vilaró MT, Palacios JM, *et al* (2013). Multiple conformations of 5-HT2A and 5-HT2C receptors in rat brain: An autoradiographic study with [125I](±)DOI. *Exp Brain Res* **230**: 395–406.

López-Giménez JF, Villazon M, Brea J, *et al* (2001). Multiple conformations of native and recombinant human 5-hydroxytryptamine(2a) receptors are labeled by agonists and discriminated by antagonists. *Mol Pharmacol* **60**: 690–699.

Lundberg J, Christophersen JS, Petersen KB, *et al* (2007). PET measurement of serotonin transporter occupancy: a comparison of escitalopram and citalopram. *Int J Neuropsychopharmacol* **10**: 777–785.

Lundberg J, Odano I, Olsson H, *et al* (2005). Quantification of 11C-MADAM binding to the serotonin transporter in the human brain. *J Nucl Med* **46**: 1505–1515.

Lundkvist C, Halldin C, Ginovart N, *et al* (1996). [11C]MDL 100907, a radioligland for selective imaging of 5-HT(2A) receptors with positron emission tomography. *Life Sci* **58**: PL 187-192.

Lundquist P, Blomquist G, Hartvig P, *et al* (2006). Validation studies on the 5-hydroxy-L-[β-11C]-tryptophan/ PET method for probing the decarboxylase step in serotonin synthesis. *Synapse* **59**: 521–531.

Lundquist P, Roman M, Syväanen S, *et al* (2007). Effect on [11C]DASB binding after tranylcypromine-induced increase in serotonin concentration: Positron emission tomography studies in monkeys and rats. *Synapse* **61**: 440–449.

Mantere T, Tupala E, Hall H, *et al* (2002). Serotonin transporter distribution and density in the cerebral cortex of alcoholic and nonalcoholic comparison subjects: A whole-hemisphere autoradiography study. *Am J Psychiatry* **159**: 599–606.

Marner L, Gillings N, Madsen K, *et al* (2010). Brain imaging of serotonin 4 receptors in humans with [11C]SB207145-PET. *Neuroimage* **50**: 855–861.

Marques TR, Natesan S, Niccolini F, *et al* (2016). Phosphodiesterase 10A in schizophrenia: A PET study using [11C]IMA107. *Am J Psychiatry* **173**: 714–721.

Martinez D, Slifstein M, Broft A, *et al* (2003). Imaging human mesolimbic dopamine transmission with positron emission tomography. Part II: amphetamine-induced dopamine release in the functional subdivisions of the striatum. *J Cereb Blood Flow Metab* **23**: 285–300.

Matthews PM, Rabiner EA, Passchier J, *et al* (2012). Positron emission tomography molecular imaging for drug development. *Br J Clin Pharmacol* **73**: 175–186.

Matusch A, Hurlemann R, Rota Kops E, *et al* (2007). Acute S-ketamine application does not alter cerebral [18F] altanserin binding: A pilot PET study in humans. *J Neural Transm* **114**: 1433–1442.

Maurice DH, Ke H, Ahmad F, *et al* (2014). Advances in targeting cyclic nucleotide phosphodiesterases. *Nat Rev Drug Discov* **13**: 290–314.

McCormick PN, Ginovart N, Wilson AA (2011). Isoflurane anaesthesia differentially affects the amphetamine sensitivity of agonist and antagonist D2/D3 positron emission tomography radiotracers: Implications for in vivo imaging of dopamine release. *Mol Imaging Biol* **13**: 737–746.

Meyer JH, Cho R, Kennedy S, *et al* (1999). The effects of single dose nefazodone and paroxetine upon 5-HT(2A) binding potential in humans using [18F]-setoperone PET. *Psychopharmacology (Berl)* **144**: 279–281.

Meyer JH, Wilson AA, Sagrati S, *et al* (2004). Serotonin transporter occupancy of five selective serotonin reuptake inhibitors at different doses: an [11C]DASB positron emission tomography study. *Am J Psychiatry* **161**: 826–835.

Meyer PT, Bhagwagar Z, Cowen PJ, *et al* (2010). Simplified quantification of 5-HT2A receptors in the human brain with [11C]MDL 100,907 PET and non-invasive kinetic analyses. *Neuroimage* **50**: 984–993.

Mick I, Myers J, Ramos AC, *et al* (2016). Blunted endogenous opioid release following an oral amphetamine challenge in pathological gamblers. *Neuropsychopharmacology* **41**: 1742–1750.

Mick I, Myers J, Stokes PRA, *et al* (2014). Amphetamine induced endogenous opioid release in the human brain detected with [11C]carfentanil PET: Replication in an independent cohort. *Int J Neuropsychopharmacol* **17**: 2069–2074.

Mikami T, Sugimoto H, Naganeo R, *et al* (2008). Contribution of active and inactive states of the human 5-HT4d receptor to the functional activities of 5-HT4-receptor agonists. *J Pharmacol Sci* **107**: 251–259.

Milak MS, Ogden RT, Vinocur DN, *et al* (2005). Effects of tryptophan depletion on the binding of [11C]-DASB to the serotonin transporter in baboons: Response to acute serotonin deficiency. *Biol Psychiatry* **57**: 102–106.

Milak MS, Severance AJ, Prabhakaran J, *et al* (2011). In vivo serotonin-sensitive binding of [11C]CUMI-101: a serotonin 1A receptor agonist positron emission tomography radiotracer. *J Cereb Blood Flow Metab* **31**: 243–249.

Millan MJ, Maiofiss L, Cussac D, *et al* (2002). Differential actions of antiparkinson agents at multiple classes of monoaminergic receptor. I. A multivariate analysis of the binding profiles of 14 drugs at 21 native and cloned human receptor subtypes. *J Pharmacol Exp Ther* **303**: 791–804.

Millan MJ, Marin P, Bockaert J, *et al* (2008). Signaling at G-protein-coupled serotonin receptors: recent advances and future research directions. *Trends Pharmacol Sci* **29**: 454–464.

Millar JK, Pickard BS, Mackie S, *et al* (2005). DISC1 and PDE4B are interacting genetic factors in schizophrenia that regulate cAMP signaling. *Science (80-)* **310**: 1187–1191.

Miner LAH, Backstrom JR, Sanders-Bush E, *et al* (2003). Ultrastructural localization of serotonin2A receptors in the middle layers of the rat prelimbic prefrontal cortex. *Neuroscience* **116**: 107–117.

Miner LH, Schroeter S, Blakely RD, *et al* (2000). Ultrastructural localization of the serotonin transporter in superficial and deep layers of the rat prelimbic prefrontal cortex and its spatial relationship to dopamine. *J Comp Neurol* **234**: 220–234.

Mintun MA, Raichle ME, Kilbourn MR, *et al* (1984). A quantitative model for the in vivo assessment of drug binding sites with positron emission tomography. *Ann Neurol* **15**: 217–227.

Miyake N, Skinbjerg M, Easwaramoorthy B, *et al* (2011). Imaging changes in glutamate transmission in vivo with the metabotropic glutamate receptor 5 tracer [11C] ABP688 and N-acetylcysteine challenge. *Biol Psychiatry* **69**: 822–824.

Miyamoto S, Miyake N, Jarskog LF, *et al* (2012). Pharmacological treatment of schizophrenia: a critical review of the pharmacology and clinical effects of current and future therapeutic agents. *Mol Psychiatry* **17**: 1206–1227.

Mnie-Filali O, Amraei MG, Benmbarek S, *et al* (2010). Serotonin 4 receptor (5-HT4R) internalization is

isoform-specific: Effects of 5-HT and RS67333 on isoforms A and B. *Cell Signal* **22**: 501–509.

Montani D, Seferian A, Savale L, *et al* (2013). Drug-induced pulmonary arterialhypertension: a recent outbreak. *Eur Respir Rev* **22**: 244–250.

Morgan P, Graaf PH Van Der, Arrowsmith J, *et al* (2012). Can the flow of medicines be improved? Fundamental pharmacokinetic and pharmacological principles toward improving Phase II survival. *Drug Discov Today* **17**: 419–424.

Mørk A, Pehrson A, Brennum LT, *et al* (2012). Pharmacological effects of Lu AA21004: A novel multimodal compound for the treatment of major depressive disorder. *J Pharmacol Exp Ther* **340**: 666–675.

Narendran R, Hwang D-R, Slifstein M, *et al* (2004). In vivo vulnerability to competition by endogenous dopamine: comparison of the D2 receptor agonist radiotracer (-)-N-[11C]propyl-norapomorphine ([11C]NPA) with the D2 receptor antagonist radiotracer [11C]-raclopride. *Synapse* **52**: 188–208.

Narendran R, Mason NS, Laymon CM, *et al* (2010). A comparative evaluation of the dopamine D(2/3) agonist radiotracer [11C](-)-N-propyl-norapomorphine and antagonist [11C]raclopride to measure amphetamine-induced dopamine release in the human striatum. *J Pharmacol Exp Ther* **333**: 533–539.

Newman-Tancredi A, Cussac D, Marini L, *et al* (2003). h5-HT1B receptor-mediated constitutive Gαi3-protein activation in stably transfected Chinese hamster ovary cells: an antibody capture assay reveals protean efficacy of 5-HT. *Br J Pharmacol* **138**: 1077–1084.

Niccolini F, Foltynie T, Reis Marques T, *et al* (2015). Loss of phosphodiesterase 10A expression is associated with progression and severity in Parkinson's disease. *Brain* **138**: 3003–3015.

Nichols DE, Nichols CD (2008). Serotonin receptors. *Chem Rev* **108**: 1614–1641.

Nishi A, Kuroiwa M, Shuto T (2011). Mechanisms for the modulation of dopamine D1 receptor signaling in striatal neurons. *Front Neuroanat* **5**: 43.

Nishiyama S, Tsukada H, Sato K, *et al* (2001). Evaluation of PET ligands (+) N-[11C]ethyl-3-piperidyl benzilate and (+) N-[11C]propyl-3-piperidyl benzilate for muscarinic cholinergic receptors: A PET study with microdialysis in comparison with (+)N-[11C]methyl-3-piperidyl benzilate in the conscious mo. *Synapse* **40**: 159–169.

Nord M, Finnema SJ, Halldin C, *et al* (2013). Effect of a single dose of escitalopram on serotonin concentration in the non-human and human primate brain. *Int J Neuropsychopharmacol* **16**: 1577–1586.

Nord M, Finnema SJ, Schain M, *et al* (2014). Test-retest reliability of [11C]AZ10419369 binding to 5-HT1B receptors in human brain. *Eur J Nucl Med Mol Imaging* **41**: 301–307.

Nutt DJ, Lingford-Hughes A, Erritzoe D, *et al* (2015). The dopamine theory of addiction: 40 years of highs and lows. *Nat Rev Neurosci* **16**: 305–312.

Ohba H, Harada N, Nishiyama S, *et al* (2009). Ketamine/xylazine anesthesia alters [11C]MNPA binding to dopamine D2 receptors and response to methamphetamine challenge in monkey brain. *Synapse* **63**: 534–537.

Ooms M, Attili B, Celen S, *et al* (2016). [18F]JNJ42259152 binding to phosphodiesterase 10A, a key regulator of medium spiny neuron excitability, is altered in the presence of cyclic AMP. *J Neurochem* **139**: 897–906.

Oswald LM, Wand GS, Wong DF, *et al* (2015). Risky decision-making and ventral striatal dopamine responses to amphetamine: A positron emission tomography [11C]raclopride study in healthy adults. *Neuroimage* **113**: 26–36.

Papakostas GI, Ionescu DF (2015). Towards new mechanisms: an update on therapeutics for treatment-resistant major depressive disorder. *Mol Psychiatry* **20**: 1142–1150.

Paramonov VM, Mamaeva V, Sahlgren C, *et al* (2015). Genetically-encoded tools for cAMP probing and modulation in living systems. *Front Pharmacol* **6**: 196.

Parsey R V., Slifstein M, Hwang D-R, *et al* (2000). Validation and reproducibility of measurement of 5-HT1A

receptor parameters with [carbonyl-11C]WAY-100635 in humans: comparison of arterial and reference tisssue input functions. *J Cereb Blood Flow Metab Metab* **20**: 1111–1133.

Paterson LM, Kornum BR, Nutt DJ, *et al* (2013). 5-HT radioligands for human brain imaging with PET and SPECT. *Med Res Rev* **33**: 54–111.

Paterson LM, Tyacke RJ, Nutt DJ, *et al* (2010). Measuring endogenous 5-HT release by emission tomography: Promises and pitfalls. *J Cereb Blood Flow Metab* **30**: 1682–1706.

Pavan B, Biondi C, Dalpiaz A (2009). Adenylyl cyclases as innovative therapeutic goals. *Drug Discov Today* **14**: 982–991.

Paxinos G, Huang X-F, Michael P, *et al* (Academic Press: San Diego, California, 2008). *The Rhesus Monkey Brain in Stereotaxic Coordinates*, 2nd edn.

Pehrson AL, Cremers T, Bétry C, *et al* (2013). Lu AA21004, a novel multimodal antidepressant, produces regionally selective increases of multiple neurotransmitters-A rat microdialysis and electrophysiology study. *Eur Neuropsychopharmacol* **23**: 133–145.

Perez-Costas E, Melendez-Ferro M, Roberts RC (2010). Basal ganglia pathology in schizophrenia: Dopamine connections and anomalies. *J Neurochem* **113**: 287–302.

Perlis RH, Ostacher MJ, Patel JK, *et al* (2006). Predictors of recurrence in bipolar disorder: Primary outcomes from the Systematic Treatment Enhancement Program for Bipolar Disorder (STEP-BD). *Am J Psychiatry* **163**: 217–224.

Phelps ME (2000). Positron emission tomography provides molecular imaging of biological processes. *Proc Natl Acad Sci U S A* **97**: 9226–9233.

Phillips KA, Bales KL, Capitanio JP, *et al* (2014). Why primate models matter. *Am J Primatol* **76**: 801–827.

Pierre S, Eschenhagen T, Geisslinger G, *et al* (2009). Capturing adenylyl cyclases as potential drug targets. *Nat Rev Drug Discov* **8**: 321–335.

Pierson ME, Andersson J, Nyberg S, *et al* (2008). [11C]AZ10419369: A selective 5-HT1B receptor radioligand suitable for positron emission tomography (PET). Characterization in the primate brain. *Neuroimage* **41**: 1075–1085.

Pinborg LH, Adams KH, Yndgaard S, *et al* (2004). [18F]altanserin binding to human 5HT2A receptors is unaltered after citalopram and pindolol challenge. *J Cereb Blood Flow Metab* **24**: 1037–1045.

Pinborg LH, Feng L, Haahr ME, *et al* (2012). No change in [11C]CUMI-101 binding to 5-HT1A receptors after intravenous citalopram in human. *Synapse* **66**: 880–884.

Pindon A, Hecke G Van, Josson K, *et al* (2005). Internalization of human 5-HT4a and 5-HT4b receptors is splice variant dependent. *Biosci Rep* **24**: 215–223.

Piñeyro G, Blier P (1999). Autoregulation of serotonin neurons: role in antidepressant drug action. *Pharmacol Rev* **51**: 533–591.

Plisson C, Salinas C, Weinzimmer D, *et al* (2011). Radiosynthesis and in vivo evaluation of [11 C] MP-10 as a positron emission tomography radioligand for phosphodiesterase 10A. *Nucl Med Biol* **38**: 875–884.

Plisson C, Weinzimmer D, Jakobsen S, *et al* (2014). Phosphodiesterase 10A PET radioligand development program: from pig to human. *J Nucl Med* **55**: 595–601.

Praschak-Rieder N, Wilson AA, Hussey D, *et al* (2005). Effects of tryptophan depletion on the serotonin transporter in healthy humans. *Biol Psychiatry* **58**: 825–830.

Quednow BB, Treyer V, Hasler F, *et al* (2012). Assessment of serotonin release capacity in the human brain using dexfenfluramine challenge and [18F]altanserin positron emission tomography. *Neuroimage* **59**: 3922–3932.

Rabiner EA, Messa C, Sargent PA, *et al* (2002). A database of [(11)C]WAY-100635 binding to 5-HT(1A) receptors in normal male volunteers: Normative data and relationship to methodological, demographic,

physiological, and behavioral variables. *Neuroimage* **15**: 620–632.

Raote I, Bhattacharyya S, Panicker MM (2013). Functional selectivity in serotonin receptor 2A (5-HT2A) endocytosis, recycling, and phosphorylation. *Mol Pharmacol* **83**: 42–50.

Ren J, Xu H, Choi J-K, *et al* (2009). Dopaminergic response to graded dopamine concentration elicited by four amphetamine doses. *Synapse* **63**: 764–772.

Riad M, Garcia S, Watkins KC, *et al* (2000). Somatodendritic localization of 5-HT1A and preterminal axonal localization of 5-HT1B serotonin receptors in adult rat brain. *J Comp Neurol* **417**: 181–194.

Riad M, Watkins KC, Doucet E, *et al* (2001). Agonist-induced internalization of serotonin-1a receptors in the dorsal raphe nucleus (autoreceptors) but not hippocampus (heteroreceptors). *J Neurosci* **21**: 8378–8386.

Ridler K, Plisson C, Rabiner EA, *et al* (2011). Characterization of in vivo pharmacological properties and sensitivity to endogenous serotonin of [11C] P943: A positron emission tomography study in Papio anubis. *Synapse* **65**: 1119–1127.

Roberts JC, Reavill C, East SZ, *et al* (2002). The distribution of 5-HT6 receptors in rat brain: An autoradiographic binding study using the radiolabelled 5-HT6 receptor antagonist [125I]SB-258585. *Brain Res* **934**: 49–57.

Rohlfing T, Kroenke CD, Sullivan E V, *et al* (2012). The INIA19 template and NeuroMaps atlas for primate brain image parcellation and spatial normalization. *Front Neuroinform* **6**: 27.

Ross SB, Jackson DM (1989). Kinetic properties of the in vivo accumulation of 3H-(−)-N-n-propylnorapomorphine in mouse brain. *Naunyn Schmiedebergs Arch Pharmacol* **340**: 13–20.

Roth BL, Sheffler DJ, Kroeze WK (2004). Magic shotguns versus magic bullets: selectively non-selective drugs for mood disorders and schizophrenia. *Nat Rev Drug Discov* **3**: 353–359.

Rothman RB, Baumann MH (2002). Therapeutic and adverse actions of serotonin transporter substrates. *Pharmacol Ther* **95**: 73–88.

Rothman RB, Baumann MH, Savage JE, *et al* (2000). Evidence for possible involvement of 5-HT(2B) receptors in the cardiac valvulopathy associated with fenfluramine and other serotonergic medications. *Circulation* **102**: 2836–2841.

Ruf BM, Bhagwagar Z (2009). The 5-HT1B receptor: a novel target for the pathophysiology of depression. *Curr Drug Targets* **10**: 1118–1138.

Rush AJ, Trivedi MH, Wisniewski SR, *et al* (2006). Acute and longer-term out- comes in depressed outpatients requiring one or several treatment steps: a STAR*D report. *Am J Psychiatry* **163**: 1905–1917.

Russwurm C, Koesling D, Russwurm M (2015). Phosphodiesterase 10A is tethered to a synaptic signaling complex in striatum. *J Biol Chem* **290**: 11936–11947.

Sanchez C, Asin KE, Artigas F (2015). Vortioxetine, a novel antidepressant with multimodal activity: Review of preclinical and clinical data. *Pharmacol Ther* **145**: 43–47.

Sandiego CM, Gallezot J-D, Lim K, *et al* (2015). Reference region modeling approaches for amphetamine challenge studies with [(11)C]FLB 457 and PET. *J Cereb Blood Flow Metab* **35**: 623–629.

Sari Y (2004). Serotonin1B receptors: from protein to physiological function and behavior. *Neurosci Biobehav Rev* **28**: 565–582.

Sari Y, Lefèvre K, Bancila M, *et al* (1997). Light and electron microscopic immunocytochemical visualization of 5-HT1B receptors in the rat brain. *Brain Res* **760**: 281–286.

Sari Y, Miquel M-C, Brisorgueil MJ, *et al* (1999). Cellular and subcellular localization of 5-hydroxytryptamine(1B) receptors in the rat central nervous system: Immunocytochemical, autoradiographic and lesion studies. *Neuroscience* **88**: 899–915.

Savitz JB, Drevets WC (2013). Neuroreceptor imaging in depression. *Neurobiol Dis* **52**: 49–65.

Schmid CL, Raehal KM, Bohn LM (2008). Agonist-directed signaling of the serotonin 2A receptor depends on

beta-arrestin-2 interactions in vivo. *Proc Natl Acad Sci U S A* **105**: 1079–1084.

Schröder S, Wenzel B, Deuther-Conrad W, *et al* (2016). Novel radioligands for cyclic nucleotide phosphodiesterase imaging with positron emission tomography: An update on developments since 2012. *Molecules* **21**: 650.

Seeger TF, Bartlett B, Coskran TM, *et al* (2003). Immunohistochemical localization of PDE10A in the rat brain. *Brain Res* **985**: 113–126.

Selvaraj S, Arnone D, Cappai A, *et al* (2014). Alterations in the serotonin system in schizophrenia: A systematic review and meta-analysis of postmortem and molecular imaging studies. *Neurosci Biobehav Rev* **45**: 233–245.

Selvaraj S, Turkheimer F, Rosso L, *et al* (2012). Measuring endogenous changes in serotonergic neurotransmission in humans: a [11C]CUMI-101 PET challenge study. *Mol Psychiatry* **17**: 1254–1260.

Seneca N, Finnema SJ, Farde L, *et al* (2006). Effect of amphetamine on dopamine D2 receptor binding in nonhuman primate brain: a comparison of the agonist radioligand [11C]MNPA and antagonist [11C]raclopride. *Synapse* **59**: 260–269.

Shotbolt P, Tziortzi AC, Searle GE, *et al* (2012). Within-subject comparison of [(11)C]-(+)-PHNO and [(11)C]raclopride sensitivity to acute amphetamine challenge in healthy humans. *J Cereb Blood Flow Metab* **32**: 127–136.

Sibon I, Benkelfat C, Gravel P, *et al* (2008). Decreased [18F]MPPF binding potential in the dorsal raphe nucleus after a single oral dose of fluoxetine: a positron-emission tomography study in healthy volunteers. *Biol Psychiatry* **63**: 1135–1140.

Skinbjerg M, Liow J-S, Seneca N, *et al* (2010). D2 dopamine receptor internalization prolongs the decrease of radioligand binding after amphetamine: A PET study in a receptor internalization-deficient mouse model. *Neuroimage* **50**: 1402–1407.

Skoblenick KJ, Argintaru N, Xu Y, *et al* (2010). Role of AP-2α Transcription factor in the regulation of synapsin II gene expression by dopamine D1 and D2 receptors. *J Mol Neurosci* **41**: 267–277.

Sleight AJ, Stam NJ, Mutel V, *et al* (1996). Radiolabelling of the human 5-HT2A receptor with an agonist, a partial agonist and an antagonist: Effects on apparent agonist affinities. *Biochem Pharmacol* **51**: 71–76.

Slifstein M, Laruelle M (2001). Models and methods for derivation of in vivo neuroreceptor parameters with PET and SPECT reversible radiotracers. *Nucl Med Biol* **28**: 595–608.

Soderling SH, Bayuga SJ, Beavo JA (1999). Isolation and characterization of a dual-substrate phosphodiesterase gene family: PDE10A. *Proc Natl Acad Sci U S A* **96**: 7071–7076.

Staley JK, Dyck CH Van, Tan PZ, *et al* (2001). Comparison of [18F]altanserin and [18F]deuteroaltanserin for PET imaging of serotonin2A receptors in baboon brain: Pharmacological studies. *Nucl Med Biol* **28**: 271–279.

Steinbusch HWM (1981). Distribution of serotonin-immunoreactivity in the central nervous system of the rat-Cell bodies and terminals. *Neuroscience* **6**: 557–618.

Stenkrona P, Halldin C, Lundberg J (2013). 5-HTT and 5-HT1A receptor occupancy of the novel substance vortioxetine (Lu AA21004). A PET study in control subjects. *Eur Neuropsychopharmacol* **23**: 1190–1198.

Stokes PRA, Myers JF, Kalk NJ, *et al* (2014). Acute increases in synaptic GABA detectable in the living human brain: A [11C]Ro15-4513 PET study. *Neuroimage* **99**: 158–165.

Sun J, Xu J, Cairns NJ, *et al* (2012). Dopamine D1, D2, D3 receptors, vesicular monoamine transporter type-2 (VMAT2) and dopamine transporter (DAT) densities in aged human brain. *PLoS One* **7**: e49483.

Svenningsson P (2006). Alterations in 5-HT1B receptor function by p11 in depression-like states. *Science (80-)* **311**: 77–80.

Takano A, Halldin C, Farde L (2013). SERT and NET occupancy by venlafaxine and milnacipran in nonhuman primates: A PET study. *Psychopharmacology (Berl)* **226**: 147–153.

Takano A, Stepanov V, Gulyás B, *et al* (2015). Evaluation of a novel PDE10A PET radioligand, [11C]T-773, in nonhuman primates: Brain and whole body PET and brain autoradiography. *Synapse* **69**: 345–355.

Talbot PS, Frankle WG, Hwang D-R, *et al* (2005). Effects of reduced endogenous 5-HT on the in vivo binding of the serotonin transporter radioligand 11C-DASB in healthy humans. *Synapse* **55**: 164–175.

Talbot PS, Slifstein M, Hwang D-R, *et al* (2012). Extended characterisation of the serotonin 2A (5-HT2A) receptor-selective PET radiotracer 11C-MDL100907 in humans: quantitative analysis, test-retest reproducibility, and vulnerability to endogenous 5-HT tone. *Neuroimage* **59**: 271–285.

Tokunaga M, Seneca N, Shin R-M, *et al* (2009). Neuroimaging and physiological evidence for involvement of glutamatergic transmission in regulation of the striatal dopaminergic system. *J Neurosci* **29**: 1887–1896.

Tsukada H, Harada N, Ohba H, *et al* (2001). Facilitation of dopaminergic neural transmission does not affect [11C]SCH23390 binding to the striatal D1 dopamine receptors, but the facilitation enhances phosphodiesterase type-IV activity through D1 receptors: PET studies in the conscious monkey brain. *Synapse* **42**: 258–265.

Tsukada H, Nishiyama S, Fukumoto D, *et al* (2004). Effects of acute acetylcholinesterase inhibition on the cerebral cholinergic neuronal system and cognitive function: Functional imaging of the conscious monkey brain using animal PET in combination with microdialysis. *Synapse* **52**: 1–10.

Turner EH, Loftis JM, Blackwell AD (2006). Serotonin a la carte: Supplementation with the serotonin precursor 5-hydroxytryptophan. *Pharmacol Ther* **109**: 325–338.

Tustison NJ, Avants BB, Cook PA, *et al* (2010). N4ITK: Improved N3 bias correction. *IEEE Trans Med Imaging* **29**: 1310–1320.

Tyacke RJ, Nutt DJ (2015). Optimising PET approaches to measuring 5-HT release in human brain. *Synapse* **69**: 505–511.

Udo De Haes JI, Bosker FJ, Waarde A Van, *et al* (2002). 5-HT1A receptor imaging in the human brain: Effect of tryptophan depletion and infusion on [18F]MPPF binding. *Synapse* **46**: 108–115.

Udo de Haes JI, Harada N, Elsinga PH, *et al* (2006). Effect of fenfluramine-induced increases in serotonin release on [18F]MPPF binding: a continuous infusion PET study in conscious monkeys. *Synapse* **59**: 18–26.

Valette H, Bottlaender M, Dollé F, *et al* (2005). Acute effects of physostigmine and galantamine on the binding of [18F]fluoro-A-85380: A PET study in monkeys. *Synapse* **56**: 217–221.

Varnäs K, Halldin C, Hall H (2004). Autoradiographic distribution of serotonin transporters and receptor subtypes in human brain. *Hum Brain Mapp* **22**: 246–260.

Varnäs K, Halldin C, Pike VW, *et al* (2003). Distribution of 5-HT4 receptors in the postmortem human brain - An autoradiographic study using [125I]SB 207710. *Eur Neuropsychopharmacol* **13**: 228–234.

Varnäs K, Nyberg S, Halldin C, *et al* (2011). Quantitative analysis of [11C]AZ10419369 binding to 5-HT1B receptors in human brain. *J Cereb Blood Flow Metab* **31**: 113–123.

Varnäs K, Varrone A, Farde L (2013). Modeling of PET data in CNS drug discovery and development. *J Pharmacokinet Pharmacodyn* **40**: 267–279.

Varrone A, Sjoholm N, Eriksson L, *et al* (2009). Advancement in PET quantification using 3D-OP-OSEM point spread function reconstruction with the HRRT. *Eur J Nucl Med Mol Imaging* **36**: 1639–1650.

Verhoest PR, Chapin DS, Corman M, *et al* (2009). Discovery of a novel class of phosphodiesterase 10A inhibitors and identification of clinical candidate 2-[4-(1-methyl-4-pyridin-4-yl-1H-pyrazol-3- yl)-phenoxymethyl]-quinoline (PF-2545920) for the treatment of schizophrenia. *J Med Chem* **52**: 5188–5196.

Vilaró MT, Cortés R, Mengod G (2005). Serotonin 5-HT4 receptors and their mRNAs in rat and guinea pig brain: distribution and effects of neurotoxic lesions. *J Comp Neurol* **484**: 418–39.

Visser AKD, Waarde A Van, Willemsen ATM, *et al* (2011). Measuring serotonin synthesis: From conventional methods to PET tracers and their (pre)clinical implications. *Eur J Nucl Med Mol Imaging* **38**: 576–591.

Vizeli P, Liechti ME (2017). Safety pharmacology of acute MDMA administration in healthy subjects. *J Psychopharmacol* **31**: 576–588.

Volkow ND, Wang GJ, Fowler JS, *et al* (2011). Addiction: beyond dopamine reward circuitry. *Proc Natl Acad Sci U S A* **108**: 15037–15042.

Volkow ND, Wang GJ, Smith L, *et al* (2015). Recovery of dopamine transporters with methamphetamine detoxification is not linked to changes in dopamine release. *Neuroimage* **121**: 20–28.

Watson J, Collin L, Ho M, *et al* (2000). 5-HT(1A) receptor agonist-antagonist binding affinity difference as a measure of intrinsic activity in recombinant and native tissue systems. *Br J Pharmacol* **130**: 1108–1114.

Whiteford HA, Degenhardt L, Rehm J, *et al* (2013). Global burden of disease attributable to mental and substance use disorders: findings from the Global Burden of Disease Study 2010. *Lancet* **382**: 1575–1586.

Winter JCF De (2013). Using the Student's t-test with extremely small sample sizes. *Pract Assessment, Res Eval* **18**: .

Wong-Lin K, Joshi A, Prasad G, *et al* (2012). Network properties of a computational model of the dorsal raphe nucleus. *Neural Networks* **32**: 15–25.

Wong DF, Tauscher J, Gründer G (2009). The role of imaging in proof of concept for CNS drug discovery and development. *Neuropsychopharmacology* **34**: 187–203.

Wong EHF, Tarazi FI, Shahid M (2010). The effectiveness of multi-target agents in schizophrenia and mood disorders: Relevance of receptor signature to clinical action. *Pharmacol Ther* **126**: 173–185.

Woolley ML, Marsden CA, Fone KCF (2004). 5-ht6 Receptors. *Curr Drug Targets - CNS Neurol Disord* **3**: 59–79.

Yamamoto S, Onoe H, Tsukada H, *et al* (2007). Effects of increased endogenous serotonin on the in vivo binding of [11C]DASB to serotonin transporters in conscious monkey brain. *Synapse* **61**: 724–731.

Yamanaka H, Yokoyama C, Mizuma H, *et al* (2014). A possible mechanism of the nucleus accumbens and ventral pallidum 5-HT1B receptors underlying the antidepressant action of ketamine: a PET study with macaques. *Transl Psychiatry* **4**: e342.

Yang K-C, Stepanov V, Amini N, *et al* (2017a). Characterization of [11C]Lu AE92686 as a PET radioligand for phosphodiesterase 10A in the nonhuman primate brain. *Eur J Nucl Med Mol Imaging* **44**: 308–320.

Yang K-C, Stepanov V, Martinsson S, *et al* (2017b). Fenfluramine reduces [11C]Cimbi-36 binding to the 5-HT2A receptor in the nonhuman primate brain. *Int J Neuropsychopharmacol* **20**: 683–691.

Yatham LN, Liddle PF, Shiah IS, *et al* (2001). Effects of rapid tryptophan depletion on brain 5-HT2 receptors: A PET study. *Br J Psychiatry* **178**: 448–453.

Zanderigo F, Ogden RT, Parsey R V. (2013). Reference region approaches in PET: a comparative study on multiple radioligands. *J Cereb Blood Flow Metab* **33**: 888–897.

Zhou FC, Tao-Cheng JH, Segu L, *et al* (1998). Serotonin transporters are located on the axons beyond the synaptic junctions: Anatomical and functional evidence. *Brain Res* **805**: 241–254.

Zoghbi SS, Shetty HU, Ichise M, *et al* (2006). PET imaging of the dopamine transporter with 18F-FECNT: a polar radiometabolite confounds brain radioligand measurements. *J Nucl Med* **47**: 520–527.